Modification and validation of a commercial dynamic chamber for reactive nitrogen and greenhouse gas flux measurements

Moxy Shah[1], Kifle Z. Aregahegn[1], Danial Nodeh-Farahani[1], Leigh R. Crilley[1,‡], Tasnia Hasan[1], Yashar Ebrahimi-Iranpour[1], Fahim Sarker[1], Nick Nickerson[2], Chance Creelman[2], Sarah Ellis[2], Alexander Moravek[1,§], Trevor C. VandenBoer[1,*]

[1] Department of Chemistry, York University, Toronto, Ontario, Canada

[2] Eosense Inc., Dartmouth, Nova Scotia, Canada

[‡] Now at: Atmospheric Services, WSP Australia, Brisbane, QLD, Australia

[§] Now at: German Environment Agency, Department of Air Quality, Dessau-Rosslau, Germany

[*]Communicating author: tvandenb@yorku.ca

Abstract

Reactive nitrogen compounds (NO, NO_2, HONO, NH_3 and others; N_r) play important roles in atmospheric processes, and their cascading impacts throughout the Earth system have adverse effects on both the environment and human health. The fluxes of these gases at the surface-atmosphere interface have been studied in isolation or ~~in~~ smaller subsets ~~by micrometeorological techniques or chambers~~, but simultaneous ~~observations~~ fluxes of all N_r ~~species~~ alongside standard greenhouse gases (GHGs) ~~as a function of time~~ have not been reported. Here, a dual-dynamic chamber system was developed for N_r by modifying a commercially available system for GHG fluxes for use with destructive analyzers, ~~and~~ including a reference chamber to account for chemical ~~changes~~challenges. The resulting platform makes the measurement of N_r and, by extension other reactive gases, more widely accessible to the scientific community, as custom chambers do not need to be fabricated.

System modifications to passivate surfaces ~~were implemented, so that N_r gases like NO_2 could be effectively transferred to standard gas analyzers, with~~reduced an initial 36% loss of NO_2 due to transformations ~~ultimately minimized~~ below analyzer detection limits (~10%) ~~under~~ for relevant atmospheric conditions. The modified 72 L chamber response times did not ~~see a~~ change ~~in the~~

~~baseline response times~~ for GHGs or NO at a flow rate of 2 L min^{-1}~~. They retained the same values as an ideal non-reactive trace gas~~ (τ = 37-39 min versus 36 min). The modifications improved the transfer ~~time constants~~ of NO_2, HONO, and NH_3 by up to 2 min, but substantial surface interactions for NH_3 remain. ~~In all cases, a~~A surface interaction term ~~needs to be~~ was characterized for these gases to obtain accurate field fluxes~~. Losses of NO_2 and O_3 by known gas phase reactions, or from deposition and reaction on pristine and aged chamber surfaces, were characterized across a range of environmentally relevant relative humidities (RH) and mixing ratios. The final dual-chamber system configuration includes a measurement and reference chamber, which are necessary to implement the corrections for surface effects and chemical transformations when accurately quantifying dynamic fluxes~~ via a mass balance framework.

Proof-of-concept measurements of N_r fluxes from agricultural soil samples under controlled lab conditions as a function of soil water content were able to quantify emissions of NO, NO_2, HONO, NH_3, and N_2O simultaneously, without amendment and when subject to N_r fertilization ~~experiments using urea, ammonium carbonate and bicarbonate, and ammonium nitrate~~. Unfertilized ~~replicate agricultural~~ soils ~~samples~~ showed variability in NO_2 and HONO emissions when ~~prepared with minimal disturbance to the~~ soil structure was minimally disturbed, consistent with ~~values consistent with those reported by~~ in-situ field measurements from others. These oppose maximum potential fluxes ~~characterized~~ in prior lab soil manipulations, particularly for HONO relative to NO. Last, N_r field fluxes were quantified ~~with destructive gas analyzers in the field~~ with the dual-chamber system on an in-use agricultural soil, ~~and~~ includinged a urea-based fertilizer perturbation to stimulate microbial and chemical transformation and transfer N_r to the atmosphere. ~~The resulting fluxes observed show g~~Good agreement with ~~prior reports based on~~ other field flux techniques was found. The mass balance terms within the dual-chamber approach are fully inspected from the pilot deployment in the field, along with an error analysis, to aid in the uptake of this approach by the community.

1 Introduction

The Earth's biogeochemical nitrogen (N) cycle is a crucial biogeochemical cycle on Earth, essential for sustaining life through the production of nucleic acids, proteins, and other vital biomolecules (Lehnert et al., 2021). Although tThe carbon cycle receives the most attentionmuch focus due to looming the climatcic crises caused by impacts greenhouse gases (GHGs) like carbon dioxide (CO_2) and methane (CH_4), yet the N cycle is closely intertwined with the carbon cycle (Schlesinger, 2020). At the interface of these cycles and the Earth's surface, reactive nitrogen (N_r) species exchanged between ecosystems and the atmosphere have therefore become an area of emerging interest (Lehnert et al., 2021; Wu et al., 2020). Within the atmosphere, Atmospheric N_r species such as nitric oxide (NO) and nitrogen dioxide (NO_2) – collectively referred to as NO_x – ammonia (NH_3), and nitrous acid (HONO) can each be mediated in part through experience surface-atmosphere exchange, influencing impacting local air or water quality, ecosystem processes, and biodiversity (Lehnert et al., 2021; Richardson et al., 2023; Wu et al., 2020). Meanwhile, the non-reactive nitrous oxide (N_2O) has climate impacts due to its long ~120 year atmospheric lifetime (~120 years) and potent greenhouse effect (IPCC, 2023).

Reactive nitrogen compounds gases (NO, NO_2, HONO, and NH_3; N_r) play an important roles in atmospheric processes, contributing to the formation of pollutants like ozone (O_3) and secondary organic aerosols (SOA). The exchange of N_r between the Earth's surface and the atmosphere involves numerous production and loss processes driven by both natural and human activities. Reactive nitrogen species They are removed from the atmosphere through wet and dry deposition, and their abundance depends onreflects the net outcome relative to N_r emissions (Delaria & Cohen, 2023). At the land surface, N_r is released into the atmosphere by microbial nitrogen cycling, agricultural activities, wildfires, or fossil fuel combustion (Benedict et al., 2017; Mosier, 2008; Yang et al., 2024). Despite the wealth of knowledge on the environmental importance of N_r, sStudying N_r at the surface-atmosphere interface with high time resolution and chemical speciation remains a challenge due to its high spatial and temporal variability driven by factors like climate, vegetation cover, and soil/surface properties (Ludwig et al., 2001). For example, recent studies have demonstrated that vertically resolved HONO production observed at the ground surface demonstrated how it plays a major role in the unexplained daytime HONO source and its impact on daytime OH, with vertically resolved measurements confirming that the surface remains a dominant source at all times of day (VandenBoer et al., 2013, 2015; Young et al., 2012). Such

observations pose a challenge ~~in studying N_r~~ because suitable ~~equipment for~~ high time resolution ~~atmospheric observations~~ equipment is expensive, ~~limiting the concurrent study of~~ preventing the interplay between emission and deposition for ~~many~~ all N_r species ~~to one or a few species at a time~~from being concurrently studied. As a result, no systems are ~~currently~~ sufficiently accessible ~~enough~~ to the scientific community ~~that they may~~to be deployed ~~across~~ widely across different global landscapes, ~~but~~ particularly soils.

Soils ~~play a pivotal role in mediating N_r emissions due to their~~have a dual function as both a source and a sink of ~~nitrogenous~~ N_r species. Soil-atmosphere exchange of N_r is thought to be governed by atmospheric abundance and/or soil microbial processes such as nitrification and denitrification, with ~~soil~~ factors like pH, moisture, organic matter, and nitrogen availability ~~playing a crucial role in~~ regulating ~~N_r emission~~flux directionality (Mosier, 2008; Purchase et al., 2023; Stepniewski et al., 2015). ~~These m~~Microbial processes have been demonstrated to drive the formation and release of ~~some~~ N_r species ~~(e.g.,~~like NO, NH_3 and N_2O~~)~~ from soils, ~~in addition to~~and have assertions ~~that they can support the production and release of~~with respect to HONO ~~via partitioning~~ (Butterbach-Bahl & Dannenmann, 2011; Kool et al., 2010; Mushinski et al., 2019; Oswald et al., 2013; Su et al., 2011). Understanding the exchange of ~~these~~ all N_r gases is essential for unravelling the complex interactions between the nitrogen and carbon cycles and their broader environmental impacts from an unprecedented imbalance in the global nitrogen cycle (Richardson et al., 2023~~). Given the importance of N_r in atmospheric chemistry and its influence on ecosystem processes, it is essential to understand the mechanisms driving its exchange (~~ Fowler et al., 2013). ~~To date, comprehensive exchange systems for studying the full suite of N_r have not been reported.~~

To quantify N_r exchange for a few explicit species near the ground surface, various flux measurement techniques have been employed~~., yielding insights into their magnitude and identifying some driving factors.~~ Quantifying fluxes of atmospheric gases has been most effectively applied to GHGs at the surface-atmosphere interface. Traditional measurement methods, such as eddy covariance (EC), relaxed eddy accumulation (REA), and aerodynamic gradient (AG) methods, have been extensively used for ecosystem-scale, continuous flux monitoring, including targeted assessment of most N_r species (e.g., ~~(~~Bao et al., 2022; Geddes & Murphy, 2014; Kamp et al., 2020; Laufs et al., 2017; Min et al., 2014; Moravek et al., 2014, 2019;

Ren et al., 2011; Von Der Heyden et al., 2022; Wang et al., 2022; Wolff et al., 2010). These micrometeorological techniques measure concentrations, concentration gradients, and/or turbulence to estimate fluxes across interfaces applicable to ecosystem-scale processes. When operated continuously, they offer long-term insight without disrupting the natural system. Chamber methods have some advantages compared to micrometeorological techniques, as they are relatively inexpensive, easy to deploy, and require minimal prior meteorological training and expertise (Tang et al., 2020). Chambers are limited to small plots, ~~e.g.~~ making them suitable to study the effect of different fertilizer treatments (Anthony & Silver, 2024; Chiaravalloti et al., 2023; Manco et al., 2025; Tang et al., 2020). The chamber method is a widely used technique for measuring GHG fluxes, especially for N_2O. However, challenges remain in addressing potential biases introduced by chemical transformations occurring within the chamber and interactions with the chamber surfaces, particularly for N_r species (i.e., NO_2, HONO, NH_3).

Chemical transformations can occur on chamber surfaces or between the point of emission and measurement, where~~.~~ ~~S~~ surface interactions such as adsorption, desorption, and heterogeneous reactions can alter the apparent concentration ~~of several N_r species~~. For example, NO in a chamber could react ~~in the gas phase~~ with O_3 to form NO_2 during the day and NO_3 at night if sufficient O_3 is present to fully titrate NO (R1, R2). Heterogeneous reaction of gas-phase NO_2 on surfaces under humid conditions also produces nitric acid (HNO_3) and HONO (R3) (Kleffmann et al., 2005; Ramazan et al., 2004; VandenBoer et al., 2015). The formed HONO can undergo multiphase processes in the chamber or on enclosed surfaces by partitioning into water according to its Henry's Law constant and then dissociating into nitrite (NO_2^-) and the hydronium ion (H_3O^+) according to its acid dissociation equilibrium constant and the pH (R4, R5) (He et al., 2006; Ren et al., 2020). Nitrous acid could also photolyze, yielding NO and an OH radical (R6) (Spataro & Ianniello, 2014).

$$NO + O_3 \rightarrow NO_2 + O_2 \quad \text{(R1)}$$

$$NO_2 + O_3 \rightarrow NO_3 + O_2 \quad \text{(R2)}$$

$$2NO_{2\,(g)} + H_2O_{\,(ads)} \rightarrow HONO_{\,(g)} + HNO_{3\,(ads)} \quad \text{(R3)}$$

$$HONO_{\,(g)} \leftrightarrow HONO_{\,(aq)} \quad \text{(R4)}$$

$$HONO_{\,(aq)} + H_2O_{\,(l)} \rightleftharpoons NO_2^-{}_{(aq)} + H_3O^+{}_{(aq)} \quad \text{(R5)}$$

149 $HONO + h\nu \rightarrow NO + OH$ (R6)

150 These processes in/on the chamber can introduce uncertainty in flux measurements. Characterizing
151 and accounting for chemistry and surface effects in chamber-based flux methods are therefore
152 necessary ~~to obtain accurate flux measurements of N_r species with a chamber-based system~~. ~~While~~
153 ~~s~~Static chamber systems typically determine the flux from the change in headspace concentration
154 after closing the ~~chamber~~ cover~~,~~. ~~traditional d~~Dynamic chamber systems ~~use~~ have traditionally
155 used a controlled flow of ambient air through the headspace ~~and~~ to retrieve the flux from ~~the~~ a
156 concentration difference ~~at~~ between the chamber inlet and outlet. ~~With minor modifications, these~~
157 ~~chambers have previously been applied to agricultural soils and natural ecosystems, demonstrating~~
158 ~~their utility for measuring emissions of gases such as N_2O and NO_x (Maggiotto et al., 2000; Pape~~
159 ~~et al., 2009). Their ability to create standardized and reproducible conditions makes them~~
160 ~~particularly advantageous for studying the driving mechanisms behind gas exchange, yet their~~
161 ~~application to the full suite of relevant N_r species for surface-atmosphere exchange remains~~
162 ~~unestablished.~~

163 The dynamic chamber flux method has ~~been reported for measurements of the exchange fluxes of~~
164 measured challenging gases like biogenic volatile organic compounds ~~(BVOCs~~, such as
165 monoterpenes and isoprene~~,~~) from vegetation and farmland (Kolari et al., 2012; Mochizuki et al.,
166 2018~~)~~, Pugliese et al. 2023), NH_3 volatilization from cattle manure (Becciolini et al., 2024), N_2O
167 and NO_x from turfgrass (Maggiotto et al., 2000), and NO_x ~~fluxes~~ from grasslands (Pape et al.,
168 2009; Plake et al., 2015). Scharko et al. (2015) used sealed chambers, while ~~and~~ Tang et al. (2019)~~,~~
169 ~~using~~ used dynamic ~~chambers~~, ~~were amongst the first~~ to highlight the hotspot potential for both
170 HONO and NO_x fluxes from agricultural soils ~~as hotspots impacting atmospheric chemistry, which~~
171 ~~has been implemented in atmospheric models (Ha et al., 2023; Tian et al., 2024).~~ These are of
172 high interest due to their impacts on atmospheric chemistry from local to regional scales.

173 The complex~~ity~~ biological and chemical controls o~~f~~n nitrite (NO_2^-) ~~chemical and biological~~
174 production and loss in soils, coupled with soil properties facilitating gas exchange of HONO, has
175 led to intense interest and debate around discerning the fundamental controls on its surface-
176 atmosphere exchange (R4, R5) (Barney & Finlayson-Pitts, 2000; Huang et al., 2002; Kamboures
177 et al., 2008; Meusel et al., 2018; Mushinski et al., 2019; Purchase et al., 2023; Song et al., 2023;
178 Sörgel et al., 2015; Wang et al., 2021). The same is true for direct emissions of NO_2 from soils,

where evidence remains limited and the uncertainty is high (Huber et al., 2024; Zörner et al., 2016). ~~Only a handful of field studies have directly measured soil NO_2 measurements, making it challenging to infer how much NO_2 might be emitted from soils.~~For example, Gong et al. (2025) estimate that fertilizer-induced soil NO_x emissions contribute 0.84–2.20 Tg N yr^{-1} globally, with uncertainty~~ies~~ partly due to ~~the~~ a lack of NO_2 measurements. Their modelling ~~indicates that~~ suggests this ~~underrepresentation likely leads to~~ underestimat~~esion of~~ summertime ozone enhancements ~~(~~by 0.3–3.3 ppbv ~~)~~ in agricultural hotspot regions, and has been ~~which has been~~ implemented further in other atmospheric models (Ha et al., 2023; Tian et al., 2024)~~.~~. This N_r exchange ~~is intricately linked to~~ in agricultural ~~practices, as~~ regions from excessive nitrogen inputs ~~(e.g., fertilizers)~~ are prime targets for chamber methodologies, as they amplify emissions of all N_r species~~, namely NO_x, N_2O, HONO, and NH_3 from the impacted soils~~ (Degaspari et al., 2020; Huber et al., 2020; Manco et al., 2025). These issues highlight the need for more direct soil NO_2 and HONO measurements, as well as simultaneous constraints on the entire N_r suite being exchanged from soils.

Automated dynamic chambers deployed in situ for field observations and performing controlled experiments would provide a platform for capturing the magnitude, direction, and temporal variability of N_r species or physical variables via the headspace gas or soil amendments while retaining soils in an intact state (Aneja et al., 2006). Thus, establishing an accessible dynamic chamber method for N_r flux measurements is desirable. However, such a platform needs to undergo extensive validation to reduce flux bias from challenging N_r species such as NH_3. This important and necessary first step will allow a wider global study of surface-atmosphere N_r exchange processes. One of the best existing examples to date of automated dynamic chamber design for N_r measurements, is the custom-built system from Pape et al. (2009) who measured NO, NO_2, and O_3 to deploy an unattended array of six samplers with destructive gas analyzers. In their system, a reference chamber was used to characterize system surface effects, while using a large volume flow through the headspace during chamber closure periods to quantify fluxes on the assumption that ambient levels were not dramatically changing (e.g. due to nearby point sources). This work synthesized many advantages from similar designs to study soil- and plant-atmosphere interactions, but the technique remains accessible only to researchers with in-house engineering design and fabrication facilities. In the intervening years, dynamic chambers for GHG fluxes have become widely commercialized to improve measurement capacity compared to static chamber

determinations and to make flux observations more accessible compared to conducting eddy covariance measurements.

Here, we bridge several gaps to link the atmospheric GHG and N_r flux communities to yield a dynamic flux system for CO_2, CH_4, N_2O, NO, NO_2, HONO, and NH_3. First, we modify commercial dynamic chambers with large volume (72 L) and footprint (0.21 m^2) originally designed for trace GHG flux measurements to make them suitable for quantifying the most prevalent N_r gas exchange fluxes at surface-atmosphere interfaces, meaning the apparatus is more widely available to the atmospheric community. ~~First~~Next, we implement surface and hardware modifications to adapt the commercial chambers to minimize gas adsorption and transformations, so that more reactive gases such as HONO and NH_3 can be added to the N_r flux analyte suite. We systematically characterized the transfer of both GHGs and N_r species by calculating fill and empty rates, transformed to time constants, to identify any surface interactions and/or transformations on the chamber surfaces. We then applied our modified commercial dynamic chambers to make flux measurements by equipping them with destructive gas analyzers for HONO and NO_x and a cavity ring-down spectrometer (Picarro G2509) for NH_3, N_2O, CO_2, and CH_4 in lab experiments, or with a fully automated dual-chamber approach under field conditions through a pilot study with 30 minute closures to obtain a sufficient number of measurements to detect relevant fluxes with standard gas analyzers. Fluxes during the pilot study were assessed by rate of change determinations during closure periods and bias minimize~~dation~~ through a mass balance ~~approach during the pilot study~~ to ~~in a real agricultural field is~~ demonstrate~~d~~ system capabilities for several N_r gases in an agricultural field. This community-accessible approach addresses key needs ~~in~~ by allowing more researchers to measure N_r exchange at the surface-atmosphere interface, with the ~~capacity~~ added benefit over past systems to monitor fluxes of all species simultaneously with at least hourly time resolution when using gas analyzers with one-minute measurement frequencies.

2. Materials and methods

2.1 Dynamic Chambers for Field Fluxes

2.1.1 Description of ~~the~~ custom-modified dual-dynamic chambers ~~system for~~ fluxes ~~measurement~~

The dynamic chamber system ~~is composed of~~uses two identical commercially available ~~chambers~~ units (eosAC-LT Eosense, Dartmouth, NS). These are modified and coupled to programmable valves that control ~~the delivery of~~ sample gases delivered to a suite of instrumentation (Figure 1**)** ~~to perform reactive gas flux measurements~~.

The dynamic chambers are~~,~~ constructed ~~out of~~ with transparent polyacrylate walls and lids, ~~have~~ with an internal volume of 0.072 m^3 (72 L) and ~~can enclose a~~bottom surface area of 0.21 m^2. When used on soils ~~surfaces,~~ the chambers are secured with ~~embedded soil~~ collars ~~using~~ and custom-made polytetrafluorethylene (PTFE) rings (Figure S1) ~~and can be similarly affixed to impervious surfaces~~. A built-in fan ensures uniform distribution of gases inside the chamber. A~~mbient a~~ir temperature is measured inside ~~the chamber~~ from the fan arm, ~~whereas~~ pressure ~~sensors are~~ is ~~embedded in~~ from the control box outside the chamber, ~~. Each chamber has~~ and two auxiliary ports, one internal~~ly~~ and ~~the other~~ external~~ly~~, ~~capable of collecting measurements of~~ can collect environmental properties such as relative humidity (RH), photosynthetically active radiation (PAR), soil temperature, and/or soil volumetric water content (VWC).

For a N_r sampling approach, one ~~of the two~~ chamber~~s~~ is used as the measurement (MC) ~~to enclose~~ from an experimental surface while the second ~~chamber acts as~~ is a reference (RC) ~~by being~~ sealed at the bottom with a 51 µm (0.002") film of ~~0.002"~~ perfluoroalkoxy alkane (PFA; McMasterr-Carr®, PN: 84955K24). The inert PFA film is held in place between the chamber collar and our custom-made PTFE rings (Figure S1). ~~This modification provides~~The RC acts as a negative control ~~observation~~ for physical interactions ~~on apparatus surfaces~~ and/or associated chemistry ~~when sampling~~of reactive gases on chamber and gas transfer line surfaces. The use of the RC, therefore, is to facilitate the correction of surface-mediated effects, reactions, and reduction of bias when determining quantitative flux values.

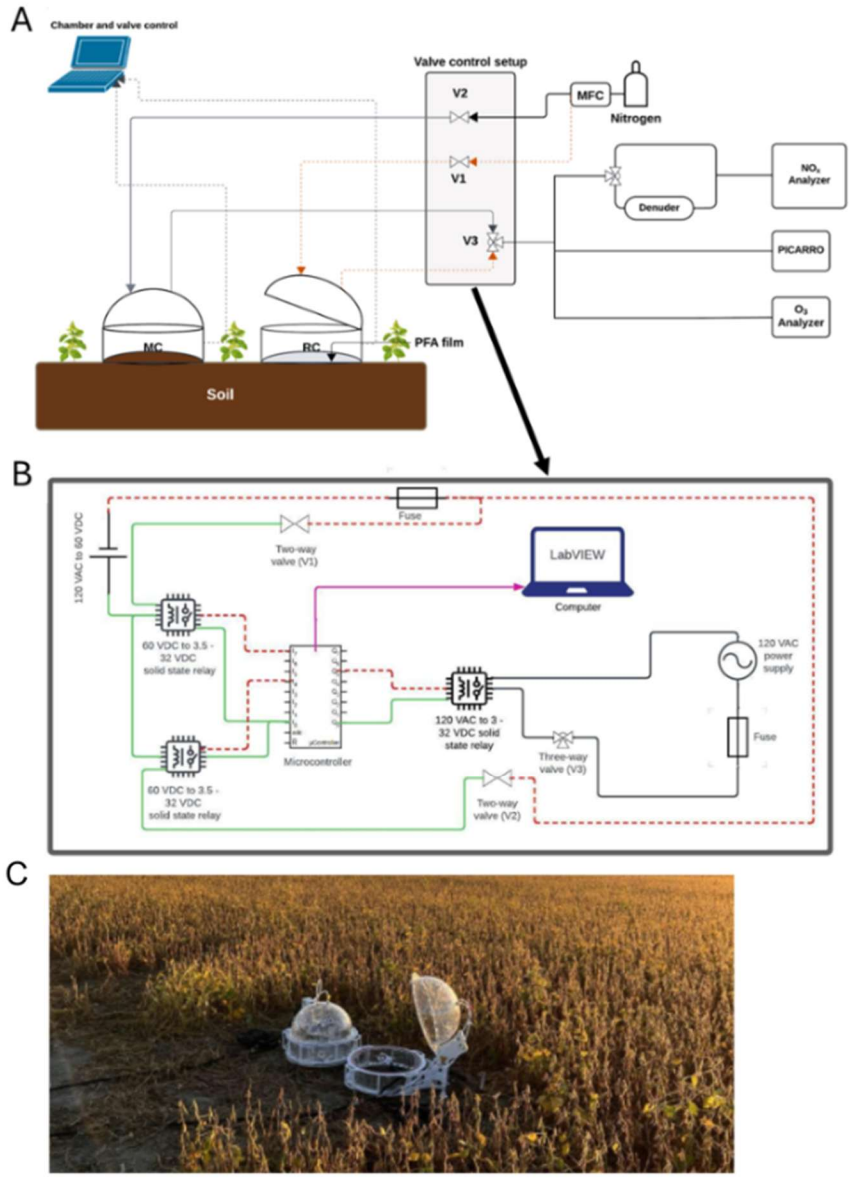

Figure 1. (**A)** Schematic of the dynamic chamber system to measure N_r and GHG fluxes. The components of the system include: the chambers, a dilution gas source (nitrogen (N_2) or zero air (ZA)), solenoid valve control, gas transfer lines, and gas analyzers. Grey lines indicate dilution gas flow from a source (e.g. cylinder) to the measurement chamber (MC) and air sampled from the MC to the analyzers. The dashed orange line represents these same flows relative to the reference chamber (RC). Communication lines from the chambers to a computer for automated control and ancillary sensor data collection using the chamber software (eoslink-AC; blue dotted lines). (**B**) The valve control setup for flow control in the complete dynamic chamber system, illustrating electrical components and lines needed for full automation using LabVIEW. It includes two 24 V DC two-way valves (V1 and V2; red dashed lines for negative electric potential, green for positive), with power supplied by solid-state relays, and a three-way 120 V AC valve (V3; black lines) with a power supply and another solid-state relay. The purple arrow represents the USB data acquisition connection from the microcontroller to a computer running the LabVIEW VI for valve

control. (**C**) Field deployment of the dynamic chamber system, where the closed chamber is the reference and the open chamber functions as the measurement chamber.

~~Reactive gases require continuous correction for surface interactions and/or transformations as ambient levels are dynamic, so t~~The RC component of this system is designed to continuously baseline~~s~~ the physical interactions and chemistry happening on its surfaces both before and after quantifying reactive gas fluxes with the MC. Thus, the measurements are taken every 30 minutes, where one chamber is closed for gas analysis while the other is open to the ambient atmosphere. The sampling time interval was determined based on i) obtaining enough measurements at 1-minute time resolution to perform a reliable accumulation or loss linear regression, and ii) an ability to readily detect the lower limit of the range of field HONO flux values reported in the literature to ensure detection in its application during our pilot field study (see Section 2.7~~6~~). For the first criterion, this also includes an exclusion of the first and last few measurements (3 to 5) to allow for complete gas replacement between the chamber lines and the analyzers, and disruption of the sealed environment as the chamber cycle alternates, respectively. The resulting accumulated mixing ratios of HONO in the chamber are well above the 1.4 parts per billion (ppbv) mixing ratio detection limit (LOD) of even a modified NO_x analyzer, such that it can be used for measuring HONO (Crilley et al., 2023; Lao et al., 2020; Zhou et al., 2018; Nodeh-Farahani et al., 2021).

Headspace recirculation to facilitate analyte mixing ratio ~~enhancements~~ accumulation or depletion for non-destructive spectroscopic GHG analysis is a common measurement approach to decrease flux observation times. Reactive nitrogen measurements, in contrast, are typically destructive techniques that change the identity of the target analyte in the act of quantifying its abundance. To interface with such instruments, the sampled air needs to be replaced (Linde Canada Plc, PN: NI LC250-230) to balance the flow demand in a closed chamber. This balance is delicate even when using mass flow controllers (MFCs) on both incoming and outgoing flows, and the best solution we identified is to provide a slight overflow that takes advantage of the chamber design to vent excess pressure through a short length (~15 cm) of 1/8" ID (3.175 mm), ¼" OD (6.35 mm) tubing that keeps the internal pressure equivalent to ambient. The flow differential between make-up gas and sampling is roughly 400 $cm^3\ min^{-1}$. Such a supply of make-up gas was explored across a range of potential flow rates when using destructive gas analyzers (e.g., three instruments each sampling at 1 - 4 standard litres per minute, L min^{-1}) to find that 6 L min^{-1} is the upper limit of flow-through

where the chamber pressure is not substantially perturbed from ambient and the chamber lid retains its seal.

In the field, a flux measurement cycle begins with closing the RC while the MC is open. At defined intervals, they alternate their open-closed states. Flows of make-up gas to each chamber are modulated with a pair of two-way solenoid valves. When sampling from the RC, one valve (V1; Figure 1) is open to permit make-up gas flow while the other valve (V2) is closed to prevent the flow from being directed to the MC. On the sampling lines, a three-way solenoid valve (V3) alternates to guide flow from whichever is closed to the suite of gas analyzers. ~~In this work, the gas instrumentation included a modified NO_x chemiluminescent analyzer (NO, NO_2, and HONO), a greenhouse gas and ammonia cavity ringdown spectrometer (H_2O, CO_2, CH_4, N_2O, NH_3), and a UV-absorption ozone (O_3) analyzer.~~ All instrument and operational details are provided in Section 2.1.3.

2.1.2 Automated controls: system, data collection and processing

The chamber eosLink-AC software (Eosense Inc., Dartmouth, NS) is used to define the duration of chamber opening and closing cycles, and logs chamber temperature, pressure, and auxiliary sensor data associated with a given eosAC-LT chamber. Each chamber requires a 12 V DC power supply connected by USB to a laptop through a weatherproof communication cable, controlling the chamber lid and data transfer.

When a chamber cycle begins, a text file is generated and includes measurement time elapsed, chamber lid status, chamber temperature and pressure, and auxiliary sensor data. This data file is updated at least once every 10 seconds, varying between 2-8 second intervals, which we average onto a 1-minute time base to match measurements from the slowest gas analyzers. The solenoid valves are modulated by the electrical circuit shown in Figure 1B. Automation is facilitated by a microcontroller (NI-6509i, National Instruments) programmed with a custom-scripted LabVIEW VI (LabVIEW version 2020). ~~The VI controls valve states (i.e., for V1, V2, and V3) and synchronization of the valve switching with respect to each chamber opening and closing cycle as described in the previous section. The VI also generates its own text file containing valve open/close state and a timestamp to be used for data processing. A custom R script (R Studio v3.0.1) was developed to process the data file generated by eoslink-AC, data from all reactive gas~~

~~analyzers, and the VI.~~ Further design information and full details of this sampling strategy and script can be found in Section S1 of the supporting information, and is available on the GitHub repository alongside our VI (https://github.com/fjs-vdblab/fluxchamber.git).

2.1.3 Reactive and greenhouse gas instrumentation for flux measurements

The mixing ratios of NO and NO_2 were measured using a commercially available chemiluminescent NO_x analyzer (EC 9841, American Ecotech, Warren, RI). The calculated LOD determined from sampling dry zero air was 0.84 ppbv, 0.67 ppbv and 1.07 ppbv for NO, NO_x, and NO_2 (or HONO when using the denuder as described below), respectively. The instrument has an operating range of 0 – 20 parts-per-million by volume (ppmv), a sample flow rate of 0.5 L min^{-1}, and reports measurements at a time resolution of 1 minute. To quantify NO_2, it is reduced to NO on a heated molybdenum catalyst (325 °C). To prevent interferences reported by others from atmospherically-relevant acidic species in this system (e.g. HONO, HNO_3, and N_2O_5) the sampled air from the chambers during field experiments was passed through a sodium carbonate (Na_2CO_3) coated annular denuder to reduce bias in the NO_2 measurement, as these species and other components of NO_y (e.g. peroxyacetyl nitrate; PAN) may also be reduced to NO (Villena et al., 2012). The Na_2CO_3 denuder was prepared according to the EPA Compendium Method IO-4.2 (Winberry Jr et al, EPA, 1999) to remove atmospheric acids by reactive uptake to the basic coating. As part of our controlled laboratory and pilot field study experiments, this denuder was also used to selectively measure HONO by scrubbing this target gas for a specified period, but would include the other known interferences. If this term is depositing, it could include the other NO_y detected by the same conversion mechanism, but if emitting we expect it to be dominated by HONO. Ideally, a platform like time-of-flight chemical ioniszation mass spectrometry (ToF-CIMS) would be used for disambiguation but was not available at this time.

A commercial O_3 analyzer (Serinus 10, American Ecotech, Warren, RI) was used to measure mixing ratios, quantify O_3 loss to surfaces, and constrain the reaction of O_3 with NO to form NO_2 in the pilot study sampling. This analyzer employs a non-dispersive UV absorption cell to quantify O_3 in the sampled air. The calculated LOD from sampling zero air is 0.95 ppbv at 1 minute time

resolution, with an operating range of 0 to 20 ppmv and a sampling flow rate of 0.5 L min^{-1}. Quality control procedures for the NO_x and O_3 instruments can be found in Section S2.

The mixing ratios of ~~greenhouse gases (~~the GHGs~~)~~ N_2O, CH_4, CO_2, H_2O, and ~~ammonia (~~NH_3~~)~~ sampled from the automated chamber system were measured using a Picarro G2509 which uses cavity ring down spectroscopy (CRDS) ~~to simultaneously measure nitrous oxide (N_2O), methane (CH_4), carbon dioxide (CO_2), and NH_3 at ppbv levels, as well as water (H_2O) vapor at ppmv~~. The analyzer has a time response of ~ 8 seconds for N_2O, CH_4, CO_2, H_2O and < 2 min for NH_3. The Picarro G2509 ~~instrument~~ was used for ~~measurements during both~~ the lab experiments and the pilot field study ~~campaign~~. The customized version of the instrument ~~had a sampling flow rate of~~ sampled at ~0.23 L min^{-1}~~,~~ and was equipped with an inlet filter. To minimize adsorption and chemical interactions of NH_3 on instrument surfaces, stainless steel gas handling components, including the inlet bulkhead, were replaced with PFA counterparts. The instrument cavity material was treated with a SilcoNert® coating by the manufacturer. We did not observe changes in its performance for the measured gases when operated according to the manufacturer guidelines. The Picarro G2509 analyzer ~~utilizes cavity ringdown~~ spectroscop~~ic~~y ~~to quantify the~~ mixing ratio ~~of the target analytes, and~~ determination means a full span calibration is not a regular necessity~~ary to be performed regularly~~. Despite this, we validated its calibration and performed quality control checks in ~~our~~ the lab~~oratory~~ to ensure the accuracy and stability of the analyzer for all aspects of this work ~~presented below~~ (Section S2).

2.2 Chamber modifications to minimize NO_2 reactions on chamber surfaces

To transfer reactive gases through these chambers, interactions with surfaces need to be limited at all points of potential adsorptive or reactive losses. The custom-made base plate~~, consisting of two rings made from PTFE sheets with a PFA film pinned between them~~ (Figure S1) was used to assess gas interactions on the commercial chamber surfaces ~~and acts as the RC for field measurements~~. ~~From this starting point, commercial components were~~ and identification ~~ed for~~ of parts for replacement. First, the gas inlet and outlet push-to-connect fittings in the original ~~chamber~~ configuration have plastic grips, with an internal component made of brass, which is informally known in the atmospheric chemistry community to have strong interactions with nitrogen oxides.

These ~~brass fittings~~ were replaced with PTFE Swagelok® bulkhead fittings (PN: T-400-1-4~~) as shown in~~; Figure S2). ~~Similarly~~Second, the polyacrylate wall and lid surfaces of the chambers ~~were considered, which are, by design, actinically transparent to ensure PAR is transferred to any contained plants or surfaces. To retain this visible radiation transparency, while also making the surface more inert, we applied~~had the 51 µm (0.002") ~~thin~~ PFA film applied to the inner surfaces using double-sided tape to retain actinic transparency and PAR transfer to contained plants and surfaces (Figure S2).

2.3 Chamber modification validation using greenhouse and reactive gases

~~The design of the chambers by the manufacturer is to transfer GHGs to non-destructive gas analyzers by recirculating the headspace.~~ Before and after our modifications, we had to ensure that the non-reactive GHG transfers ~~were still transferred through the system~~was unchanged. ~~I~~in addition~~, we~~ to challenge~~d~~ tests for the transfer of N_r gases ~~by controlled gas delivery~~. It was expected that N_r gases ~~could undergo~~ would interact~~ions~~ and/or ~~chemical transformations~~react on ~~the~~ chamber surfaces and 15 m of standard sampling tubing that would differ between the unmodified and modified variants. Determining the time constants of fill (E1, E2) and decay (E3, E4) of these interactive and/or reactive gases in the chamber system allowed us to contrast their behaviour against that expected from a modelled theoretical inert trace gas in our system (Figure 2). Equations used to model mass transfer in our chambers were derived from Pape et al. (2009). The resulting accumulation curve was modelled by the theoretical function:

$$\mu_{fill}(t) = 1 - e^{-\left(\frac{t}{\tau_{fill}}\right)} \quad \textbf{(E1)}$$

$$\tau_{fill} = V/Q_{fill} \quad \textbf{(E2)}$$

Where μ_{fill} represents the normalized mixing ratio of the gas in the chamber at the time t (min) after closing of the chamber compared to the maximum mixing ratio within the measurement cycle, τ_{fill} is theoretical accumulation timescale for transfer of an ideal inert gas (min), V is the volume of the chamber (0.072 m^3), and Q_{fill} represents the total experimental flow rate (2 L min^{-1}). Similarly, the theoretical decay curve when emptying the chamber can be obtained, where τ_{emp} is the theoretical decay timescale for gas transfer (min) and Q_{emp} is again the total experimental flow rate (2 L min^{-1}).

$$\mu_{emp}(t) = e^{\left(-\frac{t}{\tau_{emp}}\right)} \quad \textbf{(E3)}$$

$$\tau_{emp} = \frac{V}{Q_{emp}} \quad \textbf{(E4)}$$

2.3.1 Instrumentation and materials for control experiments

Control experiments for the transmission of ~~inert~~ GHG and ~~reactive~~ N_r gases were conducted by filling and emptying the chambers with known quantities ~~of the target gases~~ at mixing ratios relevant to the atmosphere, as well as ~~in~~ quantities ~~that would~~ expected to accumulate during real observations of modest emission fluxes (e.g. from a fertilized farm field). ~~Measurement of NO, NO_2 and HONO was performed using the modified NO_x analyzer, the GHGs (CO_2, CH_4 and N_2O) and NH_3 with the Picarro G2509, and O_3 with the UV-absorption instrument.~~ All assessments herein matched: the standard configuration of the chambers with all fittings, 15 m of ¼" O.D. PFA gas transfer tubing, flow rates, valves and gas transfer lines to instrumentation, with line/fitting/valve/instrumentation surfaces included. Details of the generation of gas concentrations can be found in Section S3 of the SI.

2.3.2 Filling and emptying experiments with N_r, O_3, and GHGs

The positive control experiments filled the chambers in both modified and unmodified configurations~~, where the~~ and time constants were calculated from the measurements ~~to compare against a theoretical inert and perfectly transferred gas (i.e. lost by dilution and removal to analyzers only)~~. In each filling experiment, the chamber was flushed with pure N_2 from a liquid N_2 dewar (Linde Canada, PN: NI LC250-20) until a stable baseline level of each gas mixing ratio was reached; typically, these were values at the analyzer detection limits. Then, a blend of GHGs or one of the N_r analytes was delivered into the chamber ~~along~~ with N_2 ~~as the~~ dilution flow at a total flow rate of 2 L min^{-1}, ~~and this~~ which was then sampled at ~~a total of~~ 1.8 L min^{-1} by the analyzers (Figure S4). The gases were added to the chamber from their respective calibration sources until the observed concentration (C) reached the known value being delivered (C_0), within error. Since different mixing ratios of the gases were added for these control experiments, the use of normalized concentrations was necessary to facilitate data analysis and visualization. Where surface interactions could be identified (e.g. for NH_3), the role of surfaces versus air exchange w~~h~~as ~~been~~ explored using double exponential fits (see ES-1 and ES-2 in Section S3) (Crilley et al., 2023; Ellis et al., 2010; Moravek et al., 2019). The gases were emptied back to the initial

baseline level ~~observed with clean dilution gas~~ before starting the next replicate or a new ~~filling~~ experiment with a different target gas. Time constants for filling and emptying were ~~then~~ determined by fitting the ~~experimental~~ observations in Igor Pro8 (Wavemetrics, Portland, OR, US).

Similarly, the Eosense eosMX multiplexer is designed to coordinate chamber flux measurements using eosAC chambers with non-destructive analyzers, such that headspace can be recirculated while the chambers are closed. One of these devices was also characterized ~~for the transmission of GHGs and N_r gases, alongside~~ following similar modifications. This system is appealing as it has the eosLink-MX software (Eosense, V1.9.07), which is used for communication, scheduling actions, and logging peripheral data from all connected eosAC chambers. It features dedicated chamber tubing inlets and outlets, along with a COMM port supporting up to 12 eosAC chambers. Each chamber channel includes two Swagelok gas fittings for transporting gases to analyzers and for either recirculating, or in the case of N_r measurements, supplying a ~~purging~~ clean dilution gas to the chamber headspace.

To optimize the performance for N_r species, the original stainless-steel (SS) Swagelok fittings and solenoid valves were compared against replacement PFA tube fittings, bulkhead unions (Swagelok, PFA-420-61), and a PTFE 3-way valve (Clippard, NR1-2-12-G2). A 2 L min^{-1} flow of dry zero air containing the target compounds was passed through either the SS valve with SS fittings or the PTFE valve with PFA fittings for 30 minutes each. The flow was measured before and after the valves to ensure the setup was free of leaks. The ratio of the transferred gas amount to the nominal was used to identify impacts of surface interactions on quantitative transmission to downstream gas analyzers. Further details are presented in Sections 2.7 and S4.

2.4~~.~~ Characterization of NO_2 and O_3 loss on chamber surfaces

All losses of NO_2 in the chamber were characterized by the addition of known NO_2 mixing ratios (5-10 ppbv) to the chamber under ~~a variety of~~ relevant relative humidity (RH) conditions (45-85% RH; Figure S5; Section S5). The mixing ratios of NO_2 and RH values selected for these experiments are representative of the ambient atmosphere in urban areas (Toronto North Station, ECCC), where the chamber system was envisioned to be deployed. –The experiments were performed progressively and in triplicate with 5 ppbv of NO_2 and 85% RH, starting from the unmodified configuration of the chamber, replacement of fittings, and covering the inner surface

with PFA film to quantify their efficacy in minimizing NO_2 loss and/or transformation on chamber surfaces. These were followed by varying NO_2 mixing ratios and RH to characterize the modified system.

~~Different RH values were produced inside the flux chamber by combining flows of dry zero air (ZA) and one saturated with water vapour by transiting a 500 mL Pyrex impinger filled with deionized water (e.g. equal 1 L min^{-1} flows combine to an RH of 50%). A high-precision, research-grade humidity probe (HMP60, Vaisala Oyj, Finland; ± 3% at 0 – 90% RH, ± 5% at 90 – 100% RH) was connected to the chamber to confirm the set point by measurement in the chamber. The flow from an NO_2 calibration cylinder (Linde Canada; PN: NI NX5MC-AQ; 5.9 (±5%) ppm) was adjusted using an MFC and combined with a dilution flow of ZA to achieve mixing ratios of 5, 7 and 10 ppbv. The total flow rate for these experiments was 2.0 L min^{-1} and a vacuum pump (62.3 L min^{-1}, PN: UZ-07061-22, Gast Manufacturing Inc., Benton Harbor, MI, USA) with an MFC (10 L min^{-1}, PN: 1179C01314CR1BV, MKS instruments Inc, Andover, MA, US) was used to make up the sampling flow beyond the 0.5 L min^{-1} of the NO_x analyzer. The same flow difference stated above was maintained in the chamber, using the built-in vent.~~

Quantification of NO_2 and HONO in the air sampled from the chamber can be achieved using the alternating solenoid setup depicted in Figure S5. The sampled air is switched between two channels – one directly to the NO_x analyzer and the other through a Na_2CO_3-coated denuder – modulated every 5 minutes by a three-way solenoid valve (Fluoroware Galtek 1/4" F-NPT 3-way solenoid valve, 115V, PN: 203-3414-415. Entegris Inc., MN, US). When the sampled air flows directly to the analyzer, the total mixing ratio of NO_2 and acidic NO_y species, like HONO and HNO_3, is measured and has been termed NO_2^* (Crilley et al., 2023; Lao et al., 2020; Zhou et al., 2019). When the flow is directed through a Na_2CO_3 denuder, it selectively scrubs HONO and HNO_3, leaving behind NO_2 (Possanzini et al., 1983). Under the controlled NO_2 composition used in our experiments, it is expected that HONO will be the only acid present in the sampled air, as such experimental systems have been thoroughly characterized by Finlayson-Pitts et al. (2003),~~,~~ and HNO_3 is retained on the surfaces (R3) (Barney & Finlayson-Pitts, 2000; Huang et al., 2002; Kamboures et al., 2008). As a result, by the differential measurement of mixing ratios recorded in the two channels (E5) every 5 minutes, HONO can be quantified.

$$HONO = NO_2^* - NO_2 \quad \textbf{(E5)}$$

To quantify the amount of NO_2 lost to the chamber surface relative to the mixing ratio of NO_2 added to the chamber during an experiment, the NO_2 loss fraction (f_{NO2}) ~~is~~ was found to be informative for mass balance between the two processes. ~~Comparison of each chamber modification on f_{NO2} helps identify which changes are essential in minimizing losses. Experiments using 5 ppbv of NO_2 at 85% RH added to the chamber were used to quantify f_{NO2} in the unmodified configuration (n=3), to derive an upper limit of irreversible loss to surfaces or chemical loss via surface hydrolysis (R3). Following the materials characterization experiments, additions of atmospherically relevant 5, 7 and 10 ppbv mixing ratios of NO_2 at three different RH values (45%, 65% and 85%) to the fully modified chamber were used to characterize and develop a correction methodology for the surface loss. The mixing ratios of NO_2 and RH values selected for these experiments are representative of the ambient atmosphere in urban areas (Toronto North Station, ECCC), where the chamber system was envisioned to be deployed.~~

~~2.5 Drivers of O_3 loss to chamber surfaces~~

Similarly, ~~W~~we tested ~~how~~ the modifications and aging of the ~~interior~~ installed PFA ~~chamber~~ film surfaces ~~affected~~ on O_3 transfer. It is among the most sensitive/reactive species to transfer through this new system and is expected to drive reactive loss of NO when measuring N_r fluxes. The fraction of O_3 lost to chamber surfaces was ~~first~~ quantified from 150-250 ppbv using a clean and unmodified chamber with PTFE bulkhead fittings replacing the push-to-connect brass fittings (Section S5). ~~Prior to O_3 addition, the chamber was flushed with ZA until the background level of O_3 was at the instrument detection limits. Three mixing ratios of O_3 of 150, 200 and 250 ppb generated by a GasCal 1100 dilution calibrator with integrated O_3 generator and photometer (American Ecotech, Warren, RI) and added to the chamber for 60 mins or until a constant concentration was reached. Two replicate runs of each addition level were performed.~~

The fraction of O_3 lost to chamber surfaces was then quantified in duplicate on a modified chamber with the interior chamber surfaces covered by brand new ~~0.002" thick~~ PFA film ~~in a separate set of experiments. The same mixing ratios of O_3 were delivered in duplicate to the modified chamber operated for lab and field experiments, so that the PFA film had been attached to the inner surface of the chamber and~~ or one exposed to ambient air for more than two years, with 15 days of continuous use in an agricultural field during our pilot study. ~~In all three experiments, the lost fraction of O_3 was determined for each mixing ratio delivered.~~

2.56 Proof of concept N_r fluxes from agricultural soils

2.56.1 Soil sample N_r emissions for lab experiments

Randomized soil samples weighing 4-5 kg were collected into Ziploc®k bags from an eight-plot grid established for at an agricultural field site in Lambton County, ON, Canada (43°09'36.0" N 81°55'48.0" W). The samples were used to investigate emissions in the lab with and without the addition of fertilizers. Individual and pooled samples from the field plots were used. Bulk soil samples were prepared for lab-based chamber measurements by removing debris, roots and seeds, followed by oven drying at 35 °C for 24-72 hours on a stainless-steel mesh tray covered with aluminum foil, to prevent alteration of the microbial community from exposure to unrealistic temperature regimes. After drying, samples were stored in Ziploc® bags at room temperature until use.

Ultrapure water (18 MΩ·cm; Milli-Q®, Sigma-Aldrich, St, Louis, US) was added to approximately 350 g of a dry soil sample to achieve ~28% volumetric water content (VWC). The soil sample was loaded into the chamber on a foil-lined tray, and the water content was measured using a soil moisture probe inserted fully into the sample (TEROS 11, VWC range for mineral soils: 0.00 – 0.70 m^3/m^3; accuracy: ± 0.03 m^3/m^3; resolution: 0.001 m^3/m^3, METER Group Inc., WA, USA). Zero air modified to 65% RH was delivered at 3.6 L min^{-1} to the chamber headspace where the soil was contained. The soil started the drying process from a VWC of approximately 25% with the flows held constant for around 4 days or until the VWC reached 15%. The chamber was then sealed against intrusion from room air, and dry ZA was added to the chamber during the to conduct the drying periodcycle while our . A modified NO_x analyzer measured NO, NO_2 and HONO following our usual configuration, while and the Picarro G2509 measured N_2O and NH_3 fluxes. Both instruments monitored uUnamended soil samples and others fertilized with urea ($CO(NH_2)_2$), ammonium carbonate (AC, $(NH_4)_2CO_3$), ammonium bicarbonate (ABC, NH_4HCO_3) at rates of 100 kg N ha^{-1} were assessed. A similar experiment was conducted with ammonium nitrate (NH_4NO_3) at the same fertilizer rate using only the modified NO_x analyzer. Soil VWC and headspace RH were recorded using auxiliary sensors within the chamber.

2.56.2 Field deployment of automated dynamic N_r chambers

The RC and MC setup was deployed to make automated N_r flux measurements from the same agricultural field as the lab-based soil samples described in the prior section. The observations

took place in early September 2022 at the end of a soybean cropping season. A detailed description of the campaign and its results is the subject of a separate work, so we provide a brief overview here ~~relevant to demonstrating the utility and procedure of an RC/MC chamber pair to determine fluxes from field observations~~. The total measurement period was approximately two weeks in duration to test ~~the~~ system performance ~~of the designed system~~. Generally, conditions were hot and dry, without precipitation, and the soybeans surrounding the observed soils were undergoing senescence during the measurement period. The chambers were deployed only on the soil, between crop rows, and operated to quantify fluxes as outlined in Section S7. After an initial 7-day period of observing baseline fluxes from the field, an experimental perturbation was conducted to stimulate N_r emissions through the addition of an aqueous urea solution equivalent to 22 kg N ha^{-1} of fertilizer added by broadcast application, followed by washing into the soil by an equivalen~~t~~cy of 2.5 cm (1") of rain depth. The modified NO_x analyzer and the Picarro G2509 were used to measure the N_r and GHG fluxes continuously across both periods.

2.~~7~~6 Soil flux determination

The flux of a gas is the rate at which it is ~~released and/or~~ transferred across ~~a surface or~~ an interface (e.g., soil to atmosphere) per unit area per unit time. Gas fluxes are of high interest in agriculture as they give insight into the uptake or emission of N-bearing gases that may ~~lead to~~ alter fertilizing, ~~or loss of fertilizing~~ effects~~, respectively~~. ~~Fluxes~~ They are also important for assessing the state of plants or soils at interfaces through metrics like primary productivity, in which case measurement of a GHG like CO_2 provides the insight (Anthony & Silver, 2024; Li et al., 2016; Okiti et al., 2025). The RC captures environmental fluctuations such as temperature or pressure change and directly observes the interactions of ambient gases with surfaces within the sampling setup (i.e. chambers, gas transfer lines, valves, and analyzers), as well as tracking reactions, allowing for corrections to every net flux (F_{net}) measurement cycle (E6 for reactive gases and E7 for non-reactive gases, as derived in Section S7).

$$F_{\text{net}} = (\lambda).\left(\frac{V}{A}\left(\frac{\Delta C_m}{\Delta t_m} - \frac{\Delta C_r}{\Delta t_r}\right) + \frac{Q_{\text{out}}}{A}\left(\frac{\int_{t_{1m}}^{t_{2m}} c_m(t)\ dt}{\Delta t_m} - \frac{\int_{t_{1r}}^{t_{2r}} c_r(t)\ dt}{\Delta t_r}\right) - \frac{V}{A}\left(\frac{\int_{t_{1m}}^{t_{2m}} R_m(t)\ dt}{\Delta t_m} - \frac{\int_{t_{1r}}^{t_{2r}} R_r(t)\ dt}{\Delta t_r}\right)\right) \quad \textbf{E6}$$

Where V is the volume of the chamber (m^3), A is the surface area (m^2) enclosed by the chamber and governing the gas flux; Q_{out} is the volumetric flow rate of air exiting the chamber ($m^3\ s^{-1}$; $c_m(t)$ and $c_r(t)$ are target gas concentrations within the ~~measurement~~ MC and ~~reference chamber~~ RC (mol m^{-3}), respectively; $\frac{\Delta C_m}{\Delta t_m}$ and $\frac{\Delta C_r}{\Delta t_r}$ represent their corresponding rates of change (mol $m^{-3}\ s^{-1}$); and F_{net} is the resulting net gas flux per unit area (mol $m^{-2}\ s^{-1}$).The terms R_m and R_r denote the instantaneous chemical production or loss rate expressed in units of mol $m^{-3}\ s^{-1}$ for consistency. The dimensionless attenuation factor λ is required to correct for interactions of reactive gases with surfaces. Such surface interactions, which are particularly strong for gases like NH_3, significantly reduce the measured rate of concentration change within the closed chamber (Figure 4). Thus, λ is derived as the ratio between a theoretical unattenuated gas (i.e. an inert GHG like N_2O) and the target gas concentration from controlled deliveries integrated over the chamber closure interval as derived in Section S7. This term has the surface effects from chambers, gas transfer lines, and analyzers embedded by definition and must be determined empirically for any altered configuration. The attenuation correction removes bias from surface-induced artifacts in flux estimates, so that more accurate soil–atmosphere exchange is reported.

$$F_{\text{net}} = \lambda \cdot \frac{P_{\text{air}}}{R \cdot T} \cdot \left(\frac{V}{A} \left(\frac{\Delta X_m}{\Delta t_m} - \frac{\Delta X_r}{\Delta t_r} \right) + \frac{Q_{\text{out}}}{A} \left(\frac{\int_{t_{1m}}^{t_{2m}} X_m(t)\ dt}{\Delta t_m} - \frac{\int_{t_{1r}}^{t_{2r}} X_r(t)\ dt}{\Delta t_r} \right) \right) \quad \textbf{E7}$$

For inert gases described ~~in~~ by E7**,** the fluxes can be based on mixing ratios, where X_m *and* X_r are the gas volumetric mixing ratios (mol X per mol air), P_{air} is the air pressure (Pa), T is the absolute temperature (K), and R is the universal gas constant (J $mol^{-1}\ K^{-1}$). By comparing the RC and MC observations, we isolate the effects of specific environmental conditions on N_r (E6) or GHG (E7) exchange fluxes, while accounting for surface effects and chemical transformations in the former.

3 Results

3.1 Determining time constants of reactive nitrogen and GHGs

The time constants of both filling and emptying the chambers were calculated using concentrations normalized to their initial values, for each N_r gas and GHG. These were used to quantify gas transfer times through the chambers and to confirm performance relative to theory. Where

departures were identified, we quantified the extent of surface interactions for the various target analytes so corrections for determining in situ fluxes could be implemented (Table 1, Figure 2).

3.1.1 Time constants of greenhouse gases (GHGs)

Determination of the GHG time constants allows benchmarking of the chamber performance prior to and after modifications~~, which then allows us to contrast the behaviour of transferred reactive gases through the chambers~~. In both ~~the modified and unmodified chambers,~~configurations the greenhouse gases CO_2, CH_4 and N_2O were anticipated to behave as non-reactive trace gases with little to no physical interactions on chamber surfaces, nor to undergo chemical transformations.

The theoretical fill and empty rates for the chambers with a flow rate of 2 L min^{-1} are 36 min. The average measured time constants of filling w~~ith the greenhouse gases~~for CH_4, CO_2, and N_2O in the unmodified chamber were ~~found to be~~ 37 ± 1 min, 37 ± 2 min, and 37 ± 1 min, respectively (Table 1). During ~~the~~ emptying ~~phase~~, they ~~average time constants for CH_4, CO_2, and N_2O~~ were 37 ± 1 min, 37 ± 1 min, and 38 ± 2 min, respectively. These measurements are not different from theory within the limits of experimental accuracy~~, demonstrating that GHGs do not deviate from the values modelled for an ideal trace gas~~ (Figure 2). ~~In either experiment, the time constants did not change in the presence of the chamber modifications.~~ Since the GHGs are effectively transferred through both the modified and unmodified configurations of the chamber, the baseline performance of the chambers was not affected by the hardware modifications. Therefore, comparison of these results with the time constants of N_r gases provides a description of their interaction or transformation processes on the modified chamber surfaces.

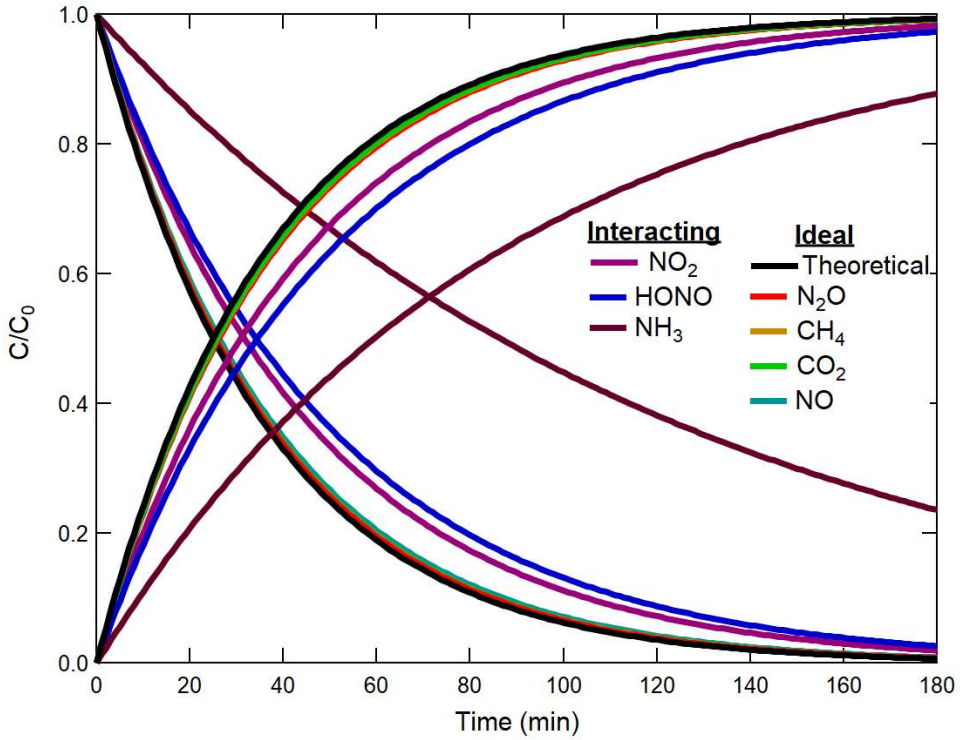

Figure 2. Addition of reactive nitrogen gases and greenhouse gases to a modified dynamic chamber. For clarity, the coloured traces show the fitting curves corresponding to the response time in concentration normalized to the delivered value of each gas while filling and emptying the chamber. The black trace corresponds to a perfect non-reactive transfer of an ideal trace gas based on volume transfer in the chamber only. Note that the N_2O, CH_4, CO_2 and NO fill and empty traces all overlap with the theoretical fill and empty curves.

3.1.2 Time constants of reactive nitrogen gases

In the modified chamber, the time constant of filling or emptying with NO was 38 ± 1 min. The obtained NO time constants are similar to GHGs, as NO is not expected to have strong surface interactions. The slower time response of the NO_2, HONO, and NH_3 measurements is determined by two processes: (1) the exchange of the sample air volume in the ~~inlet~~ gas transfer lines and the chamber, and (2) the adsorption and desorption of the gas onto and from their ~~chamber~~ surfaces (Whitehead et al., 2008). Increases in the extent of surface interactions ~~were observed for~~ followed the increasing~~ly~~ polarity, reactivity, and/or ionizability of gases in the order of NO_2, then HONO, and most for NH_3 (Figure 2). ~~The highest change in the time constants between the modified and unmodified configurations was 2.6 ± 2.5 min, observed for HONO, with smaller improvements~~

~~observed for NO_2 and NH_3 during the filling process. Improved time constants when emptying reactive nitrogen from the chambers had similar trends (Table 1).~~

~~Overall, the deviations for these gases to longer time constants than those expected from an inert molecule can be attributed to their polar, ionizable, and/or reactive nature.~~ For example, NO_2 is lost more readily than NO, possibly through its known reaction on surfaces to make HONO and HNO_3, being lost itself in the process (Finlayson-Pitts et al., 2003). It also has higher water solubility than NO, but lower than for HONO or NH_3. Similarly, a decrease in transmission efficiency for HONO could be explained by its weakly acidic nature (pKa = 3.16) (Silva et al., 2006) and solubility in water (Henry's law constant = 0.48 mol/m^3 Pa; (Schwartz & White, 1981) that facilitate partitioning and dissociation in surface water films, which could generate non-volatile nitrite (NO_2^-) on chamber surfaces. This chemistry will slow the transfer of gas-phase HONO through the chambers, as the NO_2^- would need to protonate before being lost as neutral HONO when repartitioning to the gas phase (R4, R5). Finally, the most delayed transmission rate is for NH_3, likely because it undergoes strong inter-molecule interactions and ionization on the chamber surfaces and/or any interfacial water (Henry's law constant = 5.9x10^{-1} mol/m^3 Pa (Orkin et al., 2011); pKa = 9.25 (Lide, 2009), as well as on tubing surfaces and potentially partitioning into the tubing before reaching the analyzer (Pagonis et al., 2017). The best improvement in the time constants between the modified and unmodified configurations was 2.6 ± 2.5 min for HONO, with smaller improvements observed for NO_2 and NH_3 during the filling process. Improved time constants when emptying reactive nitrogen from the chambers had similar trends (Table 1). As a result, increasing delays from NO through NH_3 exist in our N_r gas suite due to increasingly stronger interactions with chamber surfaces and gas handling lines.

The determined surface ~~impact~~ interaction values (D; Table 1; ES-2, Section S3) demonstrate an expected greater impact of surfaces when no reactive gas is present in the headspace prior to filling, and a lesser effect during emptying ~~when~~ as the exposed surface has ~~been exposed and~~ equilibrated with the analyte, which is commonly referred to as passivation. ~~As a result, increasing delays from NO through NH_3 exist in our N_r gas suite due to increasingly stronger interactions with chamber surfaces and gas handling lines.~~ For NH_3 specifically, the fill has a D value of 89%, while during emptying it is only 23%~~. This is due to all sample handling surfaces not being passivated prior to filling~~, similar to our findings with NH_3 transfer for other N_r instruments (Crilley et al., 2023). ~~In~~

~~contrast, during the emptying process, desorption occurs over previously exposed surfaces ending at the instrument, reducing the extent of surface effects.~~ The surface interactions for these gases are minimized in the modified chambers to facilitate more time-efficient measurements of surface exchange. However, they necessitate the use of the λ term when deployed in the measurement-reference configuration for those N_r species which experience partial transmission, such as NH_3. The λ term is required to obtain accurate values, as the enclosed flux measurement surface should be perturbed for the least amount of time possible when making field measurements, and the chambers cannot be closed for several hours to allow surface-active gases to passivate the lines. One potential option to improve the system performance further for NH_3 could be to heat the gas transfer lines between the chambers and gas analyzers. In addition, minimizing the potential for transformations reduces the frequency required for in-field characterization of these processes through positive and negative gas delivery controls. For NO_2, specifically, we sought to quantify this as a function of modifying components of our chambers, as NO_2 is the most reactive gas in our suite (Section S5).

Table 1. Summary of time responses of addition and removal of GHGs and N_r gases to and from a chamber at 2 L min^{-1} in unmodified and modified configurations. Time responses here correspond to a theoretical fill or empty e-folding time response of 36 minutes. Where analytes were observed to undergo surface interactions, a double exponential fit was used to characterize them, with the first time constant representing the known gas exchange rate being fixed at 36 minutes, as this was observed for the non-reactive gases, and the second time constant is reported (*) alongside an assessment of the relative magnitude of surface interactions, through the D-value (%) (Crilley et al., 2023; Ellis et al., 2010; Moravek et al., 2019). Variability shown is one standard deviation of the mean from replicate experiments (n=3).

Gas species	Direction	Unmodified (min)	Modified (min)	Improvement (min)	D (%)
NO	Fill	38.8 ± 0.7	37.8 ± 0.6	1.0 ± 0.7	-
	Empty	37.9 ± 1.5	36.0 ± 0.6	1.9 ± 2.1	-
NO_2	Fill*	18.9 ± 0.6	18.0 ± 3.1	0.9 ± 3.2	94 ± 18
	Empty*	21.2 ± 1.2	20.4 ± 1.4	0.8 ± 1.9	78 ± 21
HONO	Fill*	21.9 ± 1.1	19.3 ± 1.2	2.6 ± 1.6	74 ± 10
	Empty*	23.2 ± 1.4	21.2 ± 0.9	2.0 ± 1.7	71 ± 9

NH_3	Fill*	69.6 ± 0.4	68.2 ± 0.5	1.4 ± 0.6	89 ± 3
	Empty*	76.9 ± 0.8	75.0 ± 4.6	1.9 ± 4.7	23 ± 4
CO_2	Fill	37.9 ± 1.5	37.0 ± 1.8	0.9 ± 2.3	-
	Empty	38.0 ± 1.8	37.0 ± 1.2	1.0 ± 2.2	-
CH_4	Fill	37.9 ± 1.1	36.8± 1.2	1.1 ± 1.6	-
	Empty	39.1± 1.7	37.2 ± 1.2	1.9 ± 2.1	-
N_2O	Fill	38.6 ± 2.1	36.7 ± 1.2	1.9 ± 2.4	-
	Empty	39.7 ± 1.3	37.7 ± 1.6	2.0 ± 2.1	-

3.2 Multiplexer modification impacts on gas transfer

The multiplexer (eosMX; Eosense Inc.) allows ~~us to~~ operation of~~e~~ up to twelve dynamic chambers simultaneously with a suite of gas analyzers ~~such as the Picarro G2509, NO_x, and O_3 analyzers~~. However, t~~he commercial multiplexer~~it is constructed with stainless steel (SS) valves and fittings that would be expected to facilitate strong interactions and/or losses of target gases in the N_r analyte suite. Valves and fittings made of SS have a higher tendency to chemically interact and/or adsorb reactive gases compared to fluoropolymer replacements. To address this uncertainty, the gas transfer efficiency as a percentage loss in the multiplexer versus a bypass line was evaluated specifically for NH_3 and NO_2, alongside standard GHGs as they passed through fittings and gas handling solenoid valves made of SS or PFA and PTFE replacement parts.

The loss fractions were modest and measurable when ~~connected to the analyzers~~ using minimal lengths of PFA tubing (~50 cm) instead of the standard 15 m gas transfer lines. The most substantial loss ~~of gases~~ was observed on SS, as expected ~~in which the highest reactivity and/or adsorption were expected~~ due to its known tendenciesy ~~to interact with reactive gases~~ (Vaittinen et al., 2014). When the GHGs were delivered ~~after dry zero air into the SS setup~~ for 30 minutes, typical of a chamber closure period in the field, their losses ranged from 10% for N_2O to 19% for H_2O. Meanwhile, NO_2 exhibited 17% loss on the SS surfaces, and the greatest effect was seen for NH_3 with a loss of 38% (Figure S6). In contrast, losses on the chemically inert and hydrophobic surface of the PFA fittings and PTFE valve were negligible (<1%) for most gases, except for NH_3, which still exhibited a measurable loss of 11%. Other reports have also shown up to 15% loss of

NH_3 at atmospheric pressure on PTFE and PFA surfaces (Ellis et al., 2010; Shah et al., 2006; Vaittinen et al., 2014). While it is expected that the SS would eventually passivate and improve the transmission of the GHGs in a standard recirculation approach, this is not likely to be the case for destructively analyzed N_r and even more so if it facilitates a chemical transformation. Overall, we found that replacing the multiplexer SS valves and fittings with PFA fittings and PTFE valves provided a 9–27% reduction in surface losses of N_r compounds and GHGs. We strongly recommend the use of PTFE and/or PFA materials over SS for more accurate measurement of N_r species when interfacing the dual chamber setup with the destructive N_r analyzers needed for field flux measurements, whether using a custom setup o~~f~~r the commercially available multiplexer.

3.3 Minimizing NO_2 losses and determining controlling variables

In addition to the rate of transfer of N_r gases, chamber modifications are necessary to prevent reactive losses. ~~The lost fraction of NO_2 (f_{NO2}) to chamber surfaces was quantified by the addition of known mixing ratios of calibration gas to the chamber in both the unmodified and modified configurations under atmospherically relevant humidities.~~ These experiments enabled us to determine the magnitude of NO_2 lost to the chamber and gas transfer tubing surfaces due to chemical and/or physical transformations, as well as demonstrate the effectiveness of the different chamber modifications in minimizing these losses. For NO_2, a probable chemical transformation pathway is its heterogeneous conversion to HONO (R3), which is favourable under atmospherically relevant humidities, and the resulting water-adsorbed surfaces expected to exist throughout the chamber and sampling lines.

3.3.1. Chamber modification impacts on NO_2 losses

~~The average fractional loss (f_{NO2}) for an unmodified chamber and one modified with the PFA film and PTFE bulkhead fittings was measured under conditions of 83% RH and 5 ppb of NO_2~~. Substantial reduction in NO_2 loss fraction (f_{NO2}) and transformation was observed from the implemented PFA and PTFE modifications under conditions of 83% RH and 5 ppb of NO_2. In the original unmodified configuration of the chamber, f_{NO2} was 0.36 ± 0.02 (Figure S7)~~. When the interior chamber surfaces were covered with a film of PFA, it~~ which was reduced to 0.22 ± 0.03

with the PFA film, a relative decrease of 18%. This is consistent with the acrylic chamber surfaces and fasteners to the chamber frame, facilitating physical and/or chemical loss of NO_2.

The film of PFA, along with other fluoropolymers, is known to have excellent chemical resistance and low reactivity towards a range of chemicals, including NO_2 (Ebnesajjad, 2005; Graham et al., 1997). In addition, the superhydrophobic nature of these materials prevents the accumulation of water on the surfaces, which is known to facilitate atmospheric surface reactions of NO_2 (Finlayson-Pitts et al., 2002; Jenkin et al., 1988; Stutz et al., 2002) and create analytical bias in the measurement of trace gases like HONO, especially when instrument gas sampling inlets do not take this into account (Crilley et al., 2019; Von Der Heyden et al., 2022).

The replacement of the brass-lined push-to-connect bulkhead fittings with PTFE led to a similar decrease in f_{NO2}, which was reduced by 17% to a final value of less than 0.05 ± 0.02 (Figure S7). These fitting surfaces act as the largest surface-driven NO_2 loss despite their surface area being very small compared to that of the entire chamber configuration and with a very small contact time against the gas sample (0.012 s per fitting at a flow rate of 2 L min^{-1}).

The loss of NO_2 in the commercially available system is challenging to attribute solely to the heterogeneous hydrolysis reaction. During the characterization experiments, the conditions inside the chamber were matched to those reported by previous lab studies, which have shown that high RH, presence of NO_2, and surface adsorbed water on surfaces favour this loss mechanism (Jenkin et al., 1988; Stutz et al., 2004). The reaction is known to occur on surfaces such as Pyrex (Jenkin et al., 1988) and borosilicate glass (Finlayson-Pitts et al., 2002), but no prior studies to date, nor this study, have demonstrated metallic surfaces as facilitating this mechanism.

~~Overall, chamber modifications were effective in minimizing NO_2 losses.~~ The inert PTFE fittings dramatically minimized transformations, while PFA film lining the inner chamber surfaces was also effective, but less so. Our results indicate that water-adsorbed and metallic surfaces, such as brass, facilitate substantial loss and/or transformations of NO_2. Further investigation is required to confirm the mechanism(s) at play and is beyond the scope of this work.

3.3.2. RH-facilitated NO_2 loss as a function of concentration

A complete characterization of f_{NO2} and the amount of HONO in the fully modified chamber was determined under a range of environmentally relevant RHs and NO_2 concentrations. We found that the absolute and fractional NO_2 losses were highest under the highest RH conditions (85%; Table 2). However, the f_{NO2} does not appear to follow a concentration-dependent trend across the additions made at lower RHs, with at most 0.4 ppbv NO_2 lost across the remainder of the tests, a value which is equivalent to the LOD of the NO_x analyzer used. This would generate 0.2 ppbv of HONO according to the disproportionation of the hydrolysis mechanism, which is well below the analyzer detection limits. ~~Overall, t~~The modifications successfully reduced NO_2 losses below 10% across all environmentally relevant conditions the chambers are expected to encounter, with our findings here suggesting that the mass lost is nearly constant and independent of NO_2 mixing ratio at RHs below 85%, while being marginally higher at and above this value.

Quantifying f_{NO2} and the amount of HONO made in the chamber is required for the correction of field datasets. ~~Quantifying NO_2 loss to the chamber surfaces allows us to prevent bias when reporting NO_2 exchange processes on environmental surfaces, as the magnitude of the losses attributed to chamber surfaces versus the surface studied can be corrected.~~ The dual chamber system, via the ~~reference chamber~~RC, can also quantify any changes in these processes over time if standard ~~concentration~~ additions to the headspace are conducted. Consequently, important parameters such as NO_2 deposition fluxes on surfaces can be better estimated (Pape et al., 2009).

Since the inferred HONO mixing ratios from the chamber surfaces across various environmental RHs are nearly invariant at 0.2 ± 0.1 ppbv, it is simple to background correct any observational datasets by subtracting this amount from the total HONO measured in the chamber. ~~if a more sensitive analyzer is used during field or lab experiments.~~ In addition, as the NO_2 values expected in most atmospheric gas samples during field measurements are well into the ppbv range (>3.3 ppbv per 30-minute flux measurement for a ~~1.4~~0.08 ~~μn~~g N m^{-2} ~~min~~hr^{-1} emission), the corrections would be easy to implement in post-processing of datasets and have minimal impact on the technical aspects of the analytical determinations.

Table 2. Characterization of NO_2 lost in the modified chamber under environmentally relevant ranges of NO_2 and RH. The loss fraction (f_{NO2}) and HONO produced in the chamber were quantified ~~at each of three NO_2 mixing ratios (5, 7, 10 ppbv) delivered at varying relative humidities (RH) to the fully modified chamber~~. Variability (±) provided is one standard deviation of the mean from replicate experiments (n=3).

RH (%)	NO_2 added (ppbv)	NO_2 lost (ppbv)	f_{NO2}	HONO produced (ppbv)
85	5	0.50 ± 0.01	0.1 ± 0.02	
85	7	0.70 ± 0.04	0.1 ± 0.02	
85	10	0.50 ± 0.07	0.05 ± 0.01	
65	5	0.30 ± 0.10	0.06 ± 0.02	
65	7	0.40 ± 0.09	0.06 ± 0.02	<1.1[a]
65	10	0.30 ± 0.08	0.03 ± 0.01	
45	5	0.30 ± 0.05	0.05 ± 0.01	
45	7	0.40 ± 0.04	0.06 ± 0.00	
45	10	0.30 ± 0.08	0.03 ± 0.01	

[a] – below instrument detection limit of 1.1 ppbv determined as S/N=3 while sampling zero air

It should be noted that the amount of HONO in the chamber was below the LOD of the NO_x analyzer for HONO (1.~~07~~1 ppbv), meaning that the upper limit of HONO inferred may perhaps, in fact, be negligible. Therefore, future experiments that wish to detect small N_r fluxes accurately will need to focus on reproducing these experiments with a higher performance instrument, such as a time-of-flight chemical ionization mass spectrometer (ToF-MS) or long-path absorption photometer (LOPAP), which have lower detection limits (Crilley et al., 2019; Lee et al., 2014; Neuman et al., 2016; Reed et al., 2016).

3.~~2~~3.3 ~~Characterization~~ Loss of O_3 ~~loss in the chamber modified~~ with and without ~~PFA~~ fluoropolymer modifications

Ozone loss was observed in both modified and unmodified chamber configurations, with 18% lost to clean 15 m PFA lines alone when transferring 30 ppbv. The unmodified chambers lost 45% across ~~all~~ delivered mixing ratios spanning (150-250 ppbv~~.), which are higher than those typically expected in ambient air~~. This was reduced to 35% when the fluoropolymer modifications were implemented ~~with new clean PTFE fittings and PFA film~~. When the PFA film was aged by 15 days of ambient sampling and 2 years of exposure to lab air, the losses were substantially exacerbated, reaching 80%. Such outcomes are expected and can be attributed to several factors discussed in detail in Section S5, primarily involving surface reactions with built-up films of

deposited organics, adsorption, and material interactions (Burkholder et al., 2015,) Ebnesajjad, 2017, George et al., 2015, Plake et al., 2015). We recommend regular replacement of the PFA film as part of the N_r system maintenance, coupled with quality control procedures to characterize material performance for target gases.

Ozone is known to undergo heterogeneous surface reactions, particularly on materials like glass, metals, or polymers (Plake et al., 2015). These surfaces often contain reactive sites such as hydroxyl groups or adsorbed water molecules that can catalyze the decomposition of O_3 into molecular oxygen (O_2) and other byproducts (George et al., 2015). Adsorption of O_3 on chamber surfaces is another potential pathway for loss. When O_3 molecules interact with surfaces, they may undergo a reaction if the materials are not inert. The use of PFA here was intended to benefit the transfer of O_3, yet despite its high chemical inertness, low reactivity, and resistance to the uptake of many chemicals from gas samples, the subsequent O_3-driven surface reactions are still substantial (Ebnesajjad, 2017). This is likely because, over time, reactive substances from sampled air accumulated through adsorption on the PFA film and/or its defect sites, thereby reducing its effectiveness. The same issue is well-known for PFA tubing used in standard air quality monitoring and is a common maintenance need for O_3 analyzer inlets. Further, physical wear or surface aging might alter the material surface through product formation or exposure of new reaction sites, which makes it less resistant to further reaction with O_3, and therefore increases the rate of loss over time. This is the case in our aged PFA film results, which emphasizes the importance of regular replacement of the film as part of the N_r system maintenance and that quality control procedures characterizing the chamber material performance with respect to O_3 will provide the highest accuracy of experimental results.

3.3 Proof-of-concept reactive nitrogen fluxes using soil samples in the lab

Proof-of-concept flux measurements were performed using the modified dynamic chamber system to demonstrate that emissions of N_r gases from agricultural soil samples can be measured under controlled conditions, similar to many prior reports using custom-built soil chambers (Almand-Hunter et al., 2015; Pape et al., 2009; Tang et al., 2019, 2020).

3.3.1. Fluxes of NO, NO_2, and HONO from agricultural soil samples

Emission fluxes were measured from two pooled and two individual soil samples collected from a single agricultural field (Table 3; Section S6). The average and integrated fluxes of N_2O, NH_3, NO, NO_2, and HONO were assessed under controlled, environmentally realistic (65 % RH), drying conditions ~~of zero air modified to be 65% RH delivered at 3.6 L min^{-1} to the chamber headspace where the soil was contained. The soil started the drying process from a VWC of approximately 25% with the flows held constant for around 4 days or until the VWC reached 15%~~ (Table 3).

As the soils dried, NO and NO_2 emissions increased, with NO fluxes highest across all replicates and reaching up to 2.50 µg N m^{-2} hr^{-1}. This trend is consistent with the prior work of other researchers, showing peak NO emission potentials when VWC drops below 25% during soil drying, which is when microbial nitrification and denitrification processes are suggested to become more active (Bao et al., 2022; Oswald et al., 2013). The soil VWC at which these maxima occur can vary depending on soil type, texture, and ~~the~~ microbial diversity therein (Ludwig et al., 2001; Schindlbacher et al., 2009). ~~The p~~Plot-level replicates from our field had a higher integrated NO flux (i.e., > 2600 µg N m^{-2}), compared to the pooled replicates (<1000 µg N m^{-2}), likely indicating real differences in preserved microbial hotspots, intact plot-level soil aggregates, true spatial variability, and plot-specific N availability (Table 3). Soil texture and aggregate size, for example, play an important role in building the porous structure of soil, which has implications for the release of gases (Mangalassery et al., 2013). Soil aggregates, therefore, govern the release of gaseous N_r analytes like NO based on the aerobic or anaerobic state of the soil. Here, our low level of soil manipulation (i.e. not ground, no sieving) will drive some of the variability by preserving these features, which exist across and within real soil systems (Lipiec et al., 2007). Individual plot samples also retain plot-specific microbial communities when working with intact soil, whereas soil grinding can temporarily inhibit microbial activity. While we tried to minimize soil handling and processing extremes in these experiments, a measure of homogeneity was also pursued, and fully intact soil cores were not assessed.

Integrated NO_2 fluxes showed the same trend, with more sample-to-sample variability as one pooled replicate (R2) produced over three times the emissions of R1, despite both experiments being conducted across identical moisture content ranges (Table 3). Given the limited studies directly measuring NO_2, such as Purchase et al. (2023), this variability is difficult to interpret and

highlights the need for more assessments of its production pathways and controls, which our developed chambers show promise for.

The observed average HONO fluxes remained low across all of the samples, ranging from 0.05 to 0.25 μg N m^{-2} hr^{-1} (Table 3). These values are lower by ~~up to~~ more than an order of magnitude compared to those reported in other controlled laboratory studies, where HONO fluxes ~~were around~~ exceed 900 ~~n~~μg N m^{-2} ~~s~~hr^{-1} (Oswald et al., 2013; Su et al., 2011; Wang et al., 2021). These discrepancies are concerning, given recent emphasis from the scientific community on the atmospheric impacts of soil-derived HONO on air quality. Here, the results from our agricultural soil samples may reflect the differences in our methodology, such as the soil handling and preparation steps prior to and during experiments. Many prior reports prepare their samples in ways that strongly deviate from real-world conditions (e.g. initial soil drying temperatures above those occurring under ambient conditions, extreme storage conditions, grinding, sieving, use of dry zero air to flush chambers, etc.). Further drivers of variability within the category of heavily altered soil samples from the literature include pH, NO_2^- availability, and NH_4^+ or NO_3^- content, all of which are known to influence biotic and abiotic HONO formation pathways (Wu et al., 2019).

Our HONO fluxes from the agricultural soil samples studied here are consistent with field observations under ambient conditions, where average emissions have been reported to largely remain below ~~2 ng N m^{-2} s^{-1} or~~ 7.2 μg N m^{-2} hr^{-1} (Tang et al., 2019; Xue et al., 2024). This does suggest that greater care in sample preparation, and likely also a widely agreed-upon standard procedure, is needed to study soil HONO emissions relevant to atmospheric models.

The integrated HONO fluxes for the pooled replicates yielded 185 μg N m^{-2} and 146 μg N m^{-2}, respectively. From the individual sample replicates, which were slightly wetter than the pooled, the integrated HONO fluxes were 690 and 739 μg N m^{-2}, which was unexpected because the overall moisture regime accessed by the pooled soil experiments was not lower than those from the plot samples. The drier soils would have been expected to yield greater integrated HONO emissions (Oswald et al., 2013), yet this was not the case. Additional replicates and experimental controls, while beyond the scope of this study, would allow further attribution of the controls over the observed HONO variability.

Table 3. Average and integrated fluxes of NO, NO_2, and HONO (in μg N m^{-2} hr^{-1} and μg N m^{-2}, respectively) from agricultural soil samples across two soil VWC ranges. Both the average and integrated fluxes were calculated over a constant period within the noted range of soil VWC. Values are reported as mean ± standard error.

Soil sample	Soil VWC Range (%)	Duration (hr)	Avg Flux (μg N m^{-2} hr^{-1})			Integrated flux (μg N m^{-2})		
			NO	NO_2	HONO	NO	NO_2	HONO
Pooled R1	16-22	125	1.0 ± 0.04	0.05 ± 0.02	0.06 ± 0.02	2400 ± 120	160 ± 50	190 ± 50
Pooled R2	16-22	125	1.0 ± 0.04	0.20 ± 0.02	0.05 ± 0.01	2500 ± 130	500 ± 60	150 ± 40
Plot R1	22-27	65	1.2 ± 0.05	0.40 ± 0.03	0.20 ± 0.02	3400 ± 150	1300 ± 90	690 ± 70
Plot R2	22-27	65	1.0 ± 0.03	0.50 ± 0.04	0.30 ± 0.02	2600 ± 100	1600 ± 100	740 ± 50

These findings demonstrate the utility of the modified custom-built dynamic chambers for accurately capturing N_r fluxes under controlled laboratory settings, but they also highlight the need for more such systems to be implemented across the scientific community to better consider both biogeochemical soil properties and environmental context when interpreting the impacts of N_r fluxes obtained in the lab and scaling them to real soils. There seems to be potential for skewing the atmospheric impacts as a result, in particular for HONO, as the standard approaches have been designed to replicate NO fluxes (Behrendt et al., 2014). Most global models do not consider the effect of soil HONO on air quality through O_3 production and oxidation chemistry ~~(Ha et al., 2023)~~. Several modelling studies like Ha et al. (2023) and Tian et al. (2024) have incorporated the order of magnitude or higher HONO fluxes reported from lab studies, like those by Su et al. (2011), Wang et al. (2021), Oswald et al. (2013), and Meusel et al. (2018). They estimated significant HONO production with maximum flux potentials of 830 μg N m^{-2} hr^{-1}, 95 μg N m^{-2} hr^{-1}, 70 μg N m^{-2} hr^{-1}, 55 μg N m^{-2} hr^{-1}, respectively. In contrast, the field observations that do exist suggest that real HONO fluxes are much smaller at 2-17.5 μg N m^{-2} hr^{-1} (Song et al., 2023; Tang et al., 2019). Similarly, Wu et al. (2022) has used the regional WRF-Chem model to explore the impact of soil HONO emissions on the concentrations of atmospheric HONO, OH, and O_3.

Agricultural soil HONO emissions have been suggested to significantly contribute to OH radical production, accounting for approximately 10% to 60% of total OH formation in rural areas before noon (Oswald et al., 2013; Su et al., 2011), which often exceed the contributions from ozone photolysis. Additionally, high HONO emissions from agricultural soils have been reported to increase local O_3 concentrations by ~0.5 - 1.0 ppb in low-NO_x rural environments where VOCs are not limiting (Zhang et al., 2021), with even greater impacts observed during fertilization periods (Wu et al., 2022). Modelling studies, using GEOS-Chem and CMAQ, for example, claim that incorporating soil HONO emissions improves the agreement between observed and simulated O_3 levels, particularly during the morning (Zhang et al., 2021).

Only a few studies have conducted estimates of soil NO_x emissions under reasonable conditions, like Bao et al. (2022) and Wu et al. (2022), where the researchers tried to mimic field conditions. Even in such an area that has been long studied, large uncertainty still exists around soil sources of NO_x, particularly for agricultural activities where uncertainty is still at least ±30% due to limitations in lab characterizations and field experiments (Gong et al., 2025). It is not surprising,

then, that a similar issue exists for the very recent work on HONO soil emissions. The NO_x uncertainty range results from intricate soil biogeochemical processes and varies with crop types, soil texture, fertilizer types and application rate (Gong et al., 2025). This longstanding and established difficulty in predicting soil NO_x for use in global chemical models means that doing so for HONO without careful ground truthing of real-world emissions could lead to substantial inflation of the impacts on atmospheric chemistry and air quality. Care should be taken in using HONO emissions from lab studies in global models, as it seems they pose a risk of overestimating their atmospheric impacts until a more representative experimental design can be obtained with chamber systems like the one used here.

3.3.2 Fluxes of ~~NH_3, N_2O, NO, NO_2, and HONO~~N_r from fertilized agricultural soil samples

Agricultural soils amended with chemical fertilizers are expected to be hotspots for NH_3, N_2O, HONO, and NO_x emissions. Here, we demonstrate the use of our developed chambers to measure these analytes under controlled lab conditions using our lightly processed pooled soil samples and four fertilizers: urea, ammonium nitrate (AN), ammonium bicarbonate (ABC), and ammonium carbonate (AC) with the temperature maintained at 23 °C, VWC between 25–29%, and headspace RH held at 65% for three days, simulating realistic atmospheric and environmental N_r flux exchange conditions following farm field fertilization (Figure 3). In all experiments conducted with the Picarro G2509, the mixing ratio of N_2O began to rise approximately four hours after the experiment started. In the example shown for urea, it peaked at 0.79 ppm after 12 hours, which was followed by a gradual decline (Figure 3a). This pattern likely reflects the incubation period of nitrifying and denitrifying bacteria that leads to the subsequent release of gases like HONO, as depicted in Wang et al. (2021), and N_2O in Liu et al. (2022). In contrast, the mixing ratio of NO remained relatively constant throughout the three days (Figure 3b), with NO_2 increasing as the N_2O emissions decreased, while NO was emitted constantly throughout (Figure 3c). In this example experiment, no measurable emissions of HONO were detected despite the substantial presence of urea and evidence of active microbial nitrification and denitrification from the other emitted gases (Figure 3d). Lastly, the urea application example in Figure 3e shows the expected significant NH_3 emissions, with the integrated amount reaching 22% of the applied N over the

three-day incubation period. These findings are consistent with our existing knowledge that NH_3 volatilization as an N loss mechanism dominates early N_r losses from fertilizers.

Volatilization of NH_3 is well-characterized as a major pathway for N loss from fertilizers (Behera et al., 2013; Govoni Brondi et al., 2024; Liu et al., 2020; Moravek et al., 2019; Pan et al., 2016, 2022; Paulot et al., 2014). Besides agronomic concerns due to N loss and reduced fertilizer efficiency related to NH_3 emissions from fertilized soil (Anas et al., 2020), it is a key precursor to secondary inorganic aerosols in the atmosphere with impacts on respiratory and ecosystem health, visibility, and climate (Dennis et al., 2010; Edwards et al., 2024; Fowler et al., 2013; González Ortiz et al., 2020; Jang et al., 2025; Seinfeld and Pandis, 2006).

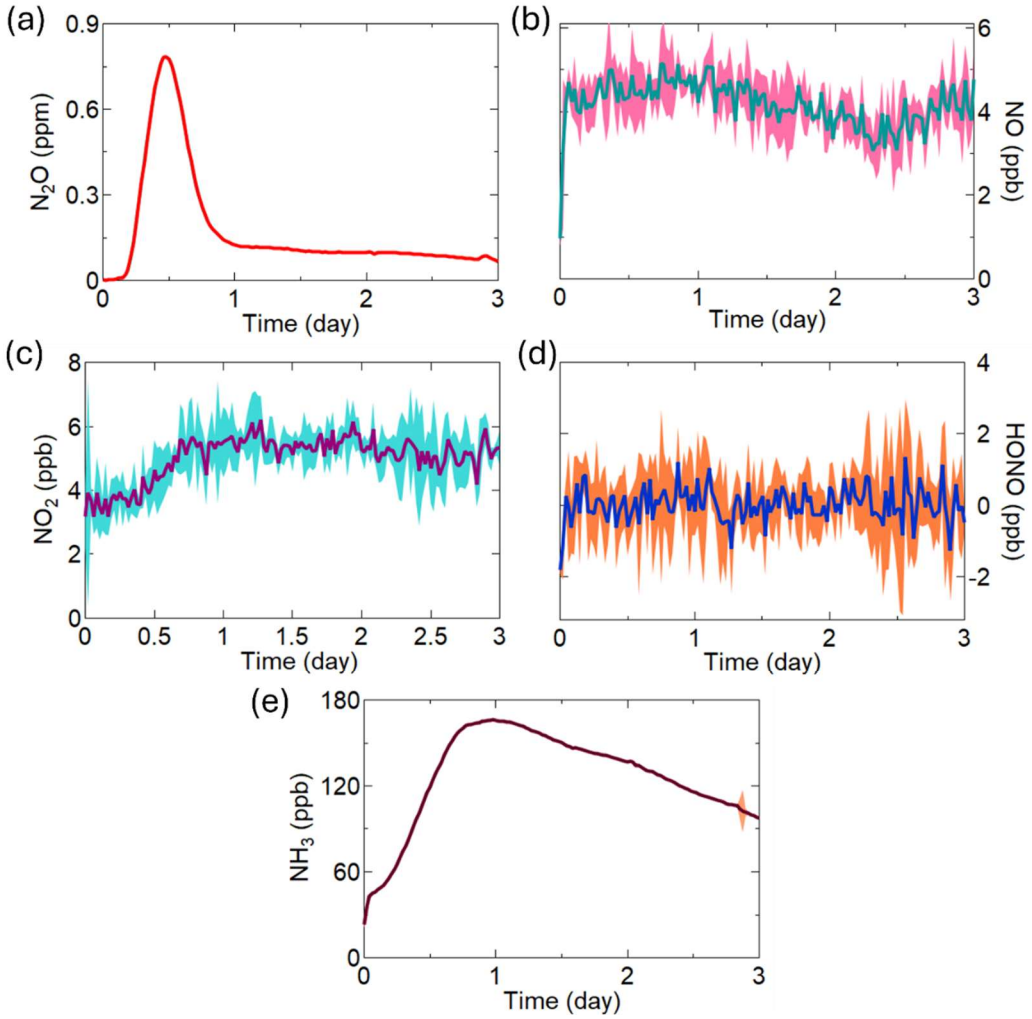

Figure 3. Soil emissions of the comprehensive suite gases from soil treated with urea, including (a) N_2O; (b) NO; (c) NO_2; (d) HONO; and (e) NH_3. The NO, NO_2 and HONO emissions were measured at 1-minute resolution and averaged to 30 min. The standard deviation (±2σ) around these averages is shaded with a lighter version of the main trace colour. Similarly, the 2-second

resolution of N_2O and NH_3 measurements were also averaged to 30-minute intervals with ±1σ provided in shading.

Emissions of NH_3 and N_2O were observed to be far greater in terms of integrated amounts from the fertilized samples (Figure 4). Integrated flux for NH_3 produced by soil treated with ABC accounted for 77% of total N_r flux (i.e., 85 900 μg N m^{-2}), followed by AC, which was 63 700 μg N m^{-2}. This is not surprising, since the use of chemical fertilizers increases the concentration of NH_4^+ in the soil that can deprotonate to emit neutral NH_3 and, in the presence of ammonia-oxidizing microorganisms, increases the production of N_2O (Luo et al., 2025). Nitrous oxide released from the addition of urea accounted for the highest integrated flux of 32 400 μg N m^{-2} observed, representing 89% of total N_r released, followed by 25 300 μg N m^{-2} and 9 600 μg N m^{-2} for ABC and AC, respectively. One way that has been proposed to reduce these large N_2O emissions from inorganic fertilizers is to change the application form to organic fertilizer, as the NH_4^+ in soil is ~~released~~ produced more slowly (Luo et al., 2025). Due to a limited duration of access to the G2509 to conduct this work, we were unable to measure the N_2O and NH_3 emitted from unamended soils or those treated with AN. Regardless, based on the obtained data, the values found here are similar to those observed under real environmental conditions (Figure 4). For our sample without N amendment, the integrated flux of NO was the largest (2 400 μg N m^{-2}; 87% of total NO_y), followed by comparable levels of NO_2 (160 μg N m^{-2}) and HONO (190 μg N m^{-2}). The fluxes of NO_x and HONO were below 1 μg N m^{-2} hr^{-1} for all the nutrient addition treatments, suggesting a similar trend as those observed under field conditions and from our lab results with unamended soils (Figure 4, Table S1, Section S6). The exact mechanism behind the HONO release, being due to nitrification and/or denitrification, cannot be definitively assigned based on flux data alone, and many ~~abiotic~~ factors ~~like soil moisture, temperature, and presence of specific microbial communities~~ drive these emissions. There are discrepancies still observed between HONO flux measured from the treated soil samples in the laboratory and similar measurements in literature (Oswald et al., 2013; Su et al., 2011), some of which report fluxes of up to ~3 600 μg N m^{-2} hr^{-1} and are likely overestimating the soil N_r fluxes found in the real world. In contrast, our results are in close agreement with the field-based measurements of Tang et al. (2020), which also used a dynamic chamber flux method.

These in-lab experiments show that simultaneous speciated N_r emissions towards mass balance analysis in a controlled environment can be conducted using a single chamber and potentially applied to an array of chambers, as others have done for a subset of gaseous N_r (Scharko et al., 2015; Tang et al., 2019). With ~~even~~ the limited replicates we ~~did~~ explored here, our results raise a question for researchers who have been using lab studies as a standard to predict and incorporate HONO soil emission values in particular~~,~~ into regional and global models.

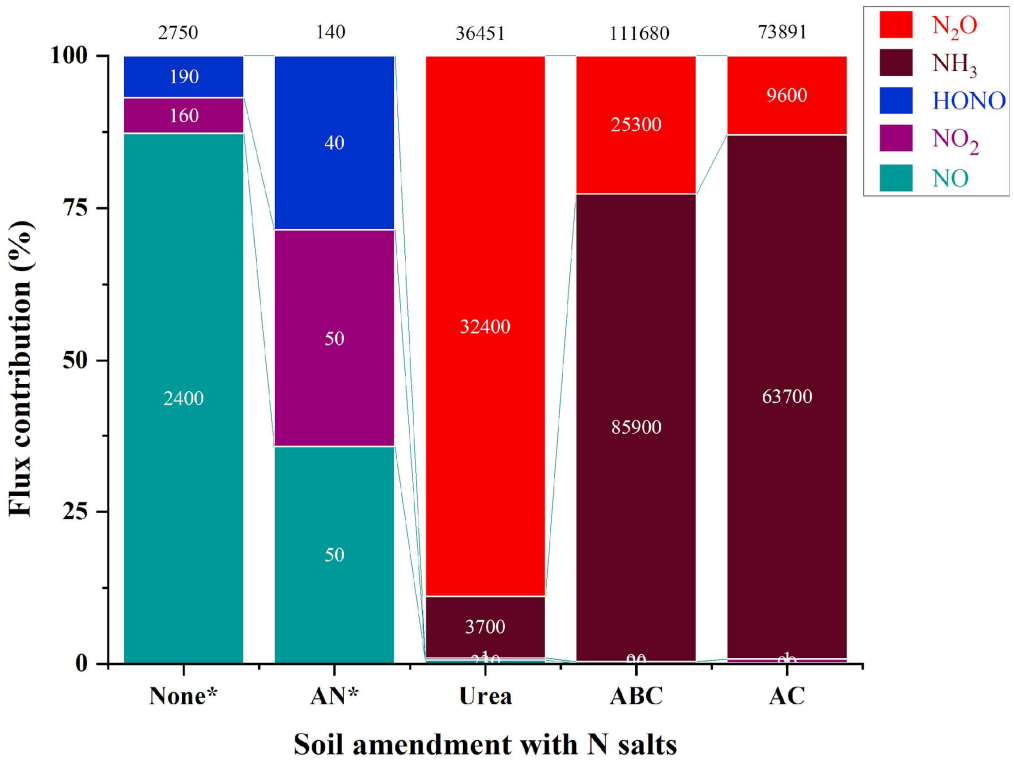

Figure 4. Relative flux contribution of soil treated with four different nitrogen-containing fertilizer salts. Each segment shows the proportion of integrated flux of NO (cyan), NO_2 (purple), HONO (blue), NH_3 (brown) and N_2O (red), with discrete flux values presented in white text, and the total flux provided in black text above the column (μg N m^{-2}). Some samples (denoted by *) were only characterized for fluxes of NO, NO_2 and HONO using the modified NO_x analyzer, as the duration of our access to the G2509 for NH_3 and N_2O measurements was limited.

3.3.3 Dual chamber field deployment for automated continuous dynamic fluxes

A pilot scale field campaign was carried out to demonstrate the application of our dual soil flux chambers in capturing N_r gas exchange processes~~, taking into account the characterized processes presented above that are necessary for accurate determinations~~. A paired ~~measurement~~ MC and ~~reference chamber~~ RC setup was deployed in the same field a year after the soil samples were

collected for our lab experiments. During a period of stimulated N_r emission from an experimental application of urea in situ, the mixing ratios of NO, N_2O, and NH_3 were impacted compared to the unfertilized state. The changes within both the ~~measurement~~ MC and ~~reference chambers~~ RC were measured and used to calculate fluxes (Figure 5). The purpose of Figure 5 is methodological to demonstrate how rate, dilution, and reaction terms combine in the observed rates of concentration change during chamber cycles. The selected data for NH_3 correspond to measurements taken after the fertilization event, while the selected NO and N_2O data segments are examples for separate observations times which best demonstrated the contributions of all terms prior to the fertilization event. ~~so that~~ Taken together, these three separate examples for the mathematical terms in E6 and E7 contributing to the net flux can be considered more easily – they are entirely ascribed to the rate term otherwise. Each set of observations span three consecutive hours of dynamic changes in gas concentrations within the chambers which allow fluxes to be calculated. manco measurement rate of the Picarro, it is clear from the accumulation and depletion of target gases in Figure 5, that a shorter observation period than 30 minutes could be used when high time resolution instrumentation across all target species is available. The benefit of this would be to reduce both the alteration of the composition of the chamber headspace and diverging physical conditions between the chamber and ambient environment; ultimately obtaining better flux estimates. However, for this pilot study, the 1-minute time resolution of the NO_x analyzer and the method for determining HONO by difference with an annular denuder every 5 minutes required the 30-minute interval. A shorter closure period could also have the drawback of worse flux detection limits when fluxes are small, and more variability due to a less robust regression of the accumulation or depletion rate. For example, this would increase the value of λ for NH_3 (Figure S11; Section S7) and its relative error (4% for a clean system, Section S7.3) as well as other surface-interacting gases.

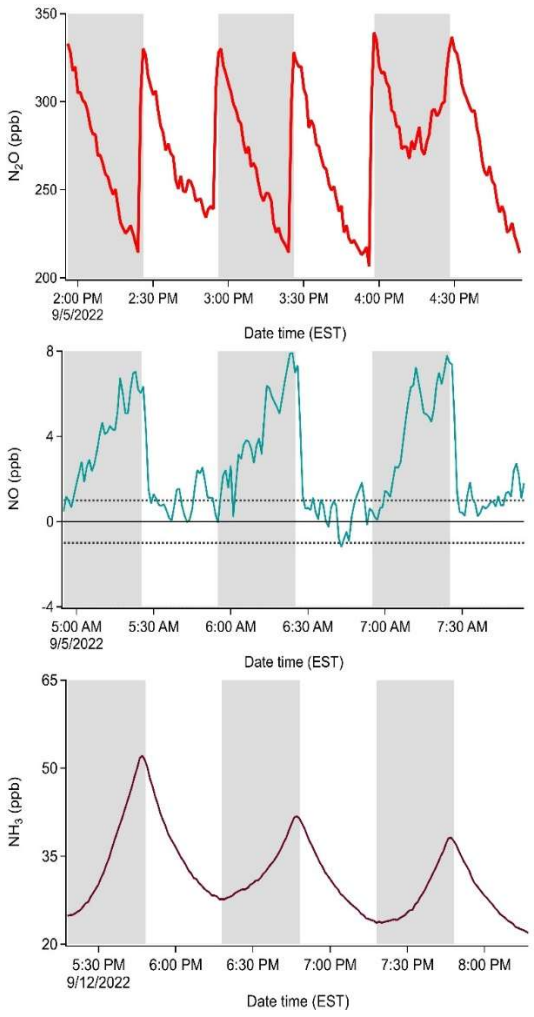

Figure 5. Mixing ratios of N_2O (ppb), NO (ppb), and NH_3 (ppb) in the measurement (grey shading) and reference (unshaded) chambers from three consecutive cycles during the pilot field study. Cycles are shown for representative, non-simultaneous periods to illustrate term contributions. The NH_3 cycles correspond to measurements taken after the fertilization perturbation, while the NO and N_2O cycles are from the same period before fertilization. The dashed lines for the NO measurements indicate ±1 ppb (3σ noise), where the positive boundary represents the detection limit of the NO_x analyzer.

The breakdown of the flux components for NH_3, N_2O, and NO can allow the contributions of the experimental setup (e.g. dilution) and environmental factors (e.g. reaction) to be considered independently (Figure 6). We consider these across a consecutive triplicate of flux determinations from the pilot field deployment, to provide meaningful examples. The uncertainty in each term is estimated from the variance between the triplicate of consecutive MC and ~~reference chamber~~ RC

observations, through the measured slopes (i.e. using E6 or E7) and assumes that ambient atmospheric composition did not change substantially during this error derivation period.

The rate term (dC/dt) is the dominant contributor to the determined flux for all three gases (Figure 6), which are all positive and indicate emissions despite their clearly differing temporal trends. Each contribution term is defined and discussed in further detail in Section S7 ~~of the Supplementary Information~~. Accurate quantification of trace gas fluxes using dynamic chamber systems requires correction for attenuation caused by surface interactions. These effects can significantly suppress the measured accumulation rate of reactive species within the closed ~~chamber~~MC~~, particularly for compounds with notable surface affinities such as NH_3, NO_2, and HONO~~ (Figure 5). To account for ~~such losses~~the, ~~an~~ the attenuation factor (λ) was introduced in this work (ES12), defined as the ratio of the theoretical concentration signal for an inert gas (e.g. as in our fill/empty experiments) to the measured signal over the chamber closure period. The value of λ is gas-specific and time-dependent, reflecting wall affinity and kinetics~~, which are therefore calculated over the first 30 min of chamber closure, as this was the duration of our field measurement closures~~. This correction reduces flux bias ~~that would otherwise result in the calculated gas exchange rates~~, independent of chamber-specific losses. The highest attenuation was observed for NH_3, for which a λ of 5.40 was determined empirically for the ~~corresponding~~ 30-minute closure period. ~~That is, substantial bias would result without this correction.~~ Comparative values for NO_2 and HONO are also provided in ~~the Supporting Information (~~Section S7.3~~)~~.

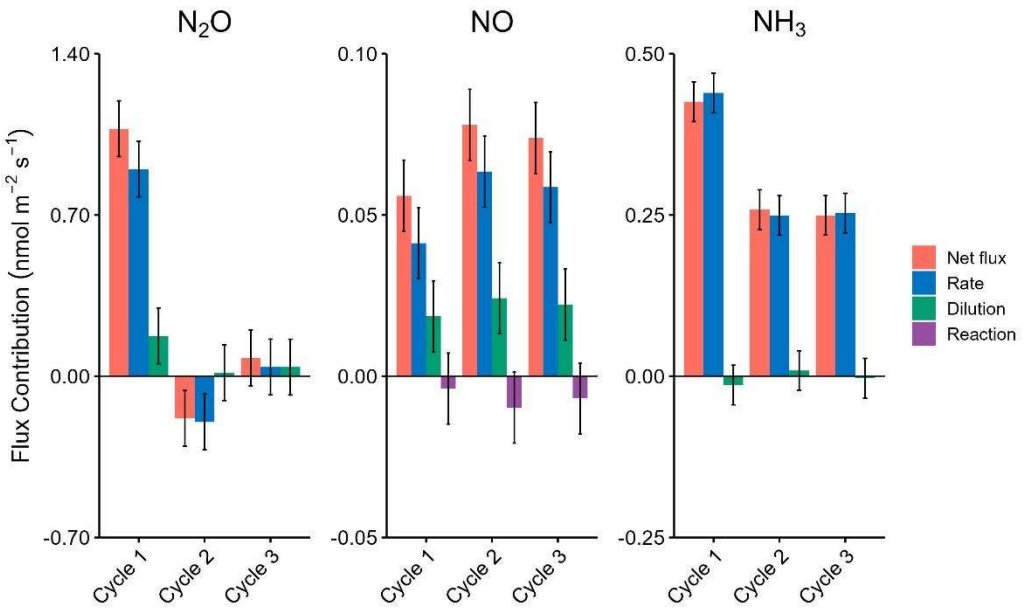

Figure 6. Contributions of different terms (rate, dilution, and reaction) to the net flux of NO, NH_3, and N_2O across three consecutive cycles (nmol m^{-2} s^{-1}). The rate represents the change in concentration measured over time, the dilution represents the integrated loss to dilution, and the reaction represents the contribution of known reactions happening inside the chamber. Error bars are calculated using the ~~mean value~~ standard deviation about the mean of the corresponding terms from three ~~reference chambers plus their standard deviation~~consecutive chamber cycles. For visual clarity, the attenuation correction ($\lambda = 5.40$) for NH_3 is not applied in this figure, as it constitutes a linear scaling factor across all NH_3 bars (Section S7.3).

For N_2O, the first cycle exhibits the highest flux (1.07±0.12 nmol m^{-2} s^{-1}), while the second cycle showed uptake by the soil (-0.18±0.12 nmol m^{-2} s^{-1}), and the final cycle showed no net flux within error (0.08±0.12 nmol m^{-2} s^{-1}). This occurs for a non-reactive greenhouse gas like N_2O despite the concentration decreasing with time for both the measurement and reference periods, as the rate of decrease during the measurement cycle is slower than that from dilution alone (Figure 6). Across the three cycles, the rate of concentration change term contributed 84±15% to the measured flux in the first cycle, 109±98% in the second cycle, and 50±171% in the third cycle. The negative rate of concentration change in all of the observation periods arises due to the use of N_2O-free purge gas delivered to the chamber headspace, which is required for the gas sample to be destructively quantified, while not introducing ambient air into the chamber (Figure 5). This simultaneously prevents sudden changes in local outdoor air composition from making small fluxes difficult to detect, as well as reduces the uncertainty in the fluxes assigned. Here, the dilution terms range

from 8 to 50% of the net flux, as would be expected from the N_2O exchange switching from emission to deposition during the three-cycle example (i.e. 3 hours). In the final measurement cycle, the rate of concentration change transitions from a loss to steady state during the observation period, suggesting that an instant of 'hot spot, hot moment' emission of N_2O was likely occurring. As such, the transition leads to no net flux for the observation period, which is a limitation of our dual-chamber approach compared to one with recirculating headspace, or that of an eddy covariance approach that can capture ~~much~~ higher temporal resolution changes in concentration. The N_2O fluxes observed here are consistent with those reported for European arable soils using both dynamic and static chambers, where event-driven N_2O peaks after fertilization commonly range between 0.2 and 2.4 nmol m^{-2} s^{-1}, and background periods can be as low as 0.08 nmol m^{-2} s^{-1} (Kong et al., 2025, Murphy et al., 2022, Maier et al., 2024, Manco et al., 2025). Field-scale eddy covariance studies, such as Maier et al. (2022), have captured post-harvest pulses up to 1.6 nmol m^{-2} s^{-1}, highlighting the capacity of EC to resolve large, rapid emission events that single-point chamber systems may miss. However, dynamic chamber systems provide high-precision, temporally resolved flux data under controlled conditions, enabling direct attribution of emissions to specific soil management or environmental factors (Butterbach-Bahl et al., 2013; Kong et al., 2025). This makes dynamic chambers, like those demonstrated here, especially valuable for mechanistic and process-level studies.

For NO, the only gas we consider in the examples here with a reaction term, the reaction contribution is the smallest among the three flux components. Over all three cycles, the reaction term opposed the net flux by less than 13%. The magnitude of the reaction term is always negligible, remaining within the ± 0.01 nmol m^{-2} s^{-1} variability caused by background correction from the ~~reference chamber~~RC. Instead, the time rate of change in concentration term drove 74–81% of the total flux for all three cycles and dilution accounted for the remaining 30–33%. The reaction term falling within the uncertainty range of no contribution in all three cycles (e.g. -0.01±0.01 nmol m^{-2} s^{-1} in the second cycle, where it had the greatest potential), indicates that its contribution is less certain than the other flux components as it is driven by the presence of O_3, which is rapidly lost upon chamber closure. Overall, the low contribution of the reaction term suggests this process has a minor role in measured NO fluxes. In other, more polluted regions, such as the North China Plain (NCP) and the Pearl River Delta (PRD), where summertime ambient O_3 concentrations ~~frequently~~ range from 60 to 275 ppbv, ~~and~~ the exceedances above 200 ppbv

~~occur~~ during pollution episodes (Wang et al., 2017)~~, this term~~ could ~~become~~ make this term very important ~~to include~~. As noted above, the PFA film on the chamber surface will change its properties with respect to O_3 transmission over time, highlighting the utility of the ~~reference chamber~~RC, which is designed to accumulate the same atmospheric compounds as the ~~measurement chamber~~ MC over time on all sampling surfaces.

The resulting emission fluxes of NO observed in these three cycles were 0.056-0.078 nmol m^{-2} s^{-1}, which ~~is~~ are well within the range reported for agricultural soils in North America and Europe, such as Taylor et al. (1999) who observed -0.07-4.2 nmol m^{-2} s^{-1} in Canadian fertilized cropland, and Pape et al. (2009) and Almand-Hunter et al. (2014) who reported values of 0.05-4.0 nmol m^{-2} s^{-1}, using dynamic chambers in grass and cropland soils. Therefore, in the case of NO for this example, the variability in the fluxes is largely driven by real fluctuations in the rate term. This highlights the sensitivity of the total flux to changes in the rate of concentration change, and the precision of the method, as the uncertainty in the final fluxes here is on the order of 14%. Compared to the dynamic chambers reported by these prior studies, ~~our~~ the ~~reference chamber~~ RC in our dual-chamber system offers a clear advantage by directly correcting for baseline fluctuations and environmental drift that can confound single-chamber approaches. This is especially important for reactive gases such as NO, which are susceptible to rapid loss to O_3 and short-term background variability (Taylor et al., 1999). The dual-chamber system provides more robust, artifact-free quantification of soil–atmosphere exchange and is less susceptible to interference from transient local emissions (e.g. from nearby traffic or agricultural equipment) than single-chamber systems. In comparison to eddy covariance or flux-gradient techniques, which integrate over larger areas but may underestimate true NO fluxes due to post-emission chemistry (Taylor et al., 1999; Plake et al., 2015), our approach yields high-frequency, process-resolving data ideal for mechanistic and plot-scale studies.

For NH_3, the rate of change term dominates the total flux, contributing 103 ± 10%, 97 ± 16%, and 101 ± 17% of the flux in cycles one, two, and three, respectively, while the dilution term contributes inconsequentially at -3 ± 7%, 3 ± 12%, and -1 ± 12% in the same three cycles, respectively. The resulting emission fluxes of NH_3 observed across these cycles ranged from 0.43 ± 0.03 nmol m^{-2} s^{-1} in cycle one down to 0.25 ± 0.03 nmol m^{-2} s^{-1} in cycle three. The relatively small contribution of the dilution term is consistent with the expectation that the ~~reference~~ RC and

measurement chambers MC exhibit similar dilution effects. The relative uncertainty in the final NH_3 fluxes is 7% for cycle one, and 12% for cycles two and three. By comparison, relative uncertainties were 14% for NO and ranged from 15% to 171% for N_2O, reflecting the greater variability and lower precision associated with the smaller flux magnitudes for those gases.

Our observed NH_3 fluxes (0.25–0.43 nmol m^{-2} s^{-1}) are consistent with literature values for managed grass and croplands. For instance, Milford et al. (2009) reported bi-directional background fluxes from –3.8 to 2.5 nmol m^{-2} s^{-1} prior to cutting intensively managed grassland, with larger diurnal emissions up to 42 nmol m^{-2} s^{-1} after cutting and maxima up to 224 nmol m^{-2} s^{-1} following fertilizer application. Abdulwahab et al. (2024) observed highly variable fluxes in intensively grazed French grassland, ranging from –6.6 to 188 nmol m^{-2} s^{-1}, with short-lived maxima above 300 nmol m^{-2} s^{-1} after slurry application, though most measurements were at much lower magnitudes. Notably, accurate quantification of NH_3 fluxes in this system critically depends on the application of the chamber-specific attenuation factor λ (Section S.7.3; Figure S11). In our study, λ for NH_3 was 5.40 for the 30-minute closure interval, meaning that wWithout this correction, true NH_3 fluxes would be underestimated by more than fivefold in our study. The necessity of such a large λ correction is due to the strong surface affinity of NH_3 and emphasizes the importance of it for gas- and chamber-specific corrections to obtain high-quality N_r fluxes. While the reference chamberRC correction plays a role in the flux calculations, its impact on NH_3 is less pronounced than on N_2O, where the correction significantly alters the net flux direction (Figure 5; first cycle). Chamber-based approaches such as ours provide a key advantage for NH_3 over micrometeorological methods like eddy covariance, which are especially prone to high-frequency attenuation and chemical interferences for reactive gases. As shown in Moravek et al. (2019), even state-of-the-art closed-path EC systems may recover less than half (as little as 46%) of true NH_3 fluxes due to instrument limitations and turbulence losses. Challenges were also evident for relaxed eddy accumulation (REA), where Xu et al. (2010) found that turbulence and surface effects complicated flux interpretation in cropland. Related methodological considerations have also been noted in other contexts. Schlossberg et al. (2017) highlighted how airflow and canopy structure can influence chamber NH_3 fluxes in turf systems, underscoring the need for chamber methods that minimize such artifacts. In contrast, our dynamic chamber system, with a chamber-specific λ correction and reference chamberRC, enables robust, bias-corrected quantification of both low and episodic NH_3 fluxes, as well as clear partitioning of emission and dilution terms, even under highly variable field

conditions. Overall, the combination of dual-chamber design with explicit λ correction in our method provides more accurate and robust quantification of soil NH_3 emissions than single-chamber, eddy covariance, or relaxed eddy accumulation techniques, particularly for short-term or low-flux events.

4. Conclusions

In this work, we presented a dynamic chamber system for ~~reactive nitrogen~~ N_r flux measurements, developed for the first time through the modification of commercially available chambers by implementing two key changes: the use of PTFE fittings instead of original brass fittings and the installation of an inert PFA film, which retains their actinic transparency. These modifications provide a targeted methodology for other researchers to convert commercially available chambers into those capable of measuring N_r. The performance of these modifications was quantified through the rise and fall time constants of target gas concentrations, as well as a reduction in reactive losses. The time constants for the transfer of GHGs were not different from those of a theoretically inert gas and showed no change from the modifications. Improved transmission for the reactive and surface-active N_r species NO_2, HONO, and NH_3 targeted here ranged from 0.8 to 2.6 minutes. Further improvement for NH_3 might be obtained by integration of heated gas transfer lines between the chambers and gas analyzers. Similarly, a commercial chamber multiplexing unit with stainless steel valves and fittings replaced with PTFE and PFA, respectively, resulted in a 9–27% reduction in surface losses of N_r compounds.

Only NO_2 showed reactive loss in the system, and the loss fraction in the chambers in their unmodified configurations was up to ~36%. Losses were reduced to the gas analyzer detection limits (<10%) with the same fluoropolymer modifications when atmospherically relevant NO_2 and RH mixtures were introduced. Lastly, O_3 loss was pervasive within chambers in both their modified and unmodified configurations at 35% and 45% respectively, demonstrating the necessity of the ~~reference chamber~~RC. It allows characterization of deposited surface film reactivity for O_3, especially when obtaining quality O_3 measurements is needed to account for the conversion of NO to NO_2 during a sampling period. Taken together, the modified commercial system is capable of measuring dynamic soil fluxes of GHGs and N_r when ~~a measurement~~ MC and ~~reference chamber~~ RC are deployed simultaneously.

Proof of concept flux measurements using this N_r dynamic chamber system were conducted using real agricultural soil samples in the lab, with a single chamber, and during a pilot study in the field with a measurement-reference chamber pair. The lab soil emissions were found to be consistent with prior field reports in the literature for NO and HONO, with unexpected emissions of NO_2 also observed. Substantial variability in NO_2 and HONO emissions between replicates demonstrates the potential heterogeneity of soil emissions that may result from samples kept intact and subject to minimal preparation conditions. Upon the addition of typical fertilizers, like urea, substantial NH_3 and N_2O emissions fluxes matched expectations, with increasing quantities of NO, NO_2, and HONO as the soil water content decreased.

Last, fully automated operation of the chambers was carried out in a field pilot study with the delivery of external fertilizer conducted at the midpoint of the ~~study~~ two-week period to stimulate N_r emissions, mainly in the form of NH_3. Continuous flux observations were made by switching sample flows between ~~a paired reference and measurement chambers~~the RC and MC with a custom-built valve system to obtain continuous N_r fluxes ~~over two weeks~~. While the details of the entire campaign will be presented in a future manuscript, it was shown here how the developed ~~methodology developed~~ measurement technique yields reliable flux determinations by accounting for known reactions and our lab-derived surface effects. The mathematical foundation of each term and its error in a mass balance equation, which are central to reducing flux bias, are fully described. The observed fluxes from our dynamic chambers are simpler to quantify with standard gas analyzers and can be compared readily with prior reports in the literature from other common flux techniques. The duration of the chamber closure for the modified NO_x analyzer used in this work made a 30-minute observation necessary to obtain sufficient measurements for a reliable flux determination. Use of higher time resolution gas analyzers can readily reduce the observation period and continue to produce reliable fluxes, depending on the flux detection limit desired, and tolerance for inflated surface effects. One key limitation of the dynamic chamber approach is the limited footprint covered in a system that is notoriously heterogeneous, where ~~EC~~ eddy covariance and ~~REA~~ relaxed eddy accumulation flux approaches are less prone to this effect. Using a multiplexer and a larger array of dynamic chambers, it is possible to reduce the susceptibility of the dynamic chamber approach to this issue. One further limitation is that the chamber and gas transfer line surfaces may accumulate material and change the mass transfer of gases, particularly NH_3, over time. This effect can be monitored using the reference chamber if sufficient quantities

are present in the ambient air, via the dilution decay rate and characterized in situ by a standard addition of the necessary gases to the headspace.

Through our modifications and validation, this work provides insight into how commercial dynamic chamber options, like those offered by Eosense, can be modified easily for scientists from various disciplines interested in studying N_r exchange at atmospheric interfaces. This is particularly important for research groups which currently do not have the expertise and resources to develop their own N_r flux measurement systems. The modified system utilizes destructive sampling techniques, as opposed to the re-circulation of chamber air, enabling integration of the dynamic chamber approach with various standard gas analysis instruments (e.g., NO_x chemiluminescence) to study their exchange. The large footprint allows gas concentrations to change in easily determined quantities even for very small fluxes. We show here, for the first time, that such a system can provide simultaneous measurement of NO, NO_2, HONO, NH_3, CO_2, H_2O, CH_4, and N_2O fluxes. In addition, we show fully automated operation of the chambers, switching of sample flows, and data collection workflows for continuous and unattended measurements of fluxes at field sites. Ideally, modern instrumentation like the ToF-CIMS would be coupled with this system to shorten the chamber closure duration, and better distinguish HONO from other NO_y fluxes, instead of a modified NO_x analyzer. Given the pressing need to understand global perturbations to the biogeochemical cycle of N, reduce nitrogen use in agriculture, and gauge the impacts of N status on biodiversity or ecosystem function, wider accessibility of N_r flux techniques for the global research community is needed to increase the pace of research outcomes and improve the capacity for interdisciplinary work between atmospheric and earth system researchers.

Data Availability: Data is available upon request from the Corresponding Author.

Competing Interests: TCV received supporting in-kind funds for this work from Eosense, Inc. and Picarro as it is mandatory in the NSERC Alliance Missions programme funding structure which facilitates research partnerships between the academy and industry. NN, CC, and SE are employed by Eosense, Inc.

Author contributions: TCV designed and oversaw the experiments, acquired funding, wrote parts of the manuscript, and guided writing and revision of all sections of the manuscript. MS wrote the

manuscript and performed all the lab experiments. KZA carried out the multiplexer experiments, conducted data analysis for the fill-empty experiment, provided guidance and feedback on the derivation of the mass balance flux model, and assisted in the revision of the manuscript. DF conducted some of the field measurements, worked up the pilot field study results and derived the dual chamber mass balance flux calculations, and made contributions to the writing and revision of the manuscript. LRC helped design the experiments, modify the chambers, write the LabVIEW code, conduct the pilot field measurements, and contributed to manuscript preparation and revision. AM contributed to the initial chamber lab setup and revision of the manuscript. FS performed some fill-empty and NO_2 loss experiments, designed the custom valve switching system, modified LabVIEW code for the pilot field measurements, and contributed to initial drafts of the manuscript. YEI and TH assisted with the GHG fill-empty experiments, YEI supported the pilot field study, and both contributed to manuscript revision. NN, CC, and SE provided technical support with setting up and modifying the chambers and multiplexer.

Acknowledgements: We gratefully acknowledge the support of Picarro for facilitating use of the G2509 analyzer during the chamber characterizations, lab experiments, and pilot study components of this work. The team at Shawnasey Farms Ltd. provided access to storage and machinery to install the experimental agricultural site for the pilot project, helped with daily campaign logistics, and the collection of soil samples.

Financial Support: All components of this work were supported by funding to TCV by the Natural Sciences and Engineering Research Council (NSERC) Alliance Missions program (ALLRP 570577-2021), with additional support from the NSERC Discovery Grants and Early Career Launch programmes (RGPIN-2020-06166 and DGECR-2020-00186). MS and YEI were supported by Ontario Graduate Scholarships, and MS was further supported by a Charles Hantho Award in Atmospheric Chemistry and the Enbridge Graduate Student Award.

5. References

Almand-Hunter, B. B., Walker, J. T., Masson, N. P., Hafford, L., & Hannigan, M. P. (2015). Development and validation of inexpensive, automated, dynamic flux chambers. *Atmospheric Measurement Techniques*, *8*(1), 267–280. https://doi.org/10.5194/amt-8-267-2015

Anas, M., Liao, F., Verma, K. K., Sarwar, M. A., Mahmood, A., Chen, Z. L., Li, Q., Zeng, X. P., Liu, Y., & Li, Y. R. (2020). Fate of nitrogen in agriculture and environment: agronomic, eco-physiological and molecular approaches to improve nitrogen use efficiency. In *Biological Research* (Vol. 53, Issue 1). BioMed Central Ltd. https://doi.org/10.1186/s40659-020-00312-4

Aneja, V. P., Blunden, J., Claiborn, C. S., & Rogers, H. H. (2006). Dynamic Chamber System to Measure Gaseous Compounds Emissions and Atmospheric-Biospheric Interactions. *Environmental Simulation Chambers: Application to Atmospheric Chemical Processes*, 97–109. https://doi.org/10.1007/1-4020-4232-9_7

Anthony, T. L., & Silver, W. L. (2024). Hot spots and hot moments of greenhouse gas emissions in agricultural peatlands. *Biogeochemistry*, *167*(4), 461–477. https://doi.org/10.1007/s10533-023-01095-y

Bao, F., Cheng, Y., Kuhn, U., Li, G., Wang, W., Kratz, A. M., Weber, J., Weber, B., Pöschl, U., & Su, H. (2022). Key Role of Equilibrium HONO Concentration over Soil in Quantifying Soil–Atmosphere HONO Fluxes. *Environmental Science & Technology*. https://doi.org/10.1021/acs.est.1c06716

Barney, W. S., & Finlayson-Pitts, B. J. (2000). Enhancement of N2O4 on Porous Glass at Room Temperature: A Key Intermediate in the Heterogeneous Hydrolysis of NO2? *Journal of Physical Chemistry A*, *104*(2), 171–175. https://doi.org/10.1021/jp993169b

Becciolini, V., Leso, L., Fuertes Gimeno, E., Rossi, G., Barbari, M., Dalla Marta, A., Orlandini, S., & Verdi, L. (2024). Nitrogen loss abatement from dairy cow excreta through urine and faeces separation: The effect of temperature and exposure period on NH3 fluxes. *Agricultural Systems*, *216*. https://doi.org/10.1016/j.agsy.2024.103898

Behera, S. N., Sharma, M., Aneja, V. P., & Balasubramanian, R. (2013). Ammonia in the atmosphere: A review on emission sources, atmospheric chemistry and deposition on terrestrial bodies. In *Environmental Science and Pollution Research* (Vol. 20, Issue 11, pp. 8092–8131). https://doi.org/10.1007/s11356-013-2051-9

Behrendt, T., Veres, P. R., Ashuri, F., Song, G., Flanz, M., Mamtimin, B., Bruse, M., Williams, J., & Meixner, F. X. (2014). Characterisation of NO production and consumption: New insights by an improved laboratory dynamic chamber technique. *Biogeosciences*, *11*(19), 5463–5492. https://doi.org/10.5194/bg-11-5463-2014

Benedict, K. B., Prenni, A. J., Carrico, C. M., Sullivan, A. P., Schichtel, B. A., & Collett, J. L. (2017). Enhanced concentrations of reactive nitrogen species in wildfire smoke. *Atmospheric Environment*, *148*, 8–15. https://doi.org/10.1016/j.atmosenv.2016.10.030

Burkholder, J. B., Cox, R. A., & Ravishankara, A. R. (2015). Atmospheric Degradation of Ozone Depleting Substances, Their Substitutes, and Related Species. *Chemical Reviews*, *115*(10), 3704–3759. https://doi.org/10.1021/cr5006759

Butterbach-Bahl, K., & Dannenmann, M. (2011). Denitrification and associated soil N2O emissions due to agricultural activities in a changing climate. *Current Opinion in Environmental Sustainability*, *3*(5), 389–395. https://doi.org/10.1016/j.cosust.2011.08.004

Chiaravalloti, I., Theunissen, N., Zhang, S., Wang, J., Sun, F., Ahmed, A. A., Pihlap, E., Reinhard, C. T., & Planavsky, N. J. (2023). Mitigation of soil nitrous oxide emissions during maize production with basalt amendments. *Frontiers in Climate*, *5*. https://doi.org/10.3389/fclim.2023.1203043

Crilley, L. R., Kramer, L. J., Ouyang, B., Duan, J., Zhang, W., Tong, S., Ge, M., Tang, K., Qin, M., Xe, P., Shaw, M. D., Lewis, A. C., Mehra, A., Bannan, T. J., Worrall, S. D., Priestley, M., Bacak, A., Coe, H., Allan, J., … Bloss, W. J. (2019). *Intercomparison of nitrous acid (HONO) measurement techniques in a megacity (Beijing)*. https://doi.org/10.5194/amt-2019-139

Crilley, L. R., Lao, M., Salehpoor, L., & VandenBoer, T. C. (2023). Emerging investigator series: an instrument to measure and speciate the total reactive nitrogen budget indoors: description and field measurements. *Environmental Science: Processes and Impacts*, *25*(3), 389–404. https://doi.org/10.1039/d2em00446a

Degaspari, I. A. M., Soares, J. R., Montezano, Z. F., Del Grosso, S. J., Vitti, A. C., Rossetto, R., & Cantarella, H. (2020). Nitrogen sources and application rates affect emissions of N2O and NH3 in sugarcane. *Nutrient Cycling in Agroecosystems*, *116*(3), 329–344. https://doi.org/10.1007/s10705-019-10045-w

Delaria, E. R., & Cohen, R. C. (2023). Measurements of Atmosphere-Biosphere Exchange of Oxidized Nitrogen and Implications for the Chemistry of Atmospheric NOx. *Accounts of Chemical Research*, *56*(13), 1720–1730. https://doi.org/10.1021/acs.accounts.3c00090

Dennis, R. L., Mathur, R., Pleim, J. E., & Walker, J. T. (2010). Fate of ammonia emissions at the local to regional scale as simulated by the Community Multiscale Air Quality model. *Atmospheric Pollution Research*, *1*(4), 207–214. https://doi.org/10.5094/APR.2010.027

Ebnesajjad, S. (2017). Introduction to Fluoropolymers. *Applied Plastics Engineering Handbook: Processing, Materials, and Applications: Second Edition*, 55–71. https://doi.org/10.1016/B978-0-323-39040-8.00003-1

Edwards, T. M., Puglis, H. J., Kent, D. B., Durán, J. L., Bradshaw, L. M., & Farag, A. M. (2024). Ammonia and aquatic ecosystems – A review of global sources, biogeochemical cycling, and effects on fish. In *Science of the Total Environment* (Vol. 907). Elsevier B.V. https://doi.org/10.1016/j.scitotenv.2023.167911

Ellis, R. A., Murphy, J. G., Pattey, E., Van Haarlem, R., O'Brien, J. M., & Herndon, S. C. (2010). Characterizing a Quantum Cascade Tunable Infrared Laser Differential Absorption Spectrometer (QC-TILDAS) for measurements of atmospheric ammonia. *Atmospheric Measurement Techniques*, *3*(2), 397–406. https://doi.org/10.5194/amt-3-397-2010

Finlayson-Pitts, B. J., Wingen, L. M., Sumner, A. L., Syomin, D., & Ramazan, K. A. (2003). The heterogeneous hydrolysis of NO2 in laboratory systems and in outdoor and indoor atmospheres: An integrated mechanism. *Physical Chemistry Chemical Physics*, *5*(2), 223–242. https://doi.org/10.1039/b208564j

Fowler, D., Coyle, M., Skiba, U., Sutton, M. A., Cape, J. N., Reis, S., Sheppard, L. J., Jenkins, A., Grizzetti, B., Galloway, J. N., Vitousek, P., Leach, A., Bouwman, A. F., Butterbach-Bahl, K., Dentener, F., Stevenson, D., Amann, M., & Voss, M. (2013). The global nitrogen cycle in the twenty-first century. *Philosophical Transactions of the Royal Society B: Biological Sciences*, *368*(1621). https://doi.org/10.1098/rstb.2013.0164

Geddes, J. A., & Murphy, J. G. (2014). Observations of reactive nitrogen oxide fluxes by eddy covariance above two midlatitude North American mixed hardwood forests. *Atmospheric Chemistry and Physics*, *14*(6), 2939–2957. https://doi.org/10.5194/acp-14-2939-2014

George, C., Ammann, M., D'Anna, B., Donaldson, D. J., & Nizkorodov, S. A. (2015). Heterogeneous Photochemistry in the Atmosphere. *Chemical Reviews*, *115*(10), 4218–4258. https://doi.org/10.1021/cr500648z

Gong, C., Wang, Y., Tian, H., Kou-Giesbrecht, S., Vuichard, N., & Zaehle, S. (2025). Uncertainties in fertilizer-induced emissions of soil nitrogen oxide and the associated impacts on ground-level ozone and methane. *EGUsphere*. https://doi.org/10.5194/egusphere-2025-1416

González Ortiz, Alberto., Guerreiro, Cristina., & Soares, Joana. (2020). *Air quality in Europe: 2020 report*. European Environment Agency. https://doi.org/10.2800/786656

Govoni Brondi, M., Bortoletto-Santos, R., Farias, J. G., Farinas, C. S., Ammar, M., Ribeiro, C., Williams, C., & Baltrusaitis, J. (2024). Mechanochemically Synthesized Nitrogen-Efficient Mg- and Zn-Ammonium Carbonate Fertilizers. *ACS Sustainable Chemistry and Engineering*, *12*(16), 6182–6193. https://doi.org/10.1021/acssuschemeng.3c07785

Ha, P. T. M., Kanaya, Y., Taketani, F., Andres Hernandez, M. D., Schreiner, B., Pfeilsticker, K., & Sudo, K. (2023). Implementation of HONO into the chemistry-climate model CHASER (V4.0): Roles in tropospheric chemistry. *Geoscientific Model Development*, *16*(3), 927–960. https://doi.org/10.5194/gmd-16-927-2023

He, Y., Zhou, X., Hou, J., Gao, H., & Bertman, S. B. (2006). Importance of dew in controlling the air-surface exchange of HONO in rural forested environments. *Geophysical Research Letters*, *33*(2). https://doi.org/10.1029/2005GL024348

Huang, G., Zhou, X., Deng, G., Qiao, H., & Civerolo, K. (2002). Measurements of atmospheric nitrous acid and nitric acid. *Atmospheric Environment*, *36*(13), 2225–2235. https://doi.org/10.1016/S1352-2310(02)00170-X

Huber, D. E., Kort, E. A., & Steiner, A. L. (2024). Soil Moisture, Soil NOx and Regional Air Quality in the Agricultural Central United States. *Journal of Geophysical Research: Atmospheres*, *129*(12). https://doi.org/10.1029/2024JD041015

IPCC. (2023). Climate Change 2021- The Physical Science Basis. *Cambridge University Press*. https://doi.org/https://doi.org/10.1017/9781009157896

Jang, J.-H., Hong, J., Kim, J. B., Park, S., Hwang, K., Kim, J., Kim, J. Y., Bae, G.-N., Kim, S., & Kim, K. H. (2025). Influence of atmospheric ammonia on secondary inorganic aerosol formation in PM2.5 during spring 2024 in the Hongseong area, Republic of Korea. *Atmospheric Environment*, 121363. https://doi.org/10.1016/j.atmosenv.2025.121363

Kamboures, M. A., Raff, J. D., Miller, Y., Phillips, L. F., Finlayson-Pitts, B. J., & Gerber, R. B. (2008). Complexes of HNO3 and NO3- with NO2 and N2O4, and their potential role in

atmospheric HONO formation. *Physical Chemistry Chemical Physics*, *10*(39), 6019–6032. https://doi.org/10.1039/b805330h

Kamp, J. N., Häni, C., Nyord, T., Feilberg, A., & Sørensen, L. L. (2020). The aerodynamic gradient method: Implications of non-simultaneous measurements at alternating heights. *Atmosphere*, *11*(10). https://doi.org/10.3390/atmos11101067

Kleffmann, J., Gavriloaiei, T., Hofzumahaus, A., Holland, F., Koppmann, R., Rupp, L., Schlosser, E., Siese, M., & Wahner, A. (2005). Daytime formation of nitrous acid: A major source of OH radicals in a forest. *Geophysical Research Letters*, *32*(5), 1–4. https://doi.org/10.1029/2005GL022524

Kolari, P., Bäck, J., Taipale, R., Ruuskanen, T. M., Kajos, M. K., Rinne, J., Kulmala, M., & Hari, P. (2012). Evaluation of accuracy in measurements of VOC emissions with dynamic chamber system. *Atmospheric Environment*, *62*, 344–351. https://doi.org/10.1016/j.atmosenv.2012.08.054

Kool, D. M., Wrage, N., Zechmeister-Boltenstern, S., Pfeffer, M., Brus, D., Oenema, O., & Van Groenigen, J. W. (2010). Nitrifier denitrification can be a source of N2O from soil: A revised approach to the dual-isotope labelling method. *European Journal of Soil Science*, *61*(5), 759–772. https://doi.org/10.1111/j.1365-2389.2010.01270.x

Lao, M., Crilley, L. R., Salehpoor, L., Furlani, T. C., Bourgeois, I., Andrew Neuman, J., Rollins, A. W., Veres, P. R., Washenfelder, R. A., Womack, C. C., Young, C. J., & VandenBoer, T. C. (2020). A portable, robust, stable, and tunable calibration source for gas-phase nitrous acid (HONO). *Atmospheric Measurement Techniques*, *13*(11), 5873–5890. https://doi.org/10.5194/amt-13-5873-2020

Laufs, S., Cazaunau, M., Stella, P., Kurtenbach, R., Cellier, P., Mellouki, A., Loubet, B., & Kleffmann, J. (2017). Diurnal fluxes of HONO above a crop rotation. *Atmospheric Chemistry and Physics*, *17*(11), 6907–6923. https://doi.org/10.5194/acp-17-6907-2017

Lee, B. H., Lopez-Hilfiker, F. D., Mohr, C., Kurtén, T., Worsnop, D. R., & Thornton, J. A. (2014). An iodide-adduct high-resolution time-of-flight chemical-ionization mass spectrometer: Application to atmospheric inorganic and organic compounds. *Environmental Science and Technology*, *48*(11), 6309–6317. https://doi.org/10.1021/es500362a

Lehnert, N., Musselman, B. W., Seefeldt, L. C., & Gutenberg-university, J. (2021). Grand Challenges in the nitrogen cycle. *Chemical Society Reviews*, *50*, 3640–3646. https://doi.org/10.1039/d0cs00923g

Li, L., Fan, W., Kang, X., Wang, Y., Cui, X., Xu, C., Griffin, K. L., & Hao, Y. (2016). Responses of greenhouse gas fluxes to climate extremes in a semiarid grassland. *Atmospheric Environment*, *142*, 32–42. https://doi.org/10.1016/j.atmosenv.2016.07.039

Lipiec, J., Walczak, R., Witkowska-Walczak, B., Nosalewicz, A., Słowińska-Jurkiewicz, A., & Sławiński, C. (2007). The effect of aggregate size on water retention and pore structure of two silt loam soils of different genesis. *Soil and Tillage Research*, *97*(2), 239–246. https://doi.org/10.1016/j.still.2007.10.001

Liu, L., Zhang, X., Xu, W., Liu, X., Li, Y., Wei, J., Wang, Z., & Lu, X. (2020). Ammonia volatilization as the major nitrogen loss pathway in dryland agro-ecosystems. *Environmental Pollution*, *265*. https://doi.org/10.1016/j.envpol.2020.114862

Liu, Zheng, X., Li, Y., Yu, J., Ding, H., Sveen, T. R., & Zhang, Y. (2022). Soil moisture determines nitrous oxide emission and uptake. *Science of the Total Environment*, *822*. https://doi.org/10.1016/j.scitotenv.2022.153566

Ludwig, J., Meixner, F. X., Vogel, B., & Forstner, J. (2001). Soil-air exchange of nitric oxide: An overview of processes, environmental factors, and modeling studies. *Biogeochemistry*, *52*(3), 225–257. https://doi.org/10.1023/A:1006424330555

Luo, X., Zhang, M., Ni, Y., & Shen, G. (2025). Mitigation strategies for NH_3 and N_2O emissions in greenhouse agriculture: Insights into fertilizer management and nitrogen emission mechanisms. *Environmental Technology and Innovation*, *37*. https://doi.org/10.1016/j.eti.2024.103995

Maggiotto, S. R., Webb, J. A., & Thurtell, G. W. (2000). Nitrous and Nitrogen Oxide Emissions from Turfgrass Receiving Different Forms of Nitrogen Fertilizer. *American Society of Agronomy, Crop Science Society of America, and Soil Science Society of America*, *29*, 621–630.

Manco, A., Giaccone, M., Vitale, L., Maglione, G., Riccardi, M., Matteo, B. Di, Esposito, A., Magliulo, V., & Tedeschi, A. (2025). Comparative Effects of Nitrogen Fertigation and Granular Fertilizer Application on Pepper Yield and Soil GHGs Emissions. *Horticulturae*, *11*(6). https://doi.org/10.3390/horticulturae11060708

Mangalassery, S., Sjögersten, S., Sparkes, D. L., Sturrock, C. J., & Mooney, S. J. (2013). The effect of soil aggregate size on pore structure and its consequence on emission of greenhouse gases. *Soil and Tillage Research*, *132*, 39–46. https://doi.org/10.1016/j.still.2013.05.003

Meusel, H., Tamm, A., Kuhn, U., Wu, D., Lena Leifke, A., Fiedler, S., Ruckteschler, N., Yordanova, P., Lang-Yona, N., Pöhlker, M., Lelieveld, J., Hoffmann, T., Pöschl, U., Su, H., Weber, B., & Cheng, Y. (2018). Emission of nitrous acid from soil and biological soil crusts represents an important source of HONO in the remote atmosphere in Cyprus. *Atmospheric Chemistry and Physics*, *18*(2), 799–813. https://doi.org/10.5194/acp-18-799-2018

Min, K. E., Pusede, S. E., Browne, E. C., LaFranchi, B. W., & Cohen, R. C. (2014). Eddy covariance fluxes and vertical concentration gradient measurements of NO and NO2 over a ponderosa pine ecosystem: Observational evidence for within-canopy chemical removal of NOx. *Atmospheric Chemistry and Physics*, *14*(11), 5495–5512. https://doi.org/10.5194/acp-14-5495-2014

Mochizuki, T., Amagai, T., & Tani, A. (2018). Effects of soil water content and elevated CO2 concentration on the monoterpene emission rate of Cryptomeria japonica. *Science of the Total Environment*, *634*, 900–908. https://doi.org/10.1016/j.scitotenv.2018.04.025

Moravek, A., Foken, T., & Trebs, I. (2014). Application of a GC-ECD for measurements of biosphere-atmosphere exchange fluxes of peroxyacetyl nitrate using the relaxed eddy accumulation and gradient method. *Atmospheric Measurement Techniques*, *7*(7), 2097–2119. https://doi.org/10.5194/amt-7-2097-2014

Moravek, A., Singh, S., Pattey, E., Pelletier, L., & Murphy, J. G. (2019). Measurements and quality control of ammonia eddy covariance fluxes: A new strategy for high-frequency attenuation correction. *Atmospheric Measurement Techniques*, *12*(11), 6059–6078. https://doi.org/10.5194/amt-12-6059-2019

Mosier, A. R. (2008). Exchange of Gaseous Nitrogen Compounds Between Terrestrial Systems and the Atmosphere. *Nitrogen in the Environment*, 443–462. https://doi.org/10.1016/B978-0-12-374347-3.00013-5

Mushinski, R. M., Phillips, R. P., Payne, Z. C., Abney, R. B., Jo, I., Fei, S., Pusede, S. E., White, J. R., Rusch, D. B., & Raff, J. D. (2019). Microbial mechanisms and ecosystem flux estimation for aerobic NOy emissions from deciduous forest soils. *Proceedings of the National Academy of Sciences of the United States of America*, *116*(6), 2138–2145. https://doi.org/10.1073/pnas.1814632116

Neuman, J. A., Trainer, M., Brown, S. S., Min, K. E., Nowak, J. B., Parrish, D. D., Peischl, J., Pollack, I. B., Roberts, J. M., Ryerson, T. B., & Veres, P. R. (2016). HONO emission and production determined from airborne measurements over the Southeast U.S. *Journal of Geophysical Research*, *121*(15), 9237–9250. https://doi.org/10.1002/2016JD025197

Nodeh-Farahani, D., Bentley, J. N., Crilley, L. R., Caputo, C. B., & VandenBoer, T. C. (2021). A boron dipyrromethene (BODIPY) based probe for selective passive sampling of atmospheric nitrous acid (HONO) indoors. *Analyst*, *146*(18), 5756–5766. https://doi.org/10.1039/d1an01089a

Okiti, I., Efakwu, G., Pindus, M., & Kasak, K. (2025). Environmental and biogeochemical drivers of CH4 and N2O flux variability in treatment wetlands. *Ecological Engineering*, *219*. https://doi.org/10.1016/j.ecoleng.2025.107705

Oswald, R., Behrendt, T., Ermel, M., Wu, D., Su, H., Cheng, Y., Breuninger, C., Moravek, A., Mougin, E., Delon, C., Loubet, B., Pommerening-Röser, A., Sörgel, M., Pöschl, U., Hoffmann, T., Andreae, M. O., Meixner, F. X., & Trebs, I. (2013). HONO emissions from soil bacteria as a major source of atmospheric reactive nitrogen. *Science*, *341*(6151), 1233–1235. https://doi.org/10.1126/science.1242266

Pan, B., Lam, S. K., Mosier, A., Luo, Y., & Chen, D. (2016). Ammonia volatilization from synthetic fertilizers and its mitigation strategies: A global synthesis. *Agriculture, Ecosystems and Environment*, *232*, 283–289. https://doi.org/10.1016/j.agee.2016.08.019

Pan, B., Xia, L., Lam, S. K., Wang, E., Zhang, Y., Mosier, A., & Chen, D. (2022). A global synthesis of soil denitrification: Driving factors and mitigation strategies. *Agriculture, Ecosystems and Environment*, *327*(September 2021), 107850. https://doi.org/10.1016/j.agee.2021.107850

Pape, L., Ammann, C., Nyfeler-Brunner, A., Spirig, C., Hens, K., & Meixner, F. X. (2009). An automated dynamic chamber system for surface exchange measurement of non-reactive and reactive trace gases of grassland ecosystems. *Biogeosciences*, *6*(3), 405–429. https://doi.org/10.5194/bg-6-405-2009

Paulot, F., Jacob, D. J., Pinder, R. W., Bash, J. O., Travis, K., & Henze, D. K. (2014). Ammonia emissions in the United States, european union, and China derived by high-resolution inversion of ammonium wet deposition data: Interpretation with a new agricultural emissions inventory (MASAGE_NH3). *Journal of Geophysical Research*, *119*(7), 4343–4364. https://doi.org/10.1002/2013JD021130

Plake, D., Sörgel, M., Stella, P., Held, A., & Trebs, I. (2015). Influence of meteorology and anthropogenic pollution on chemical flux divergence of the NO-NO2-O3 triad above and

within a natural grassland canopy. *Biogeosciences*, *12*(4), 945–959. https://doi.org/10.5194/bg-12-945-2015

Plake, D., Stella, P., Moravek, A., Mayer, J. C., Ammann, C., Held, A., & Trebs, I. (2015). Comparison of ozone deposition measured with the dynamic chamber and the eddy covariance method. *Agricultural and Forest Meteorology*, *206*, 97–112. https://doi.org/10.1016/j.agrformet.2015.02.014

Possanzini, M., Febo, A., & Liberti, A. (1983). New design of a high-performance denuder for the sampling of atmospheric pollutants. *Atmospheric Environment (1967)*, *17*(12), 2605–2610. https://doi.org/10.1016/0004-6981(83)90089-6

Pugliese, G., Ingrisch, J., Meredith, L. K., Pfannerstill, E. Y., Klüpfel, T., Meeran, K. Byron, J., Purser, G. Gil-Loaiza, J., van Haren, J., Dontsova, K., Kreuzwieser, J., Ladd, S. N., Werner, C. & Williams, J. (2023). Effects of drought and recovery on soil volatile organic compound fluxes in an experimental forest. *Nature Communications, 14:5064.* https://doi.org/10.1038/s41467-023-40661-8

Purchase, M. L., Bending, G. D., & Mushinski, R. M. (2023). Spatiotemporal Variations of Soil Reactive Nitrogen Oxide Fluxes across the Anthropogenic Landscape. *Environmental Science and Technology*, *57*(43), 16348–16360. https://doi.org/10.1021/acs.est.3c05849

Ramazan, K. A., Syomin, D., & Finlayson-Pitts, B. J. (2004). The photochemical production of HONO during the heterogeneous hydrolysis of NO2. *Physical Chemistry Chemical Physics*, *6*(14), 3836–3843. https://doi.org/10.1039/b402195a

Reed, C., Brumby, C. A., Crilley, L. R., Kramer, L. J., Bloss, W. J., Seakins, P. W., Lee, J. D., & Carpenter, L. J. (2016). HONO measurement by differential photolysis. *Atmospheric Measurement Techniques*, *9*(6), 2483–2495. https://doi.org/10.5194/amt-9-2483-2016

Ren, X., Sanders, J. E., Rajendran, A., Weber, R. J., Goldstein, A. H., Pusede, S. E., Browne, E. C., Min, K. E., & Cohen, R. C. (2011). A relaxed eddy accumulation system for measuring vertical fluxes of nitrous acid. *Atmospheric Measurement Techniques*, *4*(10), 2093–2103. https://doi.org/10.5194/amt-4-2093-2011

Ren, Y., Stieger, B., Spindler, G., Grosselin, B., Mellouki, A., Tuch, T., Wiedensohler, A., & Herrmann, H. (2020). Role of the dew water on the ground surface in HONO distribution: A case measurement in Melpitz. *Atmospheric Chemistry and Physics*, *20*(21), 13069–13089. https://doi.org/10.5194/acp-20-13069-2020

Richardson, K., Steffen, W., Lucht, W., Bendtsen, J., Cornell, S. E., Donges, J. F., Drüke, M., Fetzer, I., Bala, G., Von Bloh, W., Feulner, G., Fiedler, S., Gerten, D., Gleeson, T., Hofmann, M., Huiskamp, W., Kummu, M., Mohan, C., Nogués-Bravo, D., … Rockström, J. (2023). *Earth beyond six of nine planetary boundaries*. https://www.science.org

Scharko, N. K., Schu, U. M. E., Berke, A. E., Banina, L., Peel, H. R., Donaldson, M. A., Hemmerich, C., White, R., & Ra, J. D. (2015). *Combined Flux Chamber and Genomics Approach Links Nitrous Acid Emissions to Ammonia Oxidizing Bacteria and Archaea in Urban and Agricultural Soil*. https://doi.org/10.1021/acs.est.5b00838

Schindlbacher, A., Zechmeister-Boltenstern, S., & Jandl, R. (2009). Carbon losses due to soil warming: Do autotrophic and heterotrophic soil respiration respond equally? *Global Change Biology*, *15*(4), 901–913. https://doi.org/10.1111/j.1365-2486.2008.01757.x

Schlesinger, W. H. (2020). *Biogeochemistry: An Analysis of Global Change* (4th ed.). Academic Press. https://doi.org/https://doi.org/10.1016/C2018-0-03255-3

Seinfeld, J. H., & Pandis, S. N. (2006). *Atmospheric chemistry and physics: from air pollution to climate change.* (2nd edition). John Wiley & Sons.

Shah, S. B., Grabow, G. L., & Westerman, P. W. (2006). *Ammonia adsorption in five types of flexible tubing materials*. https://doi.org/10.13031/2013.22253

Song, Y., Xue, C., Zhang, Y., Liu, P., Bao, F., Li, X., & Mu, Y. (2023). *Measurement Report: Exchange Fluxes of HONO over Agricultural Fields in the North China Plain*. *July*, 1–38. https://zenodo.org/record/8115973

Sörgel, M., Trebs, I., Wu, D., & Held, A. (2015). A comparison of measured HONO uptake and release with calculated source strengths in a heterogeneous forest environment. *Atmospheric Chemistry and Physics*, *15*(16), 9237–9251. https://doi.org/10.5194/acp-15-9237-2015

Spataro, F., & Ianniello, A. (2014). Sources of atmospheric nitrous acid: State of the science, current research needs, and future prospects. *Journal of the Air and Waste Management Association*, *64*(11), 1232–1250. https://doi.org/10.1080/10962247.2014.952846

Stepniewski, W., Stepniewska, Z., & Rozej, A. (2015). Gas Exchange in Soils. *Soil Management: Building a Stable Base for Agriculture*, 117–144. https://doi.org/10.2136/2011.soilmanagement.c8

Su, H., Cheng, Y., Oswald, R., Behrendt, T., Trebs, I., Meixner, F. X., Andreae, M. O., Cheng, P., Zhang, Y., & Pöschl, U. (2011). Soil nitrite as a source of atmospheric HONO and OH radicals. *Science*, *333*(6049), 1616–1618. https://doi.org/10.1126/science.1207687

Tang, K., Qin, M., Duan, J., Fang, W., Meng, F., Liang, S., Xie, P., Liu, J., Liu, W., Xue, C., & Mu, Y. (2019). A dual dynamic chamber system based on IBBCEAS for measuring fluxes of nitrous acid in agricultural fields in the North China Plain. *Atmospheric Environment*, *196*(May 2018), 10–19. https://doi.org/10.1016/j.atmosenv.2018.09.059

Tang, K., Qin, M., Fang, W., Duan, J., Meng, F., Ye, K., Zhang, H., Xie, P., Liu, J., Liu, W., Feng, Y., Huang, Y., & Ni, T. (2020). An automated dynamic chamber system for exchange flux measurement of reactive nitrogen oxides (HONO and NOX) in farmland ecosystems of the Huaihe River Basin, China. *Science of the Total Environment*, *745*(X), 140867. https://doi.org/10.1016/j.scitotenv.2020.140867

Tian, H., Pan, N., Thompson, R. L., Canadell, J. G., Suntharalingam, P., Regnier, P., Davidson, E. A., Prather, M., Ciais, P., Muntean, M., Pan, S., Winiwarter, W., Zaehle, S., Zhou, F., Jackson, R. B., Bange, H. W., Berthet, S., Bian, Z., Bianchi, D., … Zhu, Q. (2024). Global nitrous oxide budget (1980-2020). *Earth System Science Data*, *16*(6), 2543–2604. https://doi.org/10.5194/essd-16-2543-2024

Vaittinen, O., Metsälä, M., Persijn, S., Vainio, M., & Halonen, L. (2014). Adsorption of ammonia on treated stainless steel and polymer surfaces. *Applied Physics B: Lasers and Optics*, *115*(2), 185–196. https://doi.org/10.1007/s00340-013-5590-3

VandenBoer, T. C., Brown, S. S., Murphy, J. G., Keene, W. C., Young, C. J., Pszenny, A. A. P. P., Kim, S., Warneke, C., De Gouw, J. A., Maben, J. R., Wagner, N. L., Riedel, T. P., Thornton, J. A., Wolfe, D. E., Dubé, W. P., Öztürk, F., Brock, C. A., Grossberg, N., Lefer, B., … Roberts, J. M. (2013). Understanding the role of the ground surface in HONO vertical structure: High resolution vertical profiles during NACHTT-11. *Journal of*

Geophysical Research Atmospheres, *118*(17), 10,155-10,171. https://doi.org/10.1002/jgrd.50721

VandenBoer, T. C., Young, C. J., Talukdar, R. K., Markovic, M. Z., Brown, S. S., Roberts, J. M., & Murphy, J. G. (2015). Nocturnal loss and daytime source of nitrous acid through reactive uptake and displacement. *Nature Geoscience*, *8*(1), 55–60. https://doi.org/10.1038/ngeo2298

Von Der Heyden, L., Wißdorf, W., Kurtenbach, R., & Kleffmann, J. (2022). A relaxed eddy accumulation (REA) LOPAP system for flux measurements of nitrous acid (HONO). *Atmospheric Measurement Techniques*, *15*(6), 1983–2000. https://doi.org/10.5194/amt-15-1983-2022

Wang, Fu, X., Wu, D., Wang, M., Lu, K., Mu, Y., Liu, Z., Zhang, Y., & Wang, T. (2021). Agricultural Fertilization Aggravates Air Pollution by Stimulating Soil Nitrous Acid Emissions at High Soil Moisture. *Environmental Science and Technology*, *55*(21), 14556–14566. https://doi.org/10.1021/acs.est.1c04134

Wang, Y., Fu, X., Wang, T., Ma, J., Gao, H., Wang, X., & Pu, W. (2022). Large Contribution of Nitrous Acid to Soil-Emitted Reactive Oxidized Nitrogen and Its Effect on Air Quality. *Environmental Science and Technology*. https://doi.org/10.1021/acs.est.2c07793

Wolff, V., Trebs, I., Ammann, C., & Meixner, F. X. (2010). Atmospheric Measurement Techniques Aerodynamic gradient measurements of the NH3-HNO3-NH4NO3 triad using a wet chemical instrument: an analysis of precision requirements and flux errors. In *Atmos. Meas. Tech* (Vol. 3). www.atmos-meas-tech.net/3/187/2010/

Wu, D., Deng, L., Liu, Y., Xi, D., Zou, H., Sha, Z., Pan, Y., Hou, L., & Liu, M. (2020). *Comparisons of the effects of different drying methods on soil nitrogen fractions: Insights into emissions of reactive nitrogen gases (HONO and NO)*. https://doi.org/10.1080/16742834.2020.1733388

Wu, D., Horn, M. A., Behrendt, T., Müller, S., Li, J., Cole, J. A., Xie, B., Ju, X., Li, G., Ermel, M., Oswald, R., Fröhlich-Nowoisky, J., Hoor, P., Hu, C., Liu, M., Andreae, M. O., Pöschl, U., Cheng, Y., Su, H., … Sörgel, M. (2019). Soil HONO emissions at high moisture content are driven by microbial nitrate reduction to nitrite: tackling the HONO puzzle. *ISME Journal*, *13*(7), 1688–1699. https://doi.org/10.1038/s41396-019-0379-y

Wu, D., Zhang, J., Wang, M., An, J., Wang, R., Haider, H., Xu-Ri, Huang, Y., Zhang, Q., Zhou, F., Tian, H., Zhang, X., Deng, L., Pan, Y., Chen, X., Yu, Y., Hu, C., Wang, R., Song, Y., … Liu, M. (2022). Global and Regional Patterns of Soil Nitrous Acid Emissions and Their Acceleration of Rural Photochemical Reactions. *Journal of Geophysical Research: Atmospheres*, *127*(6), 1–16. https://doi.org/10.1029/2021JD036379

Yang, J. Y., Drury, C. F., Jiang, R., Worth, D. E., Bittman, S., Grant, B. B., & Smith, W. N. (2024). Reactive nitrogen losses from Canadian agricultural soils over 36 years. *Ecological Modelling*, *495*. https://doi.org/10.1016/j.ecolmodel.2024.110809

Young, C. J., Washenfelder, R. A., Roberts, J. M., Mielke, L. H., Ostho, H. D., Tsai, C., Pikelnaya, O., Stutz, J., Veres, P. R., Cochran, A. K., Vandenboer, T. C., Flynn, J., Grossberg, N., Haman, C. L., Lefer, B., Stark, H., Graus, M., Gouw, J. De, Gilman, J. B., … Brown, S. S. (2012). *Vertically Resolved Measurements of Nighttime Radical Reservoirs in Los Angeles and Their Contribution to the Urban Radical Budget*.

Zhang, S., Sarwar, G., Xing, J., Chu, B., Xue, C., Sarav, A., Ding, D., Zheng, H., Mu, Y., Duan, F., Ma, T., & He, H. (2021). Improving the representation of HONO chemistry in CMAQ and examining its impact on haze over China. *Atmospheric Chemistry and Physics*, *21*(20), 15809–15826. https://doi.org/10.5194/acp-21-15809-2021

Zhou, S., Young, C. J., VandenBoer, T. C., Kowal, S. F., & Kahan, T. F. (2018). Time-Resolved Measurements of Nitric Oxide, Nitrogen Dioxide, and Nitrous Acid in an Occupied New York Home. *Environmental Science and Technology*, *52*(15), 8355–8364. https://doi.org/10.1021/acs.est.8b01792

Zörner, J., Penning De Vries, M., Beirle, S., Sihler, H., Veres, P. R., Williams, J., & Wagner, T. (2016). Multi-satellite sensor study on precipitation-induced emission pulses of NOx from soils in semi-arid ecosystems. *Atmospheric Chemistry and Physics*, *16*(14), 9457–9487. https://doi.org/10.5194/acp-16-9457-2016

Supporting Information for:

Modification and validation of a commercial dynamic chamber for reactive nitrogen and greenhouse gas flux measurements

Moxy Shah[1], Kifle Z. Aregahegn[1], Danial Nodeh-Farahani[1], Leigh R. Crilley[1,‡], Tasnia Hasan[1], Yashar Ebrahimi-Iranpour[1], Fahim Sarker[1], Nick Nickerson[2], Chance Creelman[2], Sarah Ellis[2], Alexander Moravek[1,§] , Trevor C. VandenBoer[1,*]

[1] Department of Chemistry, York University, Toronto, Ontario, Canada

[2] Eosense Inc., Dartmouth, Nova Scotia, Canada

[‡] Now at: Atmospheric Services, WSP Australia, Brisbane, QLD, Australia

[§] Now at: German Environment Agency, Department of Air Quality, Dessau-Rosslau, Germany

[*]Communicating author: tvandenb@yorku.ca

S1. Chamber customized components and LabVIEW software

To meet the performance requirements for measuring N_r gases, chamber modifications were implemented to create inert surfaces that transmit them effectively to downstream gas analyzers. In addition, a reference chamber with an inert surface at the bottom (Figure S1) was required to benchmark the performance of a modified chamber (Figure S2) where fittings and surfaces identified to be reactive or to facilitate stronger surface interactions were replaced with more inert components.

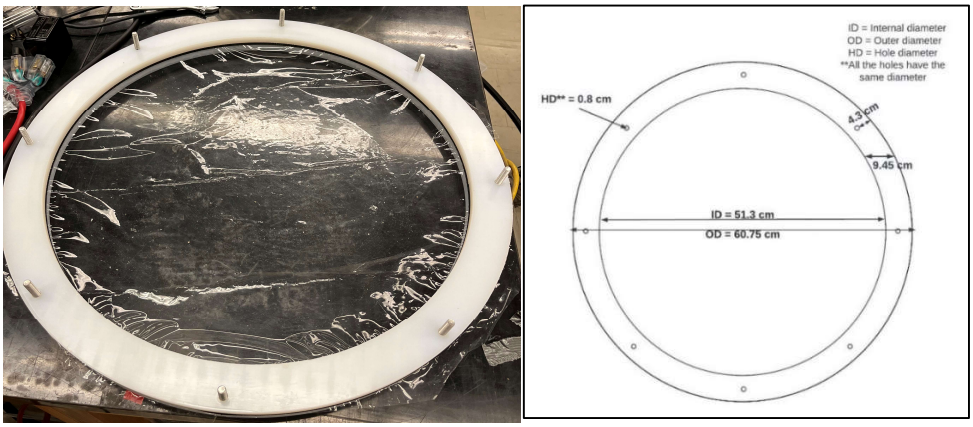

Figure S1. (left) Image of the custom-made base rings made from 1.2 cm thick PTFE with a PFA film pinned between them; all the holes have identical diameters, are located equidistant from the edges of the plate and can fit M8 bolts secured with corresponding nuts (McMasterr-Carr®, PN: 90591A161 and 91263A918). (right) Technical scale drawing of a custom-made ring for the chambers with the inner diameter, outer diameter, ring width, and diameter of holes and their distance from the outer edges denoted.

A custom LabVIEW program was created to automate control of the solenoid valves and mass flow controller in the measurement set up using the microcontroller. The front panel of the LabVIEW program (Figure S3a) allows for the timings of the solenoid valve changes to be manually set, along with the log intervals. The VI controls valve states (i.e., for V1, V2, and V3) and synchronization of the valve switching with respect to each chamber opening and closing cycle as described in the previous section. The VI also generates its own text file containing valve open/close state and a timestamp to be used for data processing. A custom R script (R Studio v3.0.1) was developed to process the data file generated by eoslink-AC, data from all reactive gas analyzers, and the VI. A graphical representation of the valve states in real time is ~~also~~ included on the front window to allow for the user to assess the measurement state. In the back window (Figure S3b), the valve timings are controlled within a state machine to allow for continuous valve

switching at the time interval selected on the front window. The MFC flow rate is controlled by sending the required voltage to the MFC ~~based on the selected flowrate~~. The data logging of the valve switching timings and MFC flowrates are handled as well within a state machine to ensure continuous logging to a csv file. The LabVIEW VI is available on the GitHub repository (https://github.com/fjs-vdblab/fluxchamber.git).

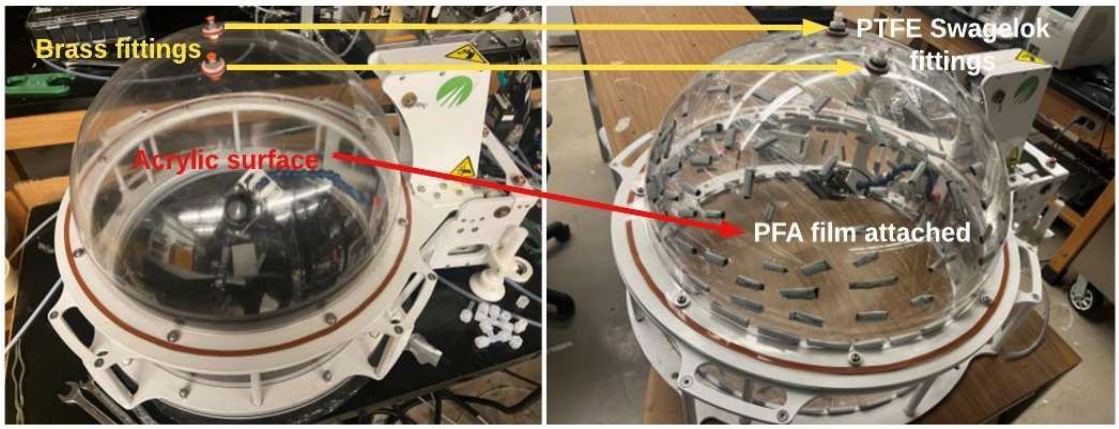

Figure S2. (left) The chamber is in its original configuration from the manufacturer with brass push-connect inlet and outlet fittings and an acrylic dome. (right) The modified chamber with 1/4" PTFE Swagelok bulkhead fittings and an attached film of PFA on the interior of the acrylic dome and all chamber sidewalls using adhesive tape.

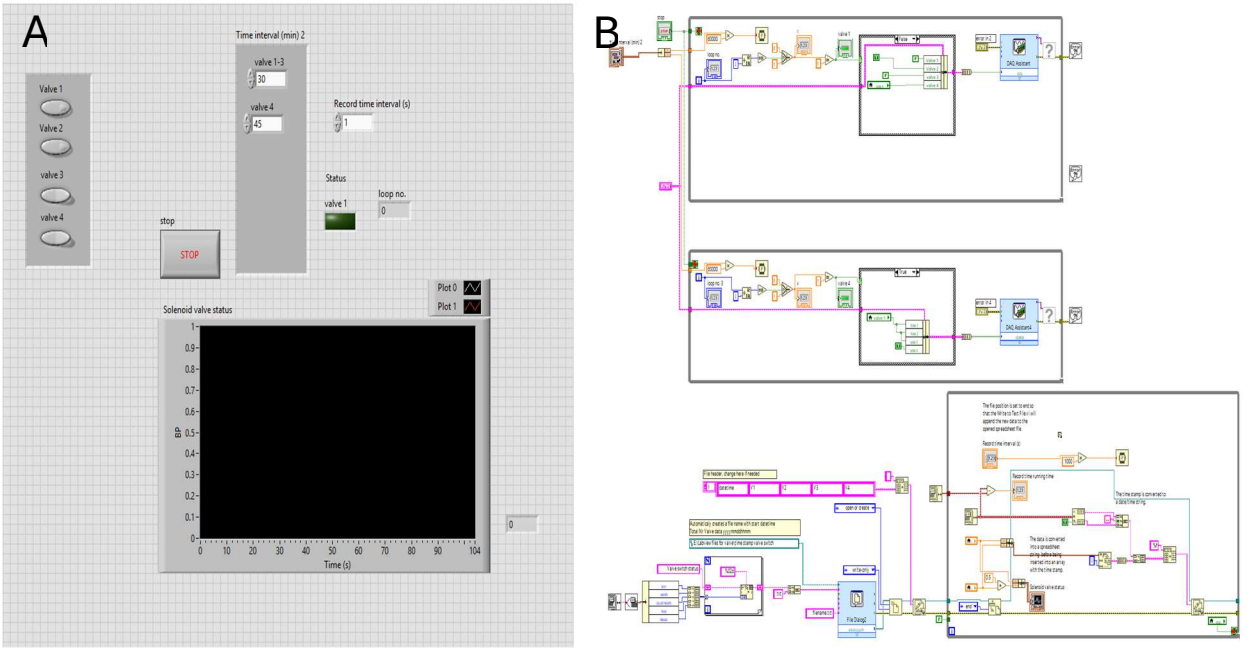

Figure S3. The custom LabVIEW VI for controlling the reference and measurement chambers (A) flows, valve states, timing for lid closures, and rate of datalogging through a graphical user interface front window, and (B) the back window virtual machines controlling the objects, voltages, and data flows.

S2. Gas analyzer quality control procedures

The NO_x analyzer is calibrated with multipoint NO and NO_2 mixing ratios to generate calibration curves on at least an annual basis, with span checks and blanks performed regularly prior to the collection of experimental data. For field use, a full calibration is performed prior to relocation of the system to the deployment site, a span check on site, and again at the end of the deployment period to account for any instrumental drift. Zero air from a gas-calibration instrument (Gascal 1100TS, American Ecotech, Warren, RI) is introduced to the analyzer through the sampling inlet to set the zero point. If the NO, NO_2 and NO_x readings are within ±0.5 ppbv of one another, the zero offset is calculated and applied. Then, an NO span check is performed using a known mixing ratio from a certified cylinder (e.g. Praxair, NI NO5MC-A3, 4.88 (±5 %) ppmv, Toronto, ON) to ensure the NO and NO_x readings are within ±1 ppbv of the true value. Next, a multi-point precision check of NO is performed at 40 ppbv, 60 ppbv, and 80 ppbv for 30 min, ensuring a stable signal has been achieved. The calibration is considered successful when the analyzer's response to

changes in NO mixing ratio is linear, with a slope of 1.00 ± 0.02 and R^2>0.98. For multi-point precision checks of NO_2, 40 ppbv, 60 ppbv, and 80 ppbv were produced using gas-phase titration of excess NO with O_3, again using the GasCal. The criteria for a successful calibration are the same as described for NO. Conversion efficiency (CE) of NO_2 to NO in the analyzer is the final parameter to be quantified, and a CE > 96% indicates that the molybdenum catalyst in the analyzer is operating reliably.

Nitrous acid (HONO) was generated using our in-house calibration source based on the reaction between gas-phase hydrochloric acid (HCl) and a $NaNO_2$ crystalline film on the surface of PFA tubing (RS-1) at 50% RH to generate gas-phase HONO and to confirm its unity conversion (Lao et al., 2020).

$$NaNO_{2(s)} + HCl_{(g)} \rightarrow HONO_{(g)} + NaCl_{(s)} \quad \textbf{RS-1}$$

In the HONO calibration source, a flow of dry carrier gas (Air Ultra Zero, 99.999%, AI 0.0UZ-K, Praxair) at 50 cm^3 min^{-1} passes through a permeation device (PD) containing HCl solution, heated to 30-40 °C. Another 50 cm^3 min^{-1} passes through a glass impinger containing deionized water to become saturated with water vapour, so the flow obtains an RH of 50% when combined with that of the HCl. This HCl-water vapour mixture enters a $NaNO_2$-coated PFA reaction device, and HONO is released by acid displacement. A delivered mixing ratio of 10-100 ppb was found to be effectively converted, in line with the performance we have previously described in detail.

Calibration for the O_3 analyzer involves a multipoint check, after one hour of warmup time to ensure lamp stability, using 100, 200, 300, and 400 ppbv mixing ratios. The procedure is considered successful if the slope falls between 0.98 and 1.02, the y-intercept between -2 and 2 ppb, and an overall R^2 > 0.99.

The calibration and precision check procedure for the Picarro G2509 involved measuring multiple known concentrations of GHGs from a calibration cylinder. The calibration cylinder contained a custom blend of GHGs (4.30 ppm (±5%) N_2O, 24.8 ppm (±5%) CH_4, 3587 ppm (±2%) CO_2), which was a certified standard grade in an air matrix (Linde Canada Plc; PN: AI CD.4MN1C-A3; CGA-590). Pure nitrogen and three calibration points at none, 4.5, and 10-times dilution of the original GHG mixing ratios in the cylinder were delivered to the Picarro analyzer until stable responses were achieved, in triplicate. The custom-built permeation oven for HONO was also used to generate known mixing ratios of NH_3 by quantification of bubbler-scrubbed NH_3 using ion

chromatography (Salehpoor and VandenBoer, 2023). A dry 90 cm^3 min^{-1} zero air flow was passed over a PD containing NH_4OH (30% v/v in 1/8" OD tubing with a 9 cm length). Calibration was performed for mixing ratios of 30 ppbv to 110 ppbv. The dilution of gases was achieved by combining the flow from a liquid N_2 dewar (Linde Canada Plc, PN: NI LC250-230). The observed versus returned slopes of 0.99 for N_2O, 0.99 for CH_4, ~~and~~ 0.98 for CO_2, and 1.37 for NH_3 when compared to the known concentrations delivered, thereby demonstrating suitable and stable calibration of the instrument, as these slopes are within the cylinder or IC mixing ratio uncertainties.

S3. Gas handling for chamber filling and emptying challenge experiments

Dilution and analyte gas flow rates were controlled using MFCs (10 L min^{-1}, PN: 1179C01314CR1BV, MKS instruments Inc, Andover, MA, US). Mixing ratios of CO_2, CH_4 and N_2O were controlled by dilution of a calibration gas cylinder containing a custom blend of the three gases (4000 ppm CO_2, 20 ppm CH_4, 3.3 ppm N_2O in zero air from Linde Canada). Known concentrations of NO and NO_2 were added from their respective calibration gas cylinders (5.9 (±5 %) ppmv of NO in air, PN: NI NO5MC-A3; 4.5 (±5 %) ppmv NO_2 in air, PN: NI NX5MC-AQ; Linde Canada plc, Toronto, ON). Production of known mixing ratios of O_3 to the chamber was achieved by combining output from the built-in ozone generator and photometer of the GasCal into dilution gas at 2 L min^{-1}. The 100 cm^3 min^{-1} flow of HONO exiting the calibration source was diluted using ZA and mixing ratios spanning 10-100 ppbv were obtained, with 2 L min^{-1} directed to the experimental setup. For NH_3, the permeation device output was also diluted with 2 L min^{-1} of zero air to generate a mixing ratio on the order of 30 ppbv.

The time response of gases for the fill and empty process was calculated from the time required to fill the chamber and completely empty the chamber (Figure S4). It can be described by a single exponential function for non-reactive gases such as N_2O, CH_4, CO_2, and NO and thus the time response, τ, for the exchange of sample gases volume (Section 2.1; E1-4). The double exponential function was used for surface-sensitive and reactive gases, such as NO_2, HONO, and NH_3 to yield two time constants, τ_1 and τ_2, the time response towards the exchange of the sample air volume and wall interactions (ES-1), respectively (Ellis et al., 2010).

$$f(t) = y_0 + A_1 \times \exp\left(\frac{-(t-t_0}{\tau_1}\right) + A_2 \times \exp\left(\frac{-(t-t_0}{\tau_2}\right) \quad \textbf{ES-1}$$

Where t_0 is the start time and y_0 is the offset that represents the measurement baseline level; A_1 and A_2 are proportionality coefficients from the contribution of the physical processes of sample volume exchange in the chamber, and reaction and wall interactions, respectively. The relative role of wall interactions or reactions, D, to the overall transfer of gases through a handling system is determined by the contribution of the A_2 term to the sum of both A terms (ES-2).

$$D = \left(\frac{A_2}{A_1+A_2}\right) \times 100\% \quad \textbf{ES-2}$$

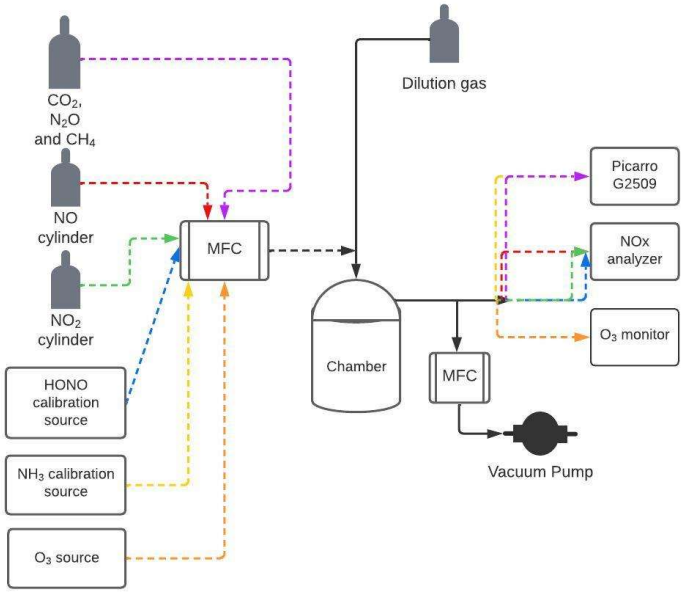

Figure S4. Experimental setup to perform fill/empty experiments in the chambers with greenhouse gases: CH_4, CO_2 and N_2O (purple); N_r gases NO (red), NO_2 (green), HONO (blue), NH_3 (yellow), and O_3 (orange); and dilution gas (black). Dashed arrows show the flow of gases from their respective sources for filling experiments to their respective gas analyzers. Emptying experiments use dilution gas alone once a steady state of the challenge gas has been obtained in the chamber.

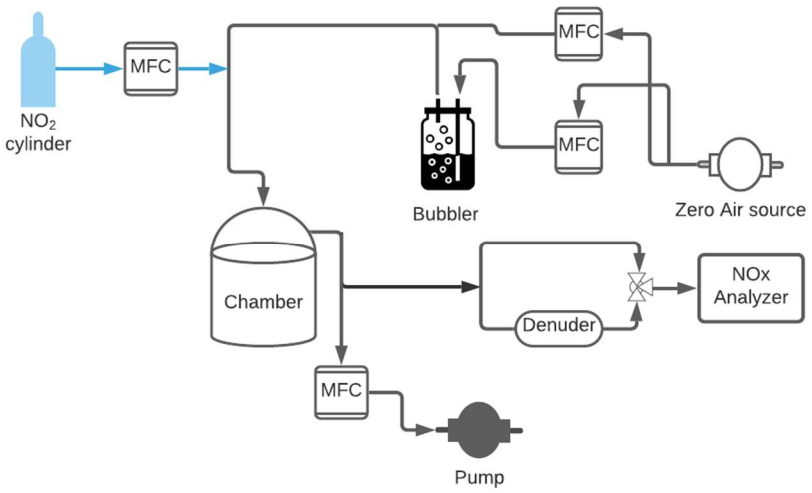

Figure S5. Experimental setup for NO_2 surface loss characterization, where arrows indicate direction of gas flows. Characterization of losses or transformation to HONO was made by a modified NO_x analyzer with experimental flow balance by an added MFC and pump.

S4. Multiplexer modification tests on gas transfer of N_r and GHGs

A 2 L min^{-1} flow of dry zero air containing 0.058 ppm of N_2O, 0.57 ppm of CH_4, and 81.5 ppm of CO_2, was passed through a multiplexer equipped with either PTFE or stainless-steel (SS) valves and fittings for 30 min to access relative losses. A separate experiment was performed with 2 L min^{-1} zero air containing a known concentration of NH_3 (0.41 ppm), which was generated based on the method described in Crilley et al. (2023) from a permeation tube containing NH_4OH. Similarly, the transfer efficiency of NO_2 was determined using a calibration cylinder (Linde Canada; PN: NI NX5MC-AQ; 5.9 (±5%) ppm) which was combined with a 2 L min^{-1} dilution flow of dry ZA to achieve a mixing ratio of 54 ppb. All challenge gases were passed through the multiplexer equipped with either PTFE or SS valves and PFA or SS fittings, respectively, to assess relative losses. All delivered and exiting flows were confirmed to be equal during these tests, ensuring no leaks led to a measured loss. The loss percentage in SS fittings and gas handling valves was measurable but generally remained below 20%, except for NH_3, which exhibited a 38% reduction. With the modifications, minimal surface loss of GHGs and NO_2 (<1%) was observed when using the PFA fittings and PTFE valves, whereas NH_3 exhibited a reduced 11% loss (Figure S6).

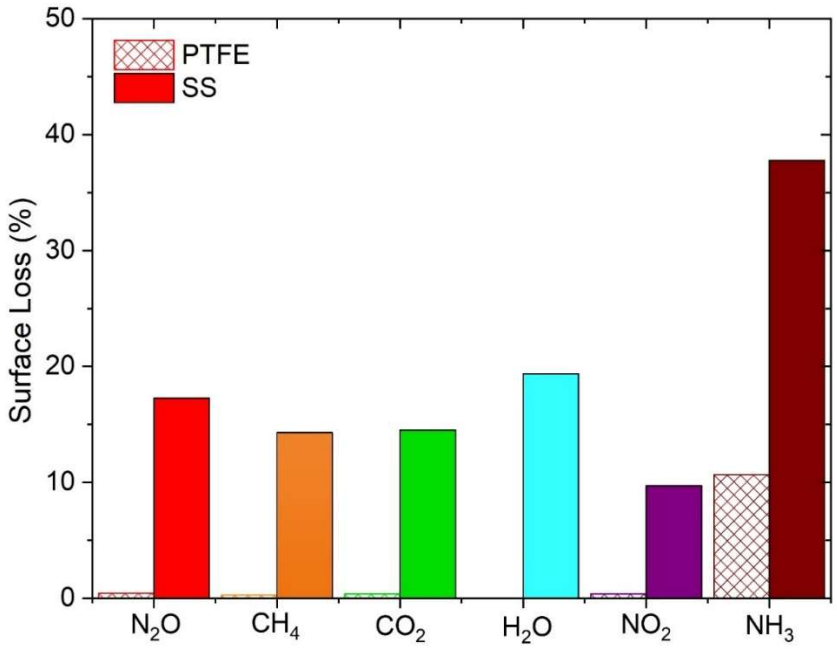

Figure S6. Loss percentage of GHGs (N_2O, CH_4, CO_2,) and N_r (NO_2, NH_3) gases on stainless steel fittings than that of a PTFE valve and unions.

The surface porosity of SS can influence its adsorption capacity for CH_4 through van der Waals interaction potentials (Sapag et al., 2010). Previous studies have shown that passivation of the SS surface via NO treatment can remove surface iron and promote the formation of chromium-enriched oxide films, which in turn govern the surface chemical reactivity toward NO (Ma et al., 2020). Furthermore, thin layers of iron oxides formed on SS surfaces can affect the interaction with N_2O and alter its decomposition pathways. Consequently, the combined effects of SS surface porosity on CH_4 van der Waals interactions, chromium-oxide passive films influencing NO reactivity, and iron-oxide layers acting as active adsorption sites for N_2O may contribute to up to a 20 % loss of these gases on SS surfaces. It is likely that the surface losses observed here for very clean SS purged extensively with dry zero air prior to these experiments is passivated over time when exposed to ambient air continuously, where the surface adsorption sites are fully occupied and losses no longer occur.

S5. Chamber modification impacts on gas transfer of NO_2 and materials for O_3

Gas interactions on chamber surfaces during challenge experiments were reversible for all N_r and GHGs tested, except NO_2, which showed reactive losses. These were characterized by calculating

the lost fraction from a small 5 ppb mixing ratio delivered into an unmodified chamber at a high relative humidity of 83%, followed by modifications to reduce this outcome under these challenging simulated environmental conditions (Figure S5). Replacement of the brass push-to-connect fittings delivered the greatest reduction in reactive losses of NO_2, with modest gains obtained from covering chamber surfaces with the PFA film (Figure S7). The final lost fraction of NO_2 in the modified system reported here is technically at the modified NO_x analyzer detection limit and therefore represents a conservative upper limit estimate.

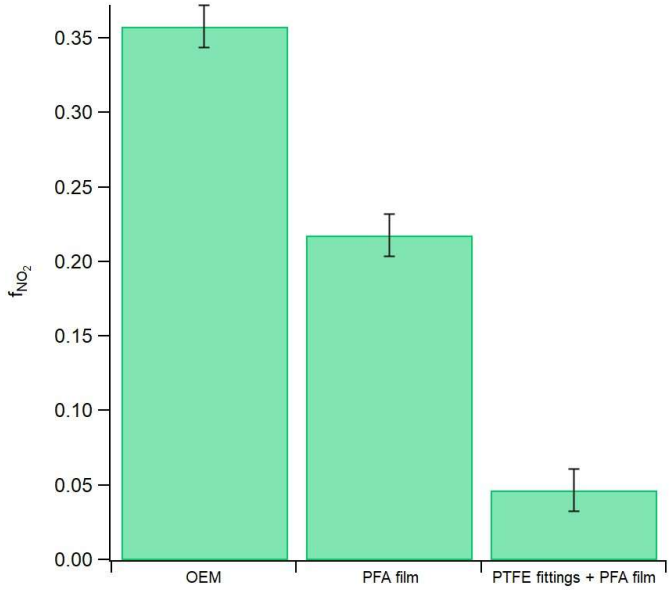

Figure S7. Average NO_2 loss fraction observed upon addition of 5 ppbv of NO_2 at 83% RH to an eosAC-LT® chamber (n = 3 each). These trials were conducted in chambers sequentially: without any modifications (original equipment manufacturer; OEM), following attachment of a PFA film to the inner surface (PFA film), and replacing brass-lined push to connect fittings with ¼" PTFE Swagelok bulkhead (PTFE fittings + PFA film).

Different RH values were produced inside the flux chamber by combining flows of dry zero air (ZA) and one saturated with water vapour by transiting a 500 mL Pyrex impinger filled with deionized water (e.g. equal 1 L min^{-1} flows combine to an RH of 50%). A high-precision, research-grade humidity probe (HMP60, Vaisala Oyj, Finland; ± 3% at 0 - 90% RH, ± 5% at 90 – 100% RH) was connected to the chamber to confirm the set point by measurement in the chamber. The flow from an NO_2 calibration cylinder (Linde Canada; PN: NI NX5MC-AQ; 5.9 (±5%) ppm) was adjusted using an MFC and combined with a dilution flow of ZA to achieve mixing ratios of 5, 7 and 10 ppbv. The total flow rate for these experiments was 2.0 L min^{-1} and a vacuum pump (62.3

L min^{-1}, PN: UZ-07061-22, Gast Manufacturing Inc., Benton Harbor, MI, USA) with an MFC (10 L min^{-1}, PN: 1179C01314CR1BV, MKS instruments Inc, Andover, MA, US) was used to make up the sampling flow beyond the 0.5 L min^{-1} of the NO_x analyzer. The same flow difference stated above was maintained in the chamber, using the built-in vent.

Prior to O_3 addition, in the characterization experiments, the chamber was flushed with ZA until the background level of O_3 was at the instrument detection limits. Three mixing ratios of O_3 of 150, 200 and 250 ppb generated by a GasCal 1100 dilution calibrator with integrated O_3 generator and photometer (American Ecotech, Warren, RI) and added to the chamber for 60 mins or until a constant concentration was reached. Two replicate runs of each addition level were performed and delivered mixing ratios were confirmed from bypassing the chambers with just the 15 m gas handling lines.

Ozone is known to undergo heterogeneous surface reactions, particularly on materials like glass, metals, or polymers (Plake et al., 2015). These surfaces often contain reactive sites such as hydroxyl groups or adsorbed water molecules that can catalyze the decomposition of O_3 into molecular oxygen (O_2) and other byproducts (George et al., 2015). Adsorption of O_3 on chamber surfaces is another potential pathway for loss. When O_3 molecules interact with surfaces, they may undergo a reaction if the materials are not inert. The use of PFA here was intended to benefit the transfer of O_3, yet despite its high chemical inertness, low reactivity, and resistance to the uptake of many chemicals from gas samples, the subsequent O_3-driven surface reactions are still substantial (Ebnesajjad, 2017). This is likely because, over time, reactive substances from sampled air accumulated through adsorption on the PFA film and/or its defect sites, thereby reducing its effectiveness. The same issue is well-known for PFA tubing used in standard air quality monitoring and is a common maintenance need for O_3 analyzer inlets. Further, physical wear or surface aging might alter the material surface through product formation or exposure of new reaction sites, which makes it less resistant to further reaction with O_3, and therefore increases the rate of loss over time. This is the case in our aged PFA film results, which emphasizes the importance of regular replacement of the film as part of the N_r system maintenance and that quality control procedures characterizing the chamber material performance with respect to O_3 will provide the highest accuracy of experimental results.

S6. Agricultural soil samples used for laboratory N_r emission measurements

A systematic method was used to collect soil samples from an agricultural field to avoid sampling bias, assuming there is no topographic reason for differences in soil properties and nutrient content within the specified plot area. The total field area was divided into eight identical plots (A-H) of 10,800 m^2 (120 m × 90 m). Soil samples were collected from four random coordinates within each plot, assuming that samples collected within 1 m^2 were homogeneous. An approximate 1 L soil core ~15 cm deep was collected with a clean shovel into a pre-labelled clean Ziploc bag. All soil samples were stored below 10 °C and transported to the laboratory within a week.

Four within-plot samples were collected to better approximate soil properties and nutrient content across the entire field. A total of 32 soil samples were collected from the field, where three of the randomly collected within-plot samples were combined generate a plot scale sample, and one sample within each plot was randomly selected to be combined into a pooled sample representative of the field scale. For the purposes of this work, we assessed the emissions of NO, NO_2, and HONO from duplicate pooled samples and from Plot D within this sampling experiment (Figure S8).

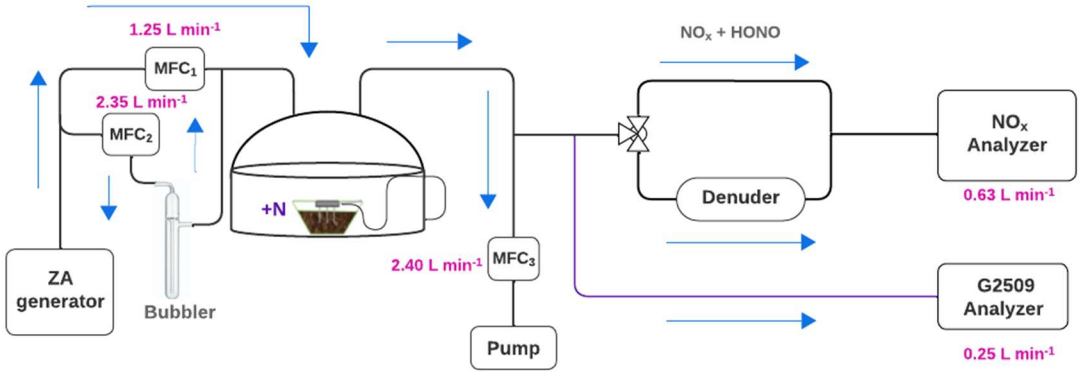

Figure S8. Schematic representation of a dynamic chamber system to measure NO, NO_2, and HONO fluxes with a modified NO_x analyzer (black lines) and NH_3 and N_2O for soil amended with fertilizer using G2509 (purple line). Zero air and humid airflow rates were set using MFC 1 and MFC 2, for a total of 3.6 L min^{-1} going into the chamber. The three-way valve either sends headspace air directly to the NO_x analyzer (measures NO and NO_2+HONO), or via the Na_2CO_3-coated denuder (measures NO, and NO_2). Blue arrows indicate the flows throughout the experimental setup, with flow rates provided in pink text.

Soil NH_3 and N_2O, along with NO, NO_2, and HONO, were measured when the pooled soil sample was amended with four different nitrogen salts (i.e., AN, urea, ABC, AC; Table S1, Figure 4). For

each experiment, 350 g of soil was used, and a corresponding fertilizer solution equivalent to 100 kg N ha^{-1} was added. Additional experimental details are provided in Section 2.~~6~~5.1 of the main manuscript. The interpretation of the full set of experimental results will be presented in a forthcoming publication on field-scale heterogeneity of N_r emissions and comments on the assumption that individual samples represent these processes across fields with similar physicochemical properties.

Table S1. The average and integrated flux for soil treated with 4 different nitrogen salts (urea, ammonium bicarbonate (ABC), ammonium carbonate (AC), and ammonium nitrate (AN)). Average fluxes were calculated over the entire experimental cycle. Integrated fluxes were obtained using the trapezoidal rule. Standard deviations reflect the variability in fluxes measured across the time points for the single sample analyzed per treatment. Replicates of urea (~40 hours) and AN (~5 hours) were analyzed with only the modified NO_x analyzer, thus lacking data for N_2O and NH_3 (represented by -).

Soil sample	Avg Flux (μg N m^{-2} hr^{-1})					Integrated flux (μg N m^{-2})				
	NO	NO_2	HONO	N_2O	NH_3	NO	NO_2	HONO	N_2O	NH_3
Urea	0.1 ± 0.06	0.03 ± 0.01	0.002 ± 0.004	9 ± 3	1 ± 0.5	230	120	1	32400	3700
ABC	0.03 ± 0.01	0.1 ± 0.01	0.03 ± 0.02	7 ± 6	20 ± 7	90	300	90	25300	85900
AC	0.03 ± 0.004	0.2 ± 0.03	0.01 ± 0.01	3 ± 2	20 ± 3	90	500	1	9600	63700
*AN	1 ± 0.1	1 ± 0.1	1 ± 0.02	-	-	50	50	40	-	-

S7. Analytical solutions to soil reactive gas flux determination with a two-chamber setup

For a single chamber system, ES1 can be used to calculate the flux of gases to and from an enclosed surface. Each of these terms and their units are provided in Section 2.~~7~~6 of the main manuscript.

$$V\frac{dC_{\text{cham}}(t)}{dt} = (A \cdot F_{\text{soil}}(t)) + (Q_{\text{in}} \cdot c_{\text{in}}(t)) - (Q_{\text{out}} \cdot c_{\text{out}}(t)) + (V \cdot R(t)) \quad \textbf{ES1}$$

Where V is the volume of the chamber (m^3), A is the surface area (m^2) enclosed by the chamber and governing the gas flux; Q_{out} is the volumetric flow rate of air exiting the chamber ($m^3\ s^{-1}$; $c_m(t)$ and $c_r(t)$ are target gas concentrations within the measurement and reference chamber (mol m^{-3}), respectively; c_{in} and c_{out} represent their corresponding rates of change (mol $m^{-3}\ s^{-1}$); and F_{net} is the resulting net gas flux per unit area (mol $m^{-2}\ s^{-1}$). The terms R_r denote the instantaneous chemical production or loss rate expressed in units of mol $m^{-3}\ s^{-1}$ for consistency.

In our field pilot study, the measurement and reference chambers were installed on clay soil using serrated collars inserted about 10 cm deep into pre-dug circles (30 cm diameter, 20 cm depth) between crop rows of senescing soybeans after removing debris. Collars were left to settle for over 24 h before the chambers were bolted securely to ensure a gas-tight seal. Flux observations were made for two weeks from 02-16 September 2022, during a period when daytime air temperatures were regularly over 25 °C and there were no instances of rain. During the second week of observations, a fertilizer addition of 25 kg N ha^{-1} was made by broadcasting urea in the chamber, followed by applying clean water to simulate 2.5 cm (1") of rainfall.

In our sampling setup, there is a negligible concentration of any target gas in the inflow ($c_{\text{in}}(t) \approx 0$) due to the use of ultra-pure zero air or nitrogen, and the air is actively mixed inside the chamber with its fan, such that $c_{\text{chamb}} = c_{\text{out}}$, so the equation simplifies to ES2. For non-steady-state conditions, where the concentration inside the chamber is changing over time, the time-varying nature of the sources and sinks needs to be accounted for. The instantaneous equation that describes the behaviour over an interval [t_1, t_2] is the integral in ES3.

$$V\frac{dC_{\text{cham}}(t)}{dt} = (A \cdot F_{\text{soil}}(t)) - (Q_{\text{out}} \cdot c_{\text{cham}}(t)) + (V \cdot R(t)) \quad \textbf{ES2}$$

$$\int_{t_1}^{t_2} V\frac{dC_{\text{cham}}(t)}{dt}\,dt = \int_{t_1}^{t_2}[(A \cdot F_{\text{soil}}(t)) - (Q_{\text{out}} \cdot c_{\text{cham}}(t)) + (V \cdot R(t))]\,dt \quad \textbf{ES3}$$

Assuming the soil flux, $F_{soil}(t)$ (mol m^{-2} s^{-1}), is constant over the time interval [t_1, t_2] is a reasonable assumption for experimental setups where the environmental conditions and, where relevant, soil-plant activity, do not change substantially over short periods of a few to tens of minutes (Pape et al., 2009). Rearranging the ES3 expression, a flux can be calculated using ES4.

$$F_{soil} = \frac{V\Delta C_{\text{cham}} + Q_{\text{out}} \int_{t_1}^{t_2} c_{\text{cham}}(t)\, dt - V \int_{t_1}^{t_2} R(t)\, dt}{A(t_2 - t_1)} \quad \textbf{ES4}$$

The volumetric mixing ratio (ES5) is often the unit of measurement for many gas analyzers and defined as the number of moles of the gas divided by the number of moles of dry air. The mixing ratio X is dimensionless and provides a way to express gas concentrations independently of changes in temperature or pressure.

$$X = \frac{n_{\text{gas}}}{n_{\text{air}}} \quad \textbf{ES5}$$

We can then write the molar concentration, c (mol m^{-3}), in the form of volumetric mixing ratio using ES6:

$$c_{\text{chamber}} = X_{\text{out}} \times \rho_d \quad \textbf{ES6}$$

Here, ρ_d (mol m^{-3}) is the molar density of the air. The total pressure P is equal to atmospheric pressure, such that by using the ideal gas law, we can define the density of air using ES7:

$$\rho_d = \frac{P}{R \cdot T} \quad \textbf{ES7}$$

Where, P (Pa) is the pressure, R (J mol^{-1} K^{-1}) is the universal gas constant, and T (K) is the absolute temperature. In ES7 it is assumed that atmospheric air behaves as an ideal gas, which is a reasonable approximation under typical environmental conditions, even at the Earth's surface. The resulting molar concentrations can then be calculated and used in the flux determinations as presented in E6 and E7 in the main manuscript.

S7.1 Dynamics and physical corrections from reference and measurement chambers

In environmental and experimental settings where gas flux is measured, it is important to capture the rate at which gas concentrations change over time. This rate reflects the net outcome from both

gas emission and deposition occurring simultaneously, influenced by the surface under study, temperature, pressure, flow, and surface interactions (ES8). The RC (r), which operates under identical conditions to the MC (m) but excludes the surface under study by isolating it beneath the PFA film, takes into account the environmental and surface effects, such that its observed flux rate is described by (ES9). To isolate the effects of the surface under study from reactions taking place in the atmospheric sample and on the chamber surfaces, the rate of change in the RC is subtracted from that in the MC, yielding the net flux through ES10.

$$F_{\mathrm{m}} = \text{surface under study} + \text{environmental and chamber effects} \quad \textbf{ES8}$$

$$F_{\mathrm{r}} = \text{environmental and chamber effects} \quad \textbf{ES9}$$

$$F_{\mathrm{net}} = F_{\mathrm{m}} - F_{\mathrm{r}} \quad \textbf{ES10}$$

The net rate of change can now be used to calculate the molar flux by substituting it into ES4 to arrive at ES11, which is the core of E6.

$$F_{\mathrm{net}} = \frac{V}{A}\left(\frac{\Delta C_m}{\Delta t_m} - \frac{\Delta C_r}{\Delta t_r}\right) + \frac{Q_{\mathrm{out}}}{A}\left(\frac{\int_{t_{1m}}^{t_{2m}} c_m(t)\ dt}{\Delta t_m} - \frac{\int_{t_{1r}}^{t_{2r}} c_r(t)\ dt}{\Delta t_r}\right) - \frac{V}{A}\left(\frac{\int_{t_{1m}}^{t_{2m}} R_m(t)\ dt}{\Delta t_m} - \frac{\int_{t_{1r}}^{t_{2r}} R_r(t)\ dt}{\Delta t_r}\right) \quad \textbf{ES11}$$

The closure period of the two chambers is matched to facilitate an accurate correction of the kinetics and surface interactions. The calculated flux from the surface under study is therefore corrected for background and environmental effects, reducing systematic bias from gas reactivity.

Last, we introduce a flux attenuation factor (λ; ES12) to correct for partial transmission of a targeted reactive gas due to adsorption to chamber walls and gas handling lines during a measurement cycle (t_1-t_2). This factor needs to be determined empirically through calibration experiments, like those presented in Figure 2, where the loss of the surface-active gas is quantified relative to the transmission of an inert gas during both filling and emptying processes.

$$\lambda = \frac{\int_{t_1}^{t_2} \left(\frac{dX}{dt}\right)_{\text{theoretical}} dt}{\int_{t_1}^{t_2} \left(\frac{dX}{dt}\right)_{\text{measured}} dt} \quad \textbf{ES12}$$

We can account for λ in ES11**,** to get the molar flux of gas inside the chamber, which accounts for flux loss (ES13) by scaling the equation directly to arrive at the full form presented as E6 in the main manuscript.

$$F_{\text{net}} = (\lambda).\left(\frac{V}{A}\left(\frac{\Delta C_m}{\Delta t_m} - \frac{\Delta C_r}{\Delta t_r}\right) + \frac{Q_{\text{out}}}{A}\left(\frac{\int_{t_{1m}}^{t_{2m}} c_m(t)\ dt}{\Delta t_m} - \frac{\int_{t_{1r}}^{t_{2r}} c_r(t)\ dt}{\Delta t_r}\right) - \frac{V}{A}\left(\frac{\int_{t_{1m}}^{t_{2m}} R_m(t)\ dt}{\Delta t_m} - \frac{\int_{t_{1r}}^{t_{2r}} R_r(t)\ dt}{\Delta t_r}\right)\right) \quad \textbf{ES13}$$

S7.2 Chemical corrections from reference and measurement chambers

For reactive species impacting our N_r suite – mainly NO, O_3, and NO_2 – flux values can be attenuated or enhanced due to the reaction of NO with O_3 (RS-2). We show below (Figure S9) that the photolysis of NO_2 and HONO are negligible due to the high-energy photon cut-off of acrylic (<400 nm threshold) (RS-3). Nevertheless, we include the NO_2 photolysis term in the rate expression for completeness, noting that under our field conditions its contribution (Section S7.2.1) is within the noise of the NO_2 fluxes. The rate of RS-2 and RS-3 for NO_2, therefore, can be expressed by ES14.

$NO + O_3 \rightarrow NO_2 + O_2$ **RS-2**

$NO_2 + h\nu \rightarrow NO + O$ **RS-3**

$$\frac{d[NO_2]}{dt} = k_{NO+O_3}[NO][O_3] - J_{NO_2}[NO_2] \quad \textbf{ES14}$$

The total change in the concentration due to reaction over a cycle can be expressed by integrating the rate equation over the cycle duration, as the start time (t_0) and end time (t) are known, therefore replacing the term *R* in ES13 (and E6) with the expression in ES15. Under our chamber conditions,

the integrated photolysis contribution was smaller than the measurement uncertainty of the NO_2 fluxes (Section S7.2.1), and therefore it was not included as an explicit term in ES15.

$$\int_{t_0}^{t} R\ d\mathrm{t} = \Delta[\mathrm{NO}] = \Delta[\mathrm{O_3}] = -\Delta[\mathrm{NO_2}] = -\int_{t_0}^{t} k\ [\mathrm{NO(t)}][\mathrm{O_3(t)}]\ d\mathrm{t} \qquad \textbf{ES15}$$

Where the R is the loss rate due to the reaction for NO and O_3 ($R \leq 0$) and simultaneous production rate for NO_2 ($R \geq 0$). For the kinetic determination, number density of the gases (molec cm^{-3}) are used to track the chemical transformations over time, but instrumentation typically measures mixing ratios. If temperature and pressure are measured alongside target gases in the dynamic chambers, then using ES6 and ES7, the reaction-corrected flux based on measured mixing ratios can be calculated using ES16.

$$F_{\mathrm{net}} = \lambda \cdot \frac{P_{\mathrm{air}}}{R \cdot T} \cdot \left(\frac{V}{A}\left(\frac{\Delta X_m}{\Delta t_m} - \frac{\Delta X_r}{\Delta t_r}\right) + \frac{Q_{\mathrm{out}}}{A}\left(\frac{\int_{t_{1m}}^{t_{2m}} X_m(t)\ dt}{\Delta t_m} - \frac{\int_{t_{1r}}^{t_{2r}} X_r(t)\ dt}{\Delta t_r} \right) \right.$$

$$\left. - \frac{V}{A}\left(\frac{P_{\mathrm{air}}}{R \cdot T}\right)\left(\frac{\int_{t_{1m}}^{t_{2m}} k \cdot X_{\mathrm{NO}_m}(t) \cdot X_{\mathrm{O3}_m}(t)\, dt}{\Delta t_m} - \frac{\int_{t_{1r}}^{t_{2r}} k \cdot X_{\mathrm{NO}_r}(t) \cdot X_{\mathrm{O3}_r}(t)\, dt}{\Delta t_r} \right) \right) \qquad \textbf{ES16}$$

Where, again, P_{air} (Pa) is the atmospheric pressure inside the measurement and reference chambers, R (J mol^{-1} K^{-1}) is the gas constant, and T (K) is the temperature inside the RC and MC. For non-reactive gases like CO_2, CH_4, and N_2O, there is no reaction term and the flux can be described simply using ES17 as below, which is presented as E7 in the main manuscript.

$$F_{\mathrm{net}} = \lambda \cdot \frac{P_{\mathrm{air}}}{R \cdot T} \cdot \left(\frac{V}{A}\left(\frac{\Delta X_m}{\Delta t_m} - \frac{\Delta X_r}{\Delta t_r}\right) + \frac{Q_{\mathrm{out}}}{A}\left(\frac{\int_{t_{1m}}^{t_{2m}} X_m(t)\, dt}{\Delta t_m} - \frac{\int_{t_{1r}}^{t_{2r}} X_r(t)\, dt}{\Delta t_r} \right) \right) \qquad \textbf{ES17}$$

S7.2.1 Losses of NO_2 or HONO due to photolysis within transparent chambers

The fraction of NO_2 or HONO lost due to photolysis depends on the photons transmitted through the chamber material (Figure S9). The photolysis rate is estimated here under a worst-case scenario with respect to our field observations, using actinic flux data collected for Lambton County,

Ontario, Canada, at 12:00 PM local time on September 10, 2022, under clear sky conditions. The effective photolysis rate constant within the chamber was calculated to be 2.62 x 10^{-4} s^{-1}, using ES18.

$$J = \int [\sigma(\lambda) \cdot \phi(\lambda) \cdot F(\lambda) \cdot T(\lambda)]\, d\lambda \qquad \textbf{ES18}$$

Where σ(λ) is the absorption cross-section of NO_2 (cm^2 $molecule^{-1}$), Φ(λ) is the quantum yield (dimensionless; 0-1), F(λ) is the actinic flux (photons cm^{-2} s^{-1} nm^{-1}), and T(λ) is the transmission of the acrylic chamber material (dimensionless) at wavelength λ (dimensionless; 0-1).

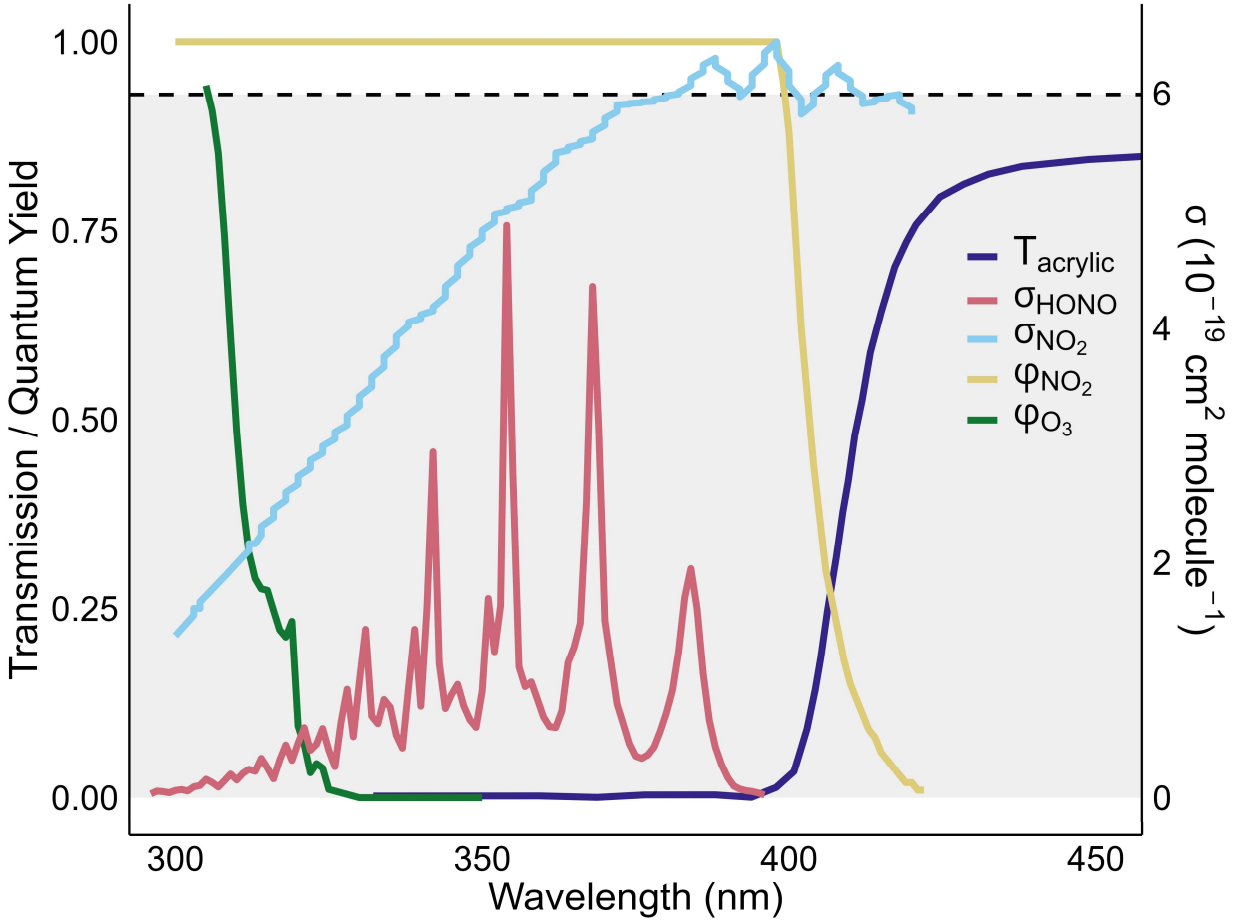

Figure S9. Transmission of light through the chamber and quantum yields for photolysis of O_3 and NO_2, along with the absorption cross section of NO_2 and HONO, as a function of wavelength. The shaded region denotes the manufacturer-specified minimum transmission (≥ 93%) for the PFA film. Note the negligible overlap for photodissociation. The acrylic effectively blocks wavelengths below approximately 400 nm, meaning the photolysis rate of NO_2 is the only one impacted by a chamber constructed from this material.

Using this attenuated loss rate in a kinetic model, we find that at most 14% of the initial NO_2 concentration is lost due to photolysis within the chamber in the first 10 minutes, and 37% within 30 minutes (Figure S10, blue trace). This rate of photolysis significantly reduces the NO_2 mixing ratio within the chamber environment. The wavelength cut-off of polyacrylate limits the penetration of shorter wavelengths, which are more effective in driving NO_2 photolysis, so the overall rate is slowed inside the chamber compared to ambient conditions (Figure S10, red trace). Despite this, within the initial 30-minute timeframe (Figure S10, vertical dashed line), the change in the fraction of NO_2 lost is relatively small due to the dynamic nature of the chamber headspace (i.e. due to continuous sampling and dilution flows), allowing for a reasonable linear approximation of the curve. The photolytic loss of HONO is much more impacted by the cutoff wavelength of the polyacrylate chamber lid, to the point where it is not substantially lost due to photolysis. As shown in Figure S9, the HONO absorption cross-section lies almost entirely below the ~400 nm transmission cutoff of the chamber lid. This spectral mismatch means that HONO photolysis is effectively suppressed inside the chamber, unlike NO_2, which still absorbs within the transmitted range. Consequently, chamber-derived HONO fluxes are not biased by photolytic loss, making their interpretation simpler than NO_2.

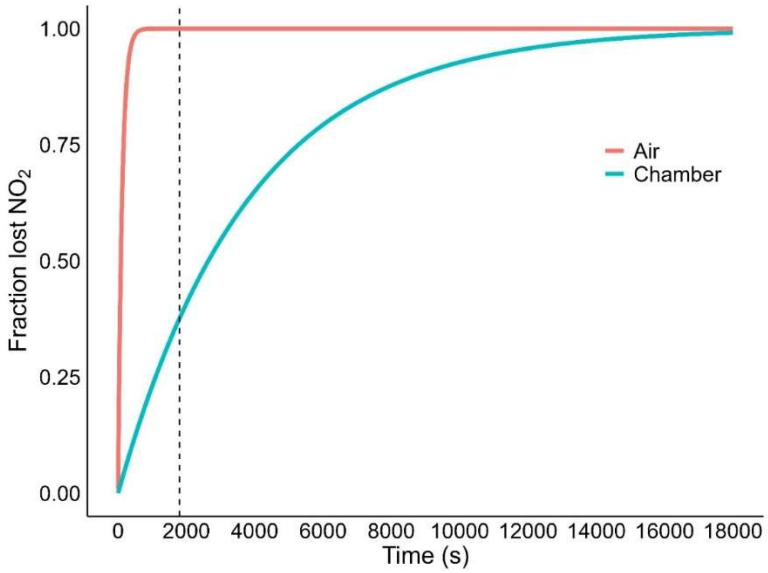

Figure S10. Fraction of NO_2 lost due to photolysis over time, both inside the chamber (blue line) and in ambient air (red line). The vertical dashed line indicates the 30-min mark, where an initial linear approximation of the loss rate can be applied.

This simplification yields an estimated initial photolysis rate loss of approximately 1% per minute for NO_2 over the initial 30-minute measurement cycle and effectively 0% per minute for HONO

under chamber conditions due to the cutoff wavelength. This linear approximation is only valid for this kind of short initial period. Beyond 30 minutes, the overall trend exhibits a steeper exponential decay, characteristic of the NO_2 photolysis process. This photolysis contribution is included within the reaction term (ES14). Its effect (~1% min^{-1} maximum at noon under clear-sky conditions) is smaller than the uncertainties of the NO_2 flux measurements, so it is not explicitly propagated into the flux equations in this work.

S7.3 Surface interaction correction using the attenuation factor (λ)

Accurate quantification of trace gas fluxes using dynamic chamber systems also requires correction for attenuation caused by gas-wall interactions and the associated sensor response delays. These effects can significantly suppress the measured accumulation rate of reactive species within the closed chamber, particularly for compounds with strong surface affinity, such as NH_3, NO_2, and HONO, requiring the use of the attenuation factor (λ; ES12).

The attenuation factor is derived from our controlled delivery experiments that simulated two sequential measurement scenarios: a filling phase, where gas is introduced and accumulates within the chamber, and an emptying phase, where the chamber is flushed and the gas signal declines (Figure 4). For an ideal gas without wall interactions, the integrated difference between theoretical and observed concentrations within a single chamber should approach zero, and λ would be approximately one. However, as shown in Figure S11, all three gases exhibited surface interactions, with NH_3 showing the largest deviation from an inert gas model.

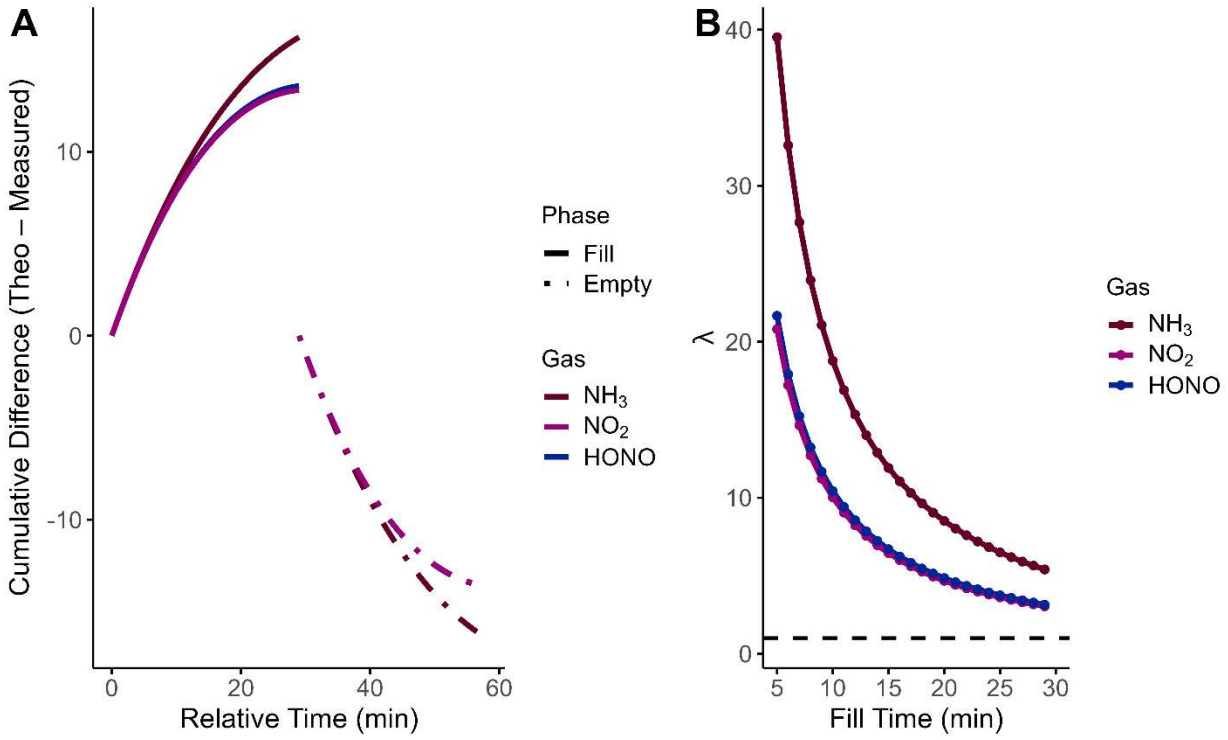

Figure S11. (A) Cumulative integration of the difference between inert and measured gas concentrations for NH_3, NO_2, and HONO over a 30-minute filling and emptying period and (B) resulting λ values for modified chambers, 15 m PFA lines, and gas analyzers as a function of filling time with a dashed line at one corresponding to the transmission of an inert gas. Theoretical concentrations represent expected values from an inert gas without attenuation, while measured values reflect signal loss due to gas–wall interactions. Solid lines correspond to the filling phase; dashed lines represent the emptying phase, together representing a full in situ measurement cycle. These ~~integrals~~ illustrate the time-dependent and nonlinear attenuation that underlies the empirical calculation of λ. Note that due to observations switching to the RC, the emptying phase does not impact the value of λ applied during field use.

When filling, the gas accumulates in the chamber, with strong initial attenuation that diminishes over time as the surfaces passivate. Conversely, adsorbed gases from surface passivation may partially desorb during emptying, offsetting some of the losses observed during filling. Two respective λ values can be derived and considered separately by integrating the filling and emptying concentration-time series independently.

Where a single-chamber is used to study an experimental system, the filling- and emptying-phase effects offset one another, masking the attenuation as all the surface interacting molecules are eventually transferred to the gas analyzer. In field applications with a dual chamber approach in

use, this symmetry is lost because the measurement chamber accumulates a real emission flux during a defined closure period, while the reference chamber does not. Hence, an empirical calculation of λ is needed which compensates for the attenuation in both the accumulation and depletion of the target gas (Table S7). For NH_3, the fill-phase difference was 16.23, dividing the expected theoretical accumulation by this measured accumulation yields a λ_{fill} of 5.40, while the empty-phase difference was −16.44, with a λ_{empty} of 0.36. Unsurprisingly, NO_2 and HONO followed a similar trend as we also noted their surface interactions, with λ_{fill} values of 3.04 and 3.14 resulting from our characterizations, respectively, and λ_{empty} values near 0.40. Uncertainties in λ were quantified from three replicate fill-empty characterizations under identical laboratory conditions, yielding one-sigma deviations of ±0.21 for NH_3, ±0.02 for NO_2, and ±0.02 for HONO. These values therefore represent attenuation behavior for a pristine or lightly used chamber system.

From a physical and mathematical standpoint, attenuation reduces all concentration-dependent components of the flux (accumulation/depletion, dilution, and reaction) by the same factor. As a result, the attenuation factor λ scales the entire net-flux expression rather than only the accumulation term. Because λ depends on surface condition, extended field use or residue accumulation may alter its value, and periodic re-characterization is recommended to maintain accurate flux estimates.

Table S7. The cumulative integrated differences between theoretical and measured values from Figure S11 for both the filling and emptying phases, and the resulting λ values. While the signed fill and empty values appear approximately balanced, their directional impact differs, and the underlying asymmetry becomes critical in real measurements.

Gas	$\int$ (Theo – Meas)$_{fill}$	$\int$ (Theo – Meas)$_{empty}$	difference	λ_{fill}	λ_{empty}
NH_3	16.23	-16.33	-0.20	5.40	0.36
NO_2	13.40	-13.64	-0.23	3.04	0.40
HONO	13.57	-13.65	-0.05	3.14	0.40

S8. References

Burkholder, J. B., Sander, S. P., Abbatt, J. P. D., Barker, J. R., Cappa, C., Crounse, J. D., Dibble, T. S., Huie, R. E., Kolb, C. E., Kurylo, M. J., Orkin, V. L., Percival, C. J., Wilmout, D. M, Wine, P. H. (2020). Chemical Kinetics and Photochemical Data for Use in Atmospheric Studies - Evaluation Number 19. NASA JPL Publication 19-5. Tables 4C-1-2, 4C-1-3, and 4C-7-2. https://jpldataeval.jpl.nasa.gov/

Crilley, L. R., Lao, M., Salehpoor, L., & VandenBoer, T. C. (2023). Emerging investigator series: an instrument to measure and speciate the total reactive nitrogen budget indoors: description and field measurements. *Environmental Science: Processes and Impacts*, *25*(3), 389–404. https://doi.org/10.1039/d2em00446a

Ebnesajjad, S. (2017). Introduction to Fluoropolymers. Applied Plastics Engineering Handbook: Processing, Materials, and Applications: Second Edition, 55–71. https://doi.org/10.1016/B978-0-323-39040-8.00003-1

Ellis, R. A., Murphy, J. G., Pattey, E., Van Haarlem, R., O'brien, J. M., & Herndon, S. C. (2010). Characterizing a Quantum Cascade Tunable Infrared Laser Differential Absorption Spectrometer (QC-TILDAS) for measurements of atmospheric ammonia. *Atmos. Meas. Tech*, *3*, 397–406.

George, C., Ammann, M., D'Anna, B., Donaldson, D. J., & Nizkorodov, S. A. (2015). Heterogeneous Photochemistry in the Atmosphere. Chemical Reviews, 115(10), 4218–4258. https://doi.org/10.1021/cr500648z

Lao, M., Crilley, L. R., Salehpoor, L., Furlani, T. C., Bourgeois, I., Andrew Neuman, J., Rollins, A. W., Veres, P. R., Washenfelder, R. A., Womack, C. C., Young, C. J., & VandenBoer, T. C. (2020). A portable, robust, stable, and tunable calibration source for gas-phase nitrous acid (HONO). *Atmospheric Measurement Techniques*, *13*(11), 5873–5890. https://doi.org/10.5194/amt-13-5873-2020

Ma, L., Pascalidou, E. M., Wiame, F., Zanna, S., Maurice, V., & Marcus, P. (2020). Passivation mechanisms and pre-oxidation effects on model surfaces of FeCrNi austenitic stainless steel. *Corrosion Science*, *167*, 108483. https://doi.org/10.1016/J.CORSCI.2020.108483

Pape, L., Ammann, C., Nyfeler-Brunner, A., Spirig, C., Hens, K., & Meixner, F. X. (2009). An automated dynamic chamber system for surface exchange measurement of non-reactive and reactive trace gases of grassland ecosystems. *Biogeosciences*, *6*(3), 405–429. https://doi.org/10.5194/bg-6-405-2009

Plake, D., Stella, P., Moravek, A., Mayer, J. C., Ammann, C., Held, A., & Trebs, I. (2015). Comparison of ozone deposition measured with the dynamic chamber and the eddy covariance method. Agricultural and Forest Meteorology, 206, 97–112. https://doi.org/10.1016/j.agrformet.2015.02.014

Salehpoor, L., & VandenBoer, T. C. (2023). Suppressor and calibration standard limitations in cation chromatography of ammonium and 10 alkylamines in atmospheric samples. *Analytical Methods*, *15*(31), 3822–3842. https://doi.org/10.1039/d3ay01158e

Sapag, K., Vallone, A., Blanco, A. A. G., & Solar, C. (2010). Adsorption of Methane in Porous Materials as the Basis for the Storage of Natural Gas. *Natural Gas*. https://doi.org/10.5772/9846